TARGETING r(CGG) REPEATS WITH SMALL MOLECULE: A THERAPEUTIC APPROACH FOR FXTAS

M.Sc. Thesis

By SOUMALYA DAS



DEPARTMENT OF BIOSCIENCES AND BIOMEDICAL ENGINEERING INDIAN INSTITUTE OF TECHNOLOGY INDORE

May 2025

TARGETING r(CGG) REPEATS WITH SMALL MOLECULE: A THERAPEUTIC APPROACH FOR FXTAS

A THESIS

Submitted in partial fulfillment of the requirements for the award of the degree

of
Master of Science

by
SOUMALYA DAS



DEPARTMENT OF BIOSCIENCES AND BIOMEDICAL ENGINEERING INDIAN INSTITUTE OF TECHNOLOGY INDORE

May 2025



INDIAN INSTITUTE OF TECHNOLOGY INDORE

CANDIDATE'S DECLARATION

I hereby certify that the work which is being presented in the thesis entitled TARGETING r(CGG) REPEATS WITH SMALL MOLECULE: A THERAPEUTIC APPROACH FOR FXTAS in the partial fulfillment of the requirements for the award of the degree of MASTER OF SCIENCE IN BIOTECHNOLOGY and submitted in the DEPARTMENT OF BIOSCIENCES AND BIOMEDICAL ENGINEERING, Indian Institute of Technology Indore, is an authentic record of my own work carried out during the time period from June 2024 to May 2025 under the supervision of Prof. Amit Kumar, BSBE, IIT Indore.

The matter presented in this thesis has not been submitted by me for the award of any other degree of this or any other institute.

Soumalya Owo 21.05.25 Signature of the student with date

(SOUMALYA DAS)

This is to certify that the above statement made by the candidate is correct to the best of my/our knowledge.

Signature of the Supervisor of M.Sc. thesis

21.05.2025(Prof. AMIT KUMAR)

SOUMALYA DAS has successfully given his M.Sc. Oral Examination held on 6th of May 2025.

Signature of Supervisor of M.Sc. thesis
Date:

21.05-2025

Convener, DPGC

Date: 21/05/2025

ACKNOWLEDGEMENTS

"The journey of a thousand miles begins with one step"

My Master's journey has been a rewarding experience, made possible by the unwavering support and encouragement of many individuals. I am deeply grateful to everyone who has contributed to my growth and success along the way. I would like to extend my sincere thanks to my supervisor, Prof. Amit Kumar, for his invaluable guidance and insightful suggestions, which have played a crucial role in shaping this journey. His enthusiasm and mentorship have made this journey both intellectually enriching and inspiring. I also acknowledge the Department of Biotechnology, Government of India, for generously supporting my studies through the awarded fellowship.

I extend my thanks to my faculty advisor Dr. Parimal Kar for his constant support and guidance throughout this journey. I am also grateful to Prof. Mirza Saqib Baig for giving me the opportunity to work on and contribute to review papers, which has greatly enriched my academic experience. I am grateful to the head of the Department of Biosciences and Biomedical Engineering for his immense support. My lab members have been a constant source of help and encouragement. I am especially thankful to Mr. Krishna Singh Solanki for his professional and personal support and guidance. He has been a great help whenever I faced problems and has always been there for valuable discussions related to my work and beyond. I would also like to express my heartfelt thanks to my lab and break time companions, Ms. Sakshi Shukla, Ms. Mansee Patel, Ms. Aditi Pramod Kumari, and Ms. Suvigya Chaturvedi as well as my batchmates Shubhi Khandelwal and Ritika Rawat, for their constant guidance and emotional support throughout my journey. I truly appreciate the engaging discussions we had during our evening snack breaks. Their valuable advice and insights have been immensely helpful, and I have gained much from their experience. I also want to thank Mr. Aritra Chakraborty and Mr. Ashmad Nayak for their meaningful scientific and non-scientific conversations. I want to acknowledge my lab seniors, Ms. Priya Gupta, Ms. Aakriti Singh, and Ms. Pronamika Chetia.

I am grateful to my dear friends Ayushi Yadav, Milan Khanda, Mahesh Sahu and Yashi Singh for their unwavering encouragement and support. I deeply appreciate their patience in tolerating my endless chatter and baseless talks. I am also grateful to my batchmates, and my seniors Khandu Wadhonkar, Sagnik Mitra, Pallabi Seal Saurav Sharma, Kapil Dattatray Ursal, and Mallar Dasgupta, who, although

not members of my lab, provided invaluable assistance with my experiments and supported me personally.

I am grateful to Mr. Kinny Pandey, Dr. Ravinder, Mr. Ghanshyam Bhavsar, and Mr. Atul Singh from SIC, IIT Indore, for their help with high-end techniques. I appreciate the assistance of departmental staff members Mr. Amit Kumar Mishra, Mr. Gaurav Kumar, and Mr. Arif Patel throughout my M.Sc. program. My sincere gratitude goes to the Director of IIT Indore, and I also thank all the non-teaching staff, housekeeping staff, and security staff at IIT Indore.

Throughout my M.Sc. journey, I have been fortunate to receive unwavering support from many individuals who helped me navigate various challenges. I am especially thankful to my family for their constant encouragement. I am deeply grateful to my parents, Mrs. Sulekha Das and Mr. Susanta Das, for fostering my curiosity and observational abilities from an early age. My grandmother, Mrs. Sova Das, has also been a consistent source of personal support. I would also like to express my heartfelt gratitude to my grandparents, who are no longer with me in this world. Their words and values continue to inspire me and have played a significant role in shaping me into the person I am today. Finally, I extend my heartfelt gratitude to the Almighty, whose blessings have been instrumental in making this journey possible.

Soumalya

Dedicated to my Parents



Abstract

Fragile X-associated Tremor/Ataxia Syndrome (FXTAS), a nucleotide repeat expansion disorder, arises from CGG repeat expansions in the 5' UTR of the FMR1 gene, leading to RNA foci formation and toxic protein aggregation via RAN translation. These fundamental mechanisms often lead to a series of consequences, including splicing defects, neuroinflammation, mitochondrial dysfunction, impaired autophagy, and neuronal cell death. Targeting toxic RNA repeats offers a promising therapeutic strategy. In this study, we identified Celecoxib, a selective COX-2 inhibitor, as a potential treatment for FXTAS. At first, we utilized various biophysical assays and molecular docking to confirm Celecoxib's strong binding affinity towards the r(CGG)_{exp} RNA. Further studies in the cellular model demonstrated the potency of Celecoxib in reducing toxic protein aggregates and improving splicing defects. Notably, it significantly reduces FMR1PolyG aggregates in the Drosophila FXTAS model, leading to improved locomotor impairments and mitigation of associated pathological consequences, including neuroinflammation, mitochondrial dysfunction, impaired autophagy and neuronal cell death. Moreover, Celecoxib treatment significantly extends the lifespan of the flies. Along with that, Celecoxib also exhibit significant effect in the muscles of *Drosophila* expressing (CGG)₉₀. There, these results collectively support the therapeutic potential of repurposing Celecoxib for the treatment of FXTAS.

Keywords: FXTAS, FMR1PolyG, $r(C\underline{G}G)_{exp}$, Celecoxib, Drug Repurposing, Trinucleotide repeats.



LIST OF PUBLICATIONS

Publication from thesis:

- 1. Soumalya Das, Aditi Pramod Kumari, Krishna Singh, Sakshi Shukla, Shubhi Khandelwal, Amit Kumar*. Molecular Repositioning of Celecoxib as a Neurotherapeutic Agent in Fragile X-associated Tremor Ataxia Syndrome (FXTAS), ACS Pharmacology & Translational Science (Manuscript ID: pt-2025-003265) (under revision).
- **2. Soumalya Das**, Sakshi Shukla, Krishna Singh, Amit Kumar*. FMR1PolyG Aggregates Induce Degeneration in Muscles. (*Manuscript to be communicated*).

Publication apart from thesis:

- 3. Wadhonkar K*, Das Soumalya*, Subramanian R, Sk MH, Singh Y, Baig MS. The effect of cancer cell-derived exosomal proteins on macrophage polarization: An in-depth review. Experimental Cell Research 2025 Jan 15;444(2):114393. doi: 10.1016/j.yexcr.2024.114393. Epub 2024 Dec 20. PMID: 39710293. (* Equal Contribution)
- Wadhonkar, K., Singh, Y., Rughetti, A., Das, Soumalya, Yangdol, R., Sk, M.H., Baig, M.S. Role of cancer cell-derived exosomal glycoproteins in macrophage polarization. Molecular Biology Reports 52, 451 (2025). https://doi.org/10.1007/s11033-025-10535-x.
- 5. Soumalya Das*, Shubhi Khandelwal*, Sakshi Shukla, Amit Kumar*. Exploring the Pleiotropic Effects of IncRNA in different Repeat Expansion Disorders. BBA Molecular Basis of Disease (Manuscript ID: BBADIS-25-1420) (* Equal Contribution) (Under review).

- 6. Soumalya Das, Mansee Patel, Shubhi Khandelwal, Ritika Rawat, Sakshi Shukla, Aditi Pramod Kumari, Krishna Singh, Amit Kumar*. From Mutations to Microbes: Investigating the Impact of the Gut Microbiome on Repeat Expansion Disorders. Journal of Neurochemistry (Manuscript ID: JNC-2025-0291) (Under review).
- 7. Shubhi Khandelwal, **Soumalya Das**, Aditi Pramod Kumari, Krishna Singh, Sakshi Shukla, Amit Kumar*. Exploring the Neuroprotective Role of P2 in the Treatment of FXTAS (*Manuscript to be communicated*).

TABLE OF CONTENTS

LIST	OF FIGURES	XIII
Nome	nclature	XVII
Acron	yms	XIX
Chapt	er 1 Introduction	1
1.1	Repeat Expansion disorders	1
1.2	Pathological mechanism driving FXTAS	2
1.3	Possible Therapeutic Strategies against FXTAS	3
1.4 disorde	Therapeutic development against repeat expansion ers	4
1.6	Repositioning of Celecoxib FXTAS therapy	5
1.6	Drosophila as a model for neurological disorders	6
1.7	The <i>Drosophila</i> genome	8
1.8	Life Cycle of <i>Drosophila</i>	8
Chapt	er 2 Literature review and Problem Formulation	13
Chapt	er 3 Materials, Methods and Instrumentation	15
3.1	Materials	15
3.2	Sample preparation and Instrumentation	15
3.2.1.	RNA synthesis and purification	15
3.2.2.	Expression and purification of DGCR8	16
3.2.3	Fluorescence Titration Assay	16
3.2.2	Isothermal Titration Calorimetry Experiment	17
3.2.3	Circular Dichroism Spectroscopy	18
3.2.4	Electrophoretic Mobility Shift Assay	19
3.2.5	PCR Stop Assay	20
3.2.8	Molecular Docking	21
3.2.9	Nuclear Magnetic Resonance Spectroscopy	21
3.2.10	Fluorescence spectroscopy	22

3.2.11	Western blot analysis22
3.2.12	Visualization of FMR1PolyG aggregation23
3.2.13	Pre-mRNA alternative splicing analysis23
3.2.14	Drosophila stocks and dietary conditions24
3.2.15	Larval Feeding Assay24
3.2.16	Eye Phenotyping25
3.2.17	Climbing Assay
3.2.18	Flight Assay
3.2.19	Larval Crawling Assay
3.2.20	Western blotting from <i>Drosophila</i> Brain tissue27
3.2.21	Histology of larval tissue staining27
3.2.22	Eye Pigmentation Analysis
3.2.23	Lifespan Analysis
3.2.24	Detection of ROS levels
Chapt	er 4 Results and Discussion 31
4.1 bindin	Primary screening of the molecules using the Fluorescence gassay
4.2 RNAs	Thermodynamic Analysis of Celecoxib Binding to CGG Repeat through Isothermal Titration Calorimetry33
4.3 CGG I	Validation of Celecoxib-Induced Conformational Changes in Repeat RNA Using Circular Dichroism Assay34
4.4 of r(C0	Electrophoretic Mobility Shift Assay and PCR-Based Inhibition GG) Repeat Expansions by Celecoxib
4.5 Using	Molecular Characterization of r(CGG) ₆ RNA–Drug Interactions Docking Studies and NMR Spectroscopy37
	Assessment of Celecoxib's effect on alterations in toxic CGG

4.7 Transla	Evaluation of Celecoxib-Mediated Inhibition of RAN ation in FXTAS Cellular Model42
4.8 Celeco	Improvement of Splicing Defects in FXTAS Cellular Model by oxib Treatment
4.9 the Flic	Assessment of Celecoxib's Effect on the Feeding Behavior of es
	Celecoxib Counteracts FMR1PolyG-Induced degeneration, Eye Abnormalities, and Pigment Loss in the phila FXTAS Model
4.10.1	Brightfield microscopy47
4.10.2	Eye pigmentation
4.10.3	FE-SEM
4.10.4	Confocal microscopy
4.11 inclusi	In vivo potency of celecoxib in reducing the FMR1PolyG on in brain tissues
4.12 Induce	Celecoxib Restores Locomotor Activity in FMR1PolyG-d FXTAS Drosophila Model53
4.13	Quantification of arbitrary ROS levels54
4.14 membr	Effect of Celecoxib on mitochondrial oxidative stress and rane potential
4.15 stainin	Visualization of neuronal cell death using Propidium Iodide g58
4.16	Analysis of Lifespan in Response to Celecoxib Dosage59
	RT-qPCR analysis of various genes involved in autophagic tion and neuroprotection
4.18 the Flic	Assessment of Celecoxib's Effect on the Feeding Behavior of es
4.19 inclusi	In vivo potency of celecoxib in reducing the FMR1PolyG on in muscles tissues
4.20 FXTA	Celecoxib Restores muscle functioning in FMR1PolyG-Induced S <i>Drosophila</i> Model
4.21	Quantification of arbitrary ROS levels in muscles68
4.22 express	Analysis of Lifespan Response to Celecoxib Dosage in flies sing (CGG) ₉₀ in the muscles69

Chapter 5 Conclusion and Future perspectives	71
Appendix	75
References	79-90

LIST OF FIGURES

Figure 1.1. Representing different types of repeat expansion disorders
Figure 1.2. Represents Represents the pathological mechanisms driving FXTAS
Figure 1.3. Represents the Possible Therapeutic Strategies against FXTAS
Figure 1.4. Represents Therapeutic development using small molecules
Figure 1.5. Represents the structure of Celecoxib
Figure 1.6. Life cycle of <i>Drosophila melanogaster</i> 14
Figure 1.7. Drosophila egg14
Figure 1.8. Drosophila larvae (1st, 2nd, and 3rd instar larval stages)
Figure 1.9. <i>Drosophila</i> pupa15
Figure 1.10. Adult <i>Drosophila</i> fly
Figure 1.11. Male and female adult flies
Figure 3.1 Jablonski diagram depicting fluorescence phenomenon where the molecule is excited to a higher energy state followed by the release of energy
Figure 3.2 Schematic representation of the heat calorimeter in ITC instrument along with example of binding isotherm
Figure 3.3. Schematic representation of Electrophoretic shift mobility
Figure 3.4. Schematic representation of PCR Stop Assay21
Figure 4.1. Fluorescence-based screening of Celecoxib's Binding Affinity to FXTAS-Associated Repeat Structures32
Figure 4.2. Isothermal calorimetry titrations of Celecoxib against different r(CGG) _{exp} and r(AUx6)
Figure 4.3. CD spectroscopy titration of r(CCG)exp and r(AUx6) duplex RNA in the presence of Celecoxib35

Figure 4.4. Gel retardation assay and PCR stop assay show alteration in r(CGG) _{exp} RNA band patterns on titration with Celecoxib
Figure 4.5. Molecular Docking, and NMR Broadening of Celecoxib and CGG RNA
Figure 4.6. CD spectroscopic analysis of r(CGGx99) RNA with increasing concentration of proteins and Celecoxib
Figure 4.7. Gel images depicting EMSA with r(CGGx99) RNA in the presence of DGCR8 and increasing concentration of Celecoxib41
Figure 4.8. Graph depicting the Fluorescence emission spectra of DGCR8 in increasing concentrations of r(CGGx99) RNA and Celecoxib
Figure 4.9. In-vitro efficacy of Celecoxib in reducing FMR1PolyG aggregates in FXTAS cellular models
Figure 4.10. In-vitro potency of Celecoxib in ameliorating splicing defects in FXTAS cellular models
Figure 4.11. Graphs representing feeding intake of Flies46
Figure 4.12. Celecoxib mitigates pigment loss and rough eye phenotype caused by PolyG toxicity in the FXTAS <i>Drosophila</i> model
Figure 4.13. Effect of Celecoxib on pigment loss and rough eye phenotype in Control Flies
Figure 4.14. Celecoxib helps to mitigate the PolyG aggregates in the FXTAS <i>Drosophila</i> model
Figure 4.15. Celecoxib improves locomotor dysfunctions in the diseased fly model
Figure 4.16. Bar graph representing % ROS production in diseased and control flies
Figure 4.17. Celecoxib treatment restores mitochondrial dysfunction in the FXTAS Drosophila model (Mitosox Staining)56
Figure 4.18. Celecoxib treatment restores mitochondrial dysfunction in the FXTAS <i>Drosophila</i> model (TMRM Staining)57
Figure 4.19. Celecoxib treatment reduces neuronal cell death in the FXTAS <i>Drosophila</i> model
Figure 4.20. Celecoxib treatment extends lifespan in the FXTAS Drosophila model

Figure 4.21. Celecoxib treatment upregulates different autophagic and neuroprotective genes in the FXTAS <i>Drosophila</i> model63
Figure 4.22. Graphs representing feeding intake of muscle specific expression flies
Figure 4.23. Celecoxib helps to mitigate the PolyG aggregates in muscle tissues in the FXTAS <i>Drosophila</i> model
Figure 4.24. Celecoxib Restores muscle functioning in larvae of FMR1PolyG-Induced FXTAS <i>Drosophila</i> Model
Figure 4.25. Celecoxib Restores muscle functioning in adult flies of FMR1PolyG-Induced FXTAS <i>Drosophila</i> Model69
Figure 4.26. Graphs representing % ROS production in muscle specific expression flies
Figure 4.27. Celecoxib treatment extends lifespan in in muscle specific expression flies



Nomenclature

Λ Wavelength

ε Extinction coefficient

°C Degree Centigrade

Δ Delta

μL Microliter

mL Milliliter

nm Nanometer

nM Nano molar

μM Micro molar

M Molar

s Seconds

min Minutes

hr Hour



Acronyms

CD Circular Dichroism

FBA Fluorescence Binding assay

D/N Drug/Nucleic Acid

DMSO Di methyl sulfoxide

EDTA Ethylenediaminetetraacetic acid

EMSA Electrophoretic Mobility Shift Assay

LB Luria Broth

PAGE Polyacrylamide gel electrophoresis

PCR Polymerase Chain Reaction

PDB Protein Data Bank

RNA Ribonucleic acid

K_d Dissociation constant

DTT Dithiothreitol

PMSF Phenylmethylsulphonyl fluoride

SDS Sodium dodecyl-sulfate

Ni-NTA Nickel-Nitrilotriacetic Acid

IPTG Isopropylthio-β-galactoside

CV Column Volume

OD Optical Density

TNR Trinucleotide repeat

UTR Untranslated region

AONs Antisense Oligonucleotides

APS Ammonium Persulphate

TEMED Tetramethylethylenediamine

Chapter 1

Introduction

Repeat-associated neurological disorders are a group of Repeat Expansion Disorders (REDs), caused by abnormal expansions of specific nucleotide repeats (e.g., trinucleotide, pentanucleotide, hexanucleotide) within the genome. These expansions can disrupt the normal functioning of the gene through various mechanisms such as toxic RNA gain-of-function, aberrant protein translation, and epigenetic changes ^{1,2}. The severity, age of onset, and progression of these disorders often correlate with the length of the repeat expansion. Some Common examples include Fragile X Syndrome, Huntington's Disease, Myotonic Dystrophies, and Spinocerebellar Ataxias ^{2,3}. Fragile X-associated Tremor/Ataxia Syndrome (FXTAS) is a late-onset neurodegenerative disorder that originates from the expansion of 55-200 CGG repeats in the 5' untranslated region (UTR) of the FMR1 gene. The pathogenesis of FXTAS includes two primary mechanisms, toxic RNA accumulation and repeat-associated non-AUG (RAN) translation of homopolymeric proteins such as FMR1PolyG. These toxic species lead to widespread cellular dysfunction, including RNA-binding protein sequestration, splicing defects, neuroinflammation, mitochondrial impairment, and neuronal death. FXTAS presents clinically with tremor, ataxia, cognitive decline, and other neurological and systemic symptoms 4,5

1.1 Repeat Expansion disorders

REDs are a complex group of genetic disorders marked by the unusual expansion of specific DNA nucleotide repeats ¹. These expansions can vary from trinucleotide repeats to more intricate ones like pentanucleotide, hexanucleotide, and even dodecanucleotide repeats ². The number of

repeats substantially influences the severity of the disease symptoms. When these repeats exceed a normal threshold, they become unstable and can lead to pathogenic consequences through various molecular mechanisms, such as RNA toxicity, protein aggregation, loss or gain of gene function, and epigenetic alterations. The length of the expanded repeat is often directly correlated with disease severity, age of onset, and rate of progression, with longer expansions typically resulting in earlier onset and more severe phenotypes. This group currently comprises about 40 different disorders, including Huntington's Disease (HD), Amyotrophic Lateral Sclerosis (ALS), Fragile X Syndrome (FXS), Fragile X-associated Tremor/Ataxia Syndrome (FXTAS), Friedreich's Ataxia (FRDA), various Myotonic Dystrophies (DMs), and Spinocerebellar Ataxias (SCAs). While many REDs predominantly affect the nervous system, recent investigations reveal they also influence other physiological systems ^{2,3}.

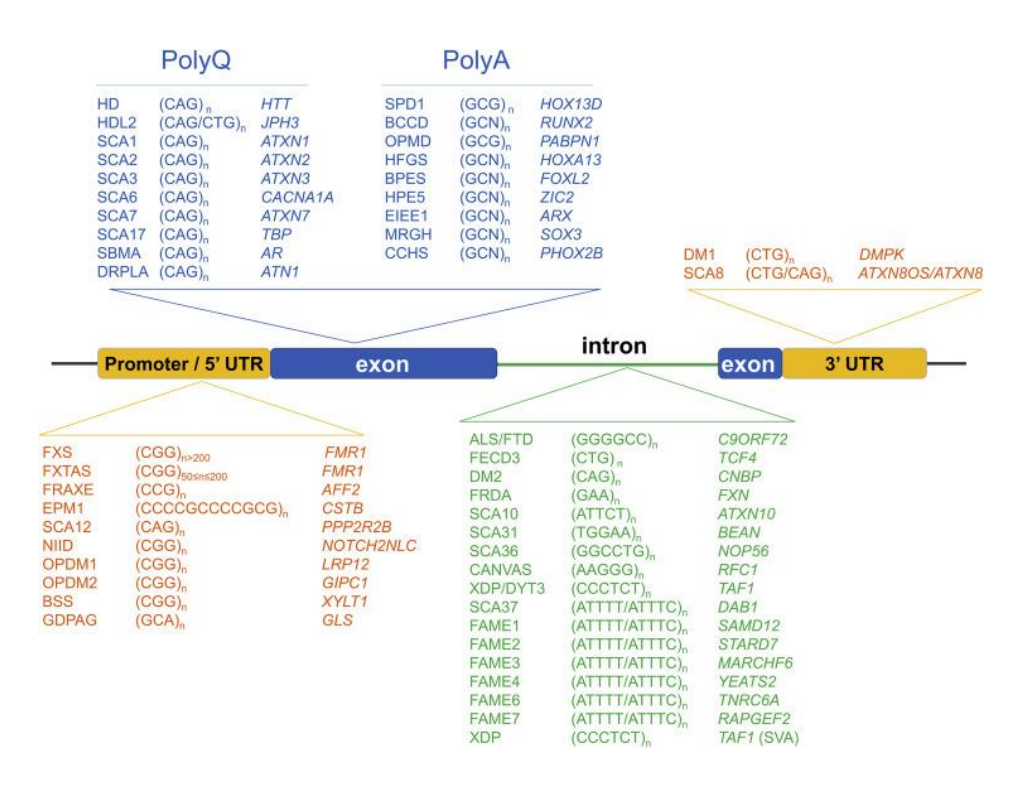


Figure 1.1 Representing different types of repeat expansion disorders ¹.

1.2 Pathological mechanism driving FXTAS

FXTAS, in particular, is a late-onset neurodegenerative disorder caused by increased CGG repeats in the 5' untranslated region (UTR) of the FMR1 gene on the X chromosome. FXTAS patients possess expansions of up to 200 CGG repeats, whereas unaffected people carry fewer than 55 repeats ^{4,5}. Expansion exceeding 200 repeats causes hypermethylation and silencing of the FMR1 (Fragile X Messenger Ribonucleoprotein 1) gene, eventually resulting in FXS. FXTAS is frequently associated with a range of clinical symptoms, including dementia, action ataxia, intention tremor, Parkinson's disease, seizures, autoimmune disorders, premature ovarian failure, and impotence ^{5,6}. The pathogenesis of FXTAS primarily involves two key mechanisms, toxic RNA accumulation and protein gain-offunction ⁵. The enlarged CGG repeats RNAs undergo Repeat-associated non-AUG (RAN) translation, resulting in the aggregation of toxic homopolymeric proteins such as FMRPolyG and FMRPolyA. Furthermore, the enlarged CGG repeats RNA forms RNA foci by sequestering crucial RNA-binding proteins (RBPs) such as DGCR8, DROSHA, Sam68, hnRNPA2/B1, CUGBP1, and Pur-alpha. This sequestration results in the production of intranuclear inclusions and extensive splicing anomalies, as seen in cellular models, animal models, and patient brain samples ⁷. Moreover, these mechanisms lead to several severe downstream pathological consequences, such as neuroinflammation ⁸, mitochondrial dysfunction ⁹, impaired autophagy ¹⁰, and neuronal cell death ¹¹, which eventually leads to a reduced lifespan ¹².

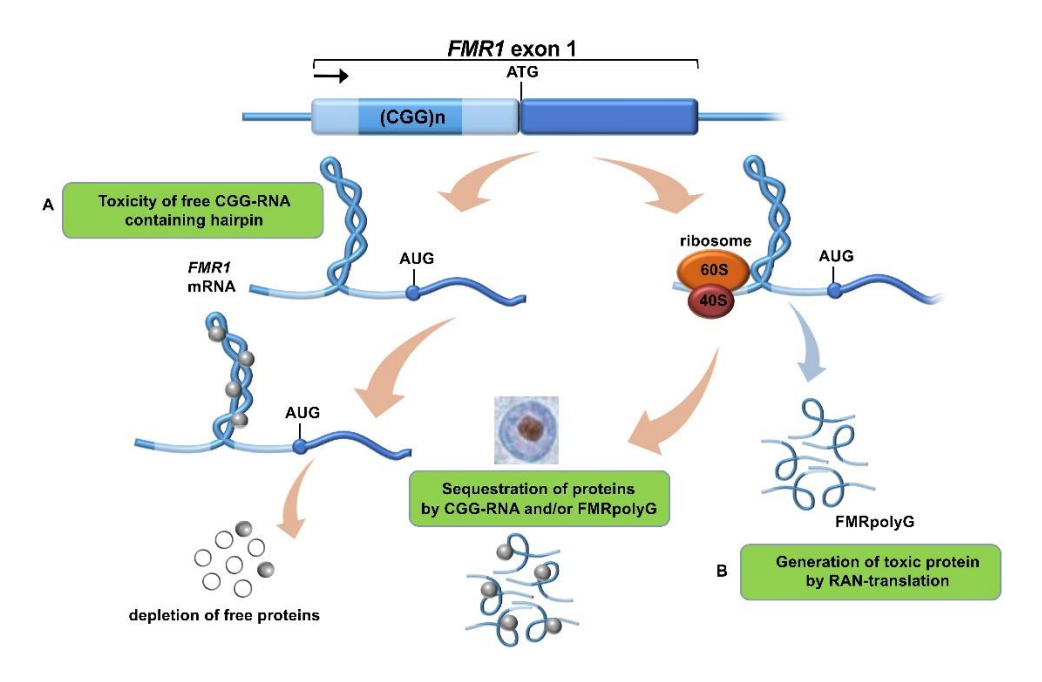


Figure 1.2 Represents the pathological mechanisms driving FXTAS ⁵.

1.3 Possible Therapeutic Strategies against FXTAS

Accumulating evidence suggests that RNA plays a fundamental role in the pathophysiology of FXTAS, acting as both a regulator of cellular processes and a mediator of disease pathology ^{7,13}. Given the involvement of expanded CGG repeat RNA in the disease pathogenesis, targeting this biomacromolecule appears to be a potential therapeutic strategy. While previous efforts have utilized RNA-targeted Cas9, CRISPR-Cas13a, antisense oligonucleotides (ASOs), and RNA interference to target these expanded RNAs, small-molecule approaches have distinct advantages ^{7,14}. Small molecules can preferentially target toxic repeat RNAs, efficiently pass the blood-brain barrier, and have lower immunogenicity than conventional therapeutic modalities ¹⁵. Potential candidate molecules have been discovered as well as repurposed to target the toxic expanded RNA repeats associated with several REDs, including r(CAG)_{exp} in HD¹⁶⁻¹⁸, r(CGG)_{exp} in FXTAS ¹⁹⁻²³, and r(CUG)_{exp} in DM1 ²⁴⁻²⁶. Developing novel

small molecules is often a time-consuming procedure with considerable safety challenges. Therefore, drug repurposing offers an appealing alternative by utilizing previously licensed drugs, allowing for a more rapid and safer approach to discovering potential treatment strategies ^{27,28}.

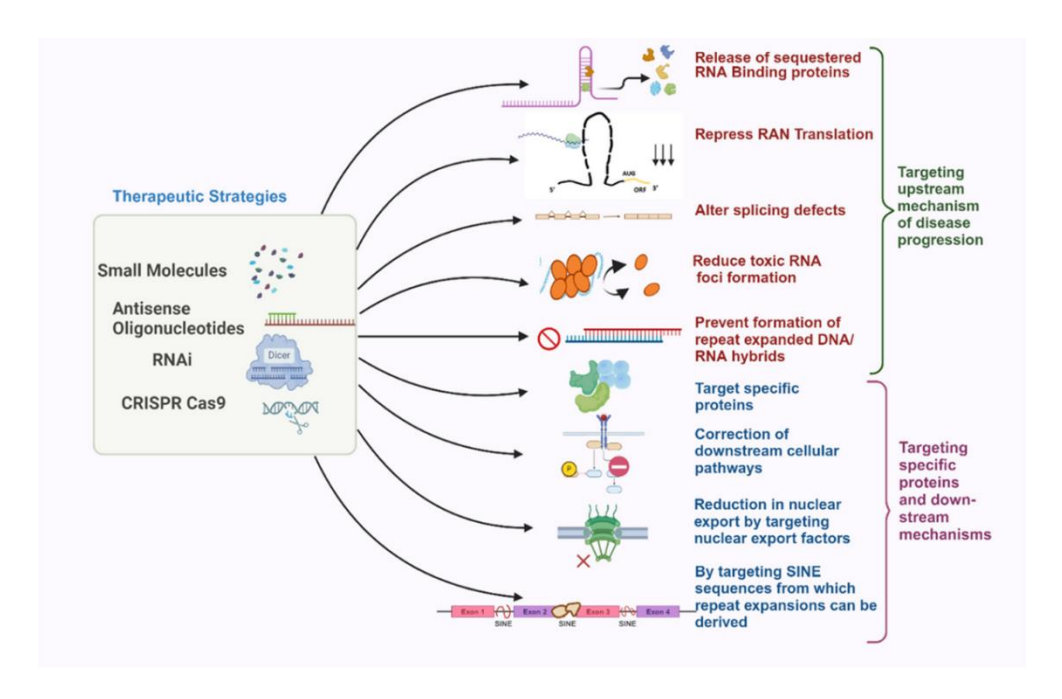


Figure 1.3 Represents the Possible Therapeutic Strategies against FXTAS 13

1.4 Rationale for Selecting Small molecule based therapeutics

Several studies have indicated that small molecules, particularly Non-Steroidal Anti-Inflammatory Drugs (NSAIDs), hold promise as a therapeutic strategy in various neurological diseases by modulating neuroinflammation and its downstream effects ^{29,30}. Additionally, previous studies have revealed that small molecules with planar structures tend to have a higher binding affinity towards the toxic RNA loops, a key structural feature implicated in RNA-mediated REDs ²⁰⁻²². Building on these studies, we chose Celecoxib as our molecule of interest for treating FXTAS, given its planar structure and demonstrated efficacy in various

neurological disorders ³¹⁻³³. Herein, we aimed to explore the neuroprotective potential of celecoxib in FXTAS, leveraging its anti-inflammatory property, as recent research has indicated the involvement of toxic r(CGG)_{exp} RNAs and FMR1PolyG (Fragile X Messenger Ribonucleoprotein 1) proteins in activating neuroinflammatory pathways and their downstream process that further accelerate the disease progression ³⁴⁻³⁸.

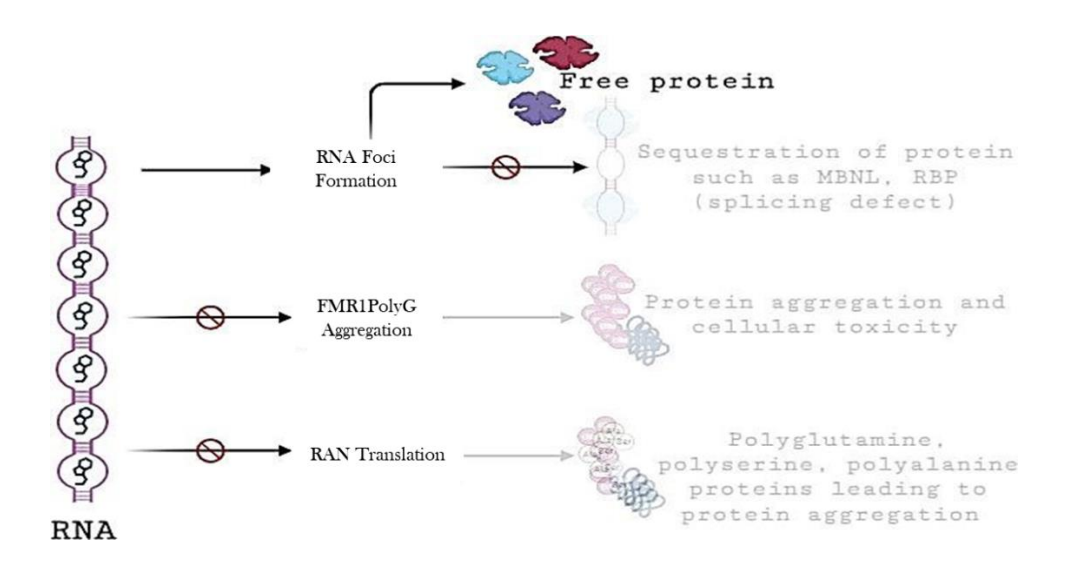


Figure 1.4 Represents Therapeutic development using small molecules ¹⁹.

1.5 Repositioning of Celecoxib FXTAS therapy

Celecoxib is a selective cyclooxygenase-2 (COX-2) inhibitor primarily known for its effective analgesic, anti-inflammatory, and antipyretic properties, offering the advantage of reduced gastrointestinal side effects compared to non-selective NSAIDs. Its versatility makes it valuable for managing osteoarthritis, rheumatoid arthritis, dysmenorrhea, and acute pain while improving patient tolerability. Its favorable pharmacokinetic

properties, proven through years of clinical use, position it as a potential candidate for repurposing ^{39 40}. Recent research has demonstrated the neuroprotective potential of Celecoxib, primarily by attenuating neuroinflammation in various neurological disorders ^{29,41,42,43}. Additionally, Celecoxib has been reported to cross the blood-brain barrier ^{29,44}, further supporting its potential for therapeutic repurposing in the treatment of neurodegenerative diseases such as FXTAS.

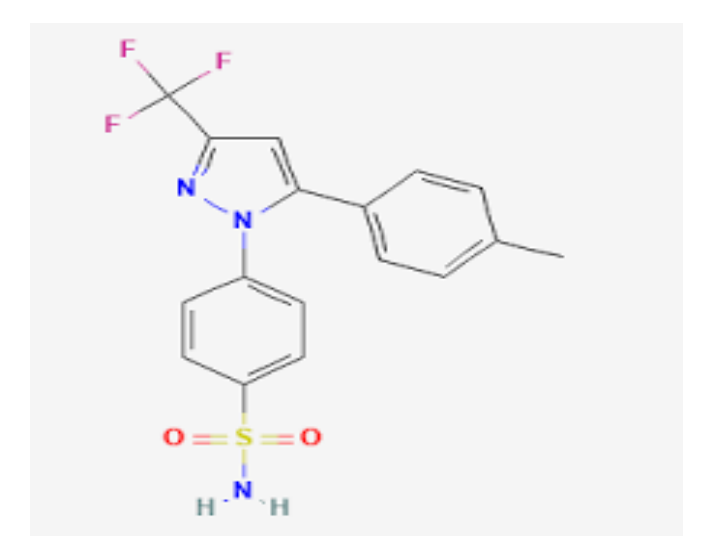


Figure 1.5 Represents the structure of Celecoxib. (PubChem CID: 2662)

1.6 Drosophila as a model for neurodegenerative disorders

Drosophila melanogaster, commonly known as fruit fly, is a holometabolous arthropod that becomes an invaluable model for studying the molecular underpinnings of repeat expansion disorders. Being an extensively studied model system for genetics and developmental biology for decades, the *Drosophila* genome sequence has shown that 77% of human diseases causing genes are preserved in the fly.

Drosophila melanogaster has been the most common animal model in genetic research for over many decades. Interestingly, despite its tiny size and seemingly distant relation to humans, these tiny animals share many genetic similarities with us, making it an excellent model organism for studying various genetic phenomena, including repeat expansion disorders ^{75,77}. Here's how *Drosophila* can be used to study repeat expansion disorders:

<u>Conserved Genetic Pathways</u>: Many of the genetic pathways involved in fundamental biological processes are conserved between *Drosophila* and humans. This includes pathways related to DNA replication, repair, and gene expression regulation, which are crucial in understanding repeat expansion disorders. This provides a controlled platform to dissect the mechanisms driving disease progression.

<u>Genetic Manipulation</u>: It offers powerful genetic manipulation techniques. Researchers can easily create transgenic flies carrying expanded repeat sequences associated with specific disorders. By introducing these repeats into Drosophila, scientists can study the effects of repeat expansion on gene expression, protein aggregation, and cellular toxicity.

<u>Behavioral Studies</u>: It exhibits complex behaviors that can be easily observed and quantified in the laboratory. Locomotion defects, learning and memory impairments, and other measurable behaviors can be observed and analyzed in a short time span, allowing researchers to link molecular changes with functional outcomes.

<u>High Throughput Screening</u>: It allows for high throughput genetic and pharmacological screens. Researchers can quickly screen large numbers of flies for modifiers of repeat expansion phenotypes. This approach can identify potential therapeutic targets or drugs that alleviate the symptoms associated with repeat expansion disorders.

<u>Neurodegeneration Models</u>: Several repeat expansion disorders, such as FXTAS, are characterized by progressive neurodegeneration. *Drosophila* models of these disorders recapitulate key features of neurodegeneration, including neuronal loss, toxic protein aggregation, and associated downstream mechanisms. Studying these tiny models can uncover molecular mechanisms underlying neurodegeneration and identify potential interventions.

In summary, *Drosophila melanogaster* offers a cost-effective, genetically tractable, and biologically relevant system to explore the complex landscape of repeat expansion disorders. Its contributions extend beyond disease modeling and thereby helping to unravel basic biological processes such as cell death, development, proliferation, and migration, all of which are closely tied to human health and disease ^{75,77}.

Complex behaviors of these tiny animals also include circadian rhythms, memory and learning, sleep, and aggression. Studies have shown that some of these once believed to be exclusive in humans also have genetic roots in other species.

Drosophila melanogaster mimics the cellular environment associated with genetic versions of the diseases utilizing transgenic techniques, while offering the convenience of small size, small genome size, low chromosome number, quick generation time, giant salivary gland chromosomes, and the capacity to produce a huge number of flies at a relatively low cost and time.

Drosophila melanogaster, or the fruit fly, has been a key model in genetics and developmental biology for many years because it is easy to work with in the lab. Studies in fruit flies have helped scientists discover many important genes and processes that are also found in other animals, including humans. In fact, many of the genes that play a role in human

development were first found in fruit flies, showing how useful this tiny insect is for understanding how living things grow and develop ^{75,77}.

1.7 The Drosophila genome

The haploid genome of *Drosophila* composed of approximately 170,000 kilobases of DNA, housing around 13,600 genes, making it roughly 5% of the size of the human genome. Its genetic material is organized into four chromosomes: chromosome 1 represents the X chromosome, while chromosomes 2 through 4 are autosomes. In Drosophila, sex determination follows the XY system, where females possess two X chromosomes (XX) and males have one X and one Y chromosome (XY). The ratio of X chromosomes to autosomes (the X:A ratio) governs the determination of sex.

Classification of *Drosophila melanogaster*

Table 1. Classification of Drosophila melanogaster

Kingdom	Animalia
Phylum	Arthropoda
Class	Insecta
Order	Diptera
Family	Drosophilidae
Genes	Drosophila
Species	melanogaster

1.8 Life Cycle of *Drosophila*

Drosophila melanogaster, or the fruit fly, has a fast and efficient life cycle. When grown on the proper dietary conditions, it takes just about 10 days to

develop from a fertilized egg into an adult fly. Female flies are extremely fertile and can produce up to 3,000 offspring during their lifetime. Fertilization usually happens as the egg is being laid. Each egg is about 1 mm long and contains enough yolk to support early development.

The embryo grows quickly and hatches within 24 hours into a small, worm-like larva whose main job is to feed. Over the next 2 days, the larva molts twice, growing into second and then third instar stages. Three days after its second molt, the third instar larva stops feeding and crawls out of the food to begin pupariation, forming a protective pupal case.

Inside this case, the larva undergoes metamorphosis over 4 days. Most larval tissues break down, and adult structures form, eventually resulting in a fully developed adult fly.

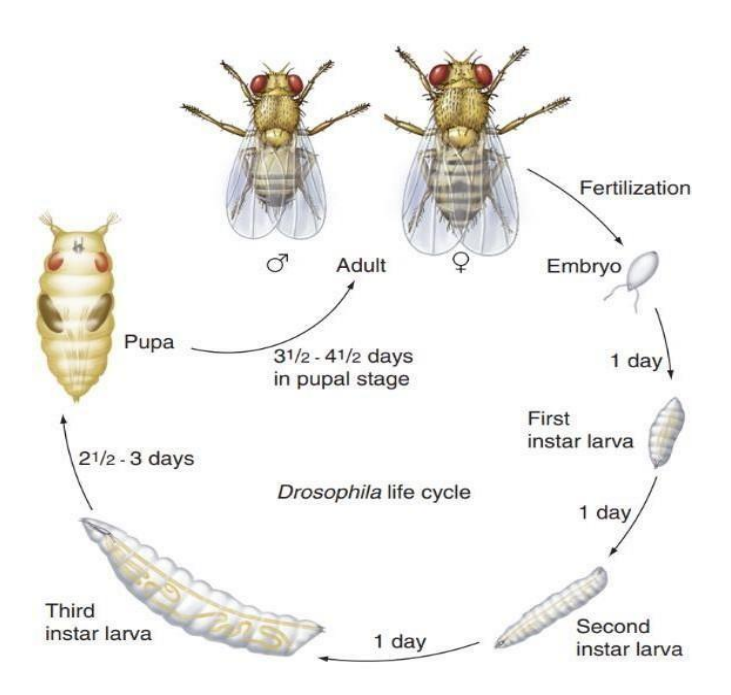


Figure 1.6 Life cycle of *Drosophila melanogaster* (Figure adapted from T.H. Morgan 1910)

Different Stages in the life cycle of *Drosophila melanogaster* –

Egg Stage: The life cycle of *Drosophila melanogaster* begins when fertilized eggs are laid by mated females. Each egg measures approximately 0.5 mm in length and is enveloped by two distinct layers: an inner vitelline membrane and an outer, rigid chorion, which displays a characteristic hexagonal pattern and provides structural protection. The anterior end of the egg features two respiratory filaments (spiracles) and a micropyle, a specialized opening that facilitates sperm entry during fertilization. Upon sperm entry through the micropyle, the completion of maternal meiotic divisions results in the formation of the female pronucleus. The male and female pronuclei align side-by-side, subsequently fusing to form the diploid zygotic nucleus. This zygote undergoes synchronous nuclear divisions, initiating the early stages of embryogenesis. The complete development of the embryo occurs within approximately 24 hours post-fertilization.



Figure 1.7 *Drosophila* egg (Adapted from T.H. Morgan 1910).

<u>Larval Stages</u>: Following embryogenesis, a wormlike larva hatches that is particular for feeding and grows dramatically. They voraciously feed and grow. This is commonly known as the mobile phase. The larvae show three growth stages: 1st instar, 2nd instar and 3rd instar. 24 and 48 hours post hatching, the larva moults produce 2nd and 3rd instar larvae. The 3rd instar larvae complete its growth after 3 daysof 2nd molt. Pulses of ecdysone which is a steroid molting hormone controls the timing of each larval molt and pupation.

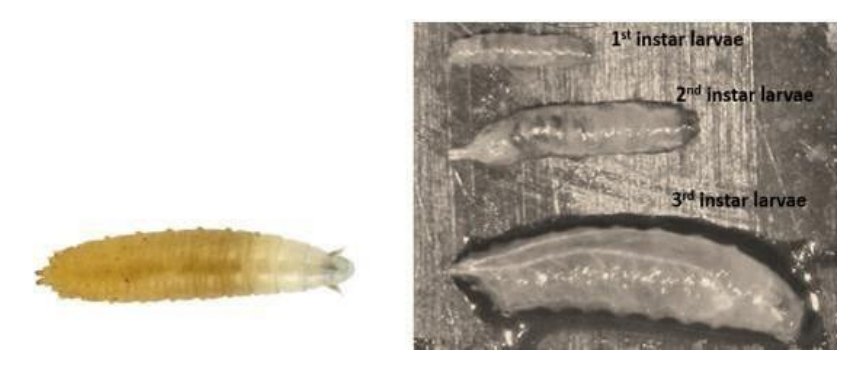


Figure 1.8 Drosophila larvae (Adapted from T.H. Morgan 1910).

<u>Pupa</u>: Larval stages are followed by pupa. This is also known as the static phase. Pupa consists of three stages – pre-pupal stage, mid-pupal stage, and late pupal stage. Once, under the pupal case, the larvae undergo metamorphosis. On getting pupate, they creep from the culture medium and adhere to some dry place, such as at the side of the bottle.



Figure 1.9 *Drosophila* pupa (Adapted from T.H. Morgan 1910).

<u>Adult</u>: At the end of the metamorphosis, the adult emerges from the pupal case through eclosion, its wings expand, and the entire exoskeleton hardens and becomes pigmented. Then adult fly forms with three predominant body parts- Head, thorax, and abdomen.

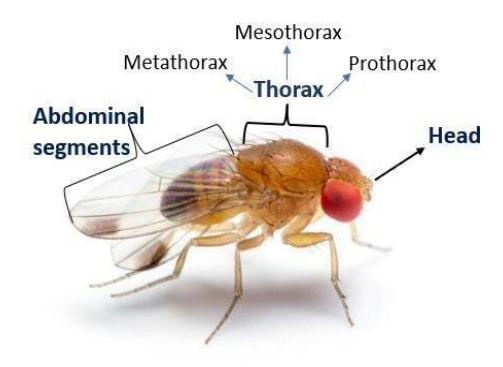


Figure 1.10 Adult *Drosophila melanogaster* (Adapted from T.H. Morgan 1910).

<u>Identification of male and female *Drosophila melanogaster*</u>: Female flies are larger than the male. Tip of the abdomen is pointed in the female, while males have a round abdomen tip. The color of the last two segments of the abdomen is darker in males as compared to the females. Females have 7 abdominal segments, whilethe males have 6 abdominal segments. A group of bristles called sex combs are present on the 3rd tarsal segments of the first pair of legs in male *drosophila*. The ovipositor of the female is pointed, while the clasper of the male is darkblack and circular.

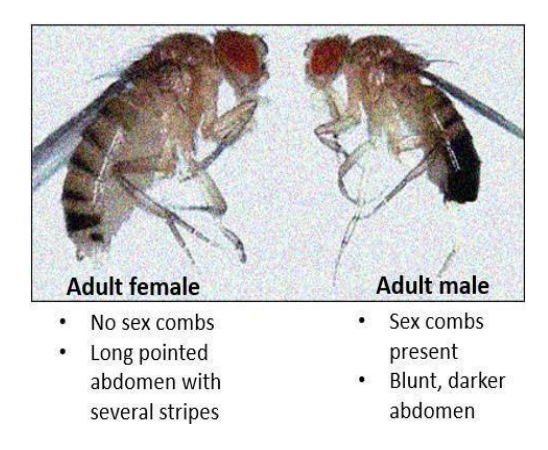


Figure 1.11 Male and female adult flies (Adapted from T.H. Morgan 1910).

Chapter 2

Literature Review and Hypothesis Framing

Repeat Expansion Disorders (REDs) are a group of genetically distinct yet mechanistically convergent conditions driven by the expansion of short nucleotide repeats in specific genomic regions. These repeats—ranging from trinucleotides to hexanucleotides and beyond—disrupt gene function through multiple pathways, often leading to severe, progressive, and largely untreatable diseases. REDs include Huntington's Disease (HD), Amyotrophic Lateral Sclerosis (ALS), Myotonic Dystrophies (DM1, DM2), Fragile X-associated disorders, and various Spinocerebellar Ataxias (SCAs). While many primarily affect the central nervous system, emerging studies underscore systemic effects, including endocrine, immune, and metabolic reinforcing disturbances, the complexity of their pathophysiology ^{2,3}. Fragile X-associated Tremor/Ataxia Syndrome (FXTAS) is a late-onset RED resulting from a premutation (55-200 CGG repeats) in the 5' untranslated region (UTR) of the FMR1 gene. Unlike full mutations that silence the gene and cause Fragile X Syndrome (FXS), FXTAS retains transcriptional activity, giving rise to pathologic RNA molecules and noncanonical peptides through Repeat-Associated Non-AUG (RAN) translation. These expanded RNAs fold into secondary structures, sequestering RNA-binding proteins (RBPs) critical for splicing and RNA regulation, such as DGCR8 and hnRNPA2/B1. Simultaneously, RAN-translated peptides like FMRpolyG accumulate and form inclusions, triggering mitochondrial dysfunction, neuroinflammation, and cellular apoptosis ^{4,5}. Current therapeutic efforts are increasingly focused on targeting the toxic RNA species. While antisense oligonucleotides (ASOs) and RNA-editing technologies offer precision, small molecules remain attractive for their blood-brain barrier permeability and oral bioavailability. Repurposing FDA-approved drugs shortens development timelines and enhances clinical translatability. Among potential candidates, Celecoxib, a COX-2-selective Non-Steroidal Anti-Inflammatory Drug (NSAID), has shown neuroprotective properties in other neurodegenerative models. Its ability to attenuate microglial activation, suppress oxidative stress, and cross the blood-brain barrier makes it a compelling molecule for FXTAS. Furthermore, Celecoxib's planar aromatic structure suggests potential for direct interaction with structured CGG repeat RNAs ^{29,30,34-38}. These attributes position it as a strong candidate in the expanding search for RNA-targeted therapeutics in REDs.

Fragile X-associated Tremor/Ataxia Syndrome (FXTAS) is a progressive neurodegenerative disorder caused by a premutation CGG-repeat expansion (55–200 repeats) in the 5' UTR of the FMR1 gene. Despite increasing recognition of RNA toxicity and repeat-associated non-AUG (RAN) translation as central drivers of FXTAS pathogenesis, effective disease-modifying therapies remain unavailable. The expanded CGGrepeat RNA forms abnormal secondary structures that sequester RNAbinding proteins and undergo RAN translation to produce toxic polyglycine and polyalanine peptides, leading to neuronal dysfunction through mechanisms such as mitochondrial impairment, RNA splicing defects, and neuroinflammation. Recent studies underscore the importance of targeting the CGG-repeat RNA and its downstream toxic effects as a viable therapeutic strategy. However, most RNA-targeting approaches face delivery challenges or have not advanced clinically. Small molecules such as non-steroidal anti-inflammatory drugs (NSAIDs) show promise due to their ability to cross the blood-brain barrier and mitigate inflammation. Among them, Celecoxib, a selective COX-2 inhibitor with a favorable safety and pharmacokinetic profile, has shown neuroprotective effects in other neurodegenerative diseases but remains unexplored in the context of FXTAS. Celecoxib mitigates neurodegeneration in FXTAS by targeting key pathogenic mechanisms such as RNA-induced neuroinflammation, oxidative stress, and mitochondrial dysfunction. Through its planar structure and ability to cross the blood-brain barrier, Celecoxib is hypothesized to reduce the toxic consequences of CGG-repeat RNA and associated RAN translation products, thereby improving cellular homeostasis and neuronal survival.

Chapter 3

Materials, Methods, and Instrumentation

3.1 Materials

NaCl, KCl, MgCl₂, K₂HPO₄, KH₂PO₄, NaH₂PO₄, Na₂HPO₄, NaOH, HCl, Tris-base, EDTA, DMSO, APS, TEMED, Acrylamide, Bis-Acrylamide, ethanol, isopropanol, 2-butanol, methanol, urea, Triton-X 100 and others, were sourced from Sigma- Aldrich Chemicals Ltd., based in St. Louis, Missouri, USA, and Sisco Research Laboratories Pvt. Ltd. in Mumbai, India. The dNTPs and rNTPs used for PCR and in vitro transcription reactions were also obtained from Sigma-Aldrich Chemicals Ltd. Additional materials such as Agarose, Luria broth, Luria agar, GC agar, and antibiotics like ampicillin, chloramphenicol, Taq polymerase, and others were procured from Himedia Laboratories in India. Standard plastic wares were supplied by Tarsons Products Pvt. Ltd. from Kolkata, India, while glasswares were sourced from Borosil.

For the cell culture experiments, growth media DMEM (Dulbecco's Modified Eagle Medium), FBS (Fetal bovine serum), PBS (Phosphate buffer saline), and ABAM (Antibiotic solution) were used from Gibco. Tissue culture plates and plasticware were obtained from Thermo Fisher and Tarsons. Anti-PolyG and Anti-β-actin antibodies were procured from Sigma-Aldrich and Santa Cruz Biotechnology. Lipofectamine 3000 was obtained from Invitrogen-Thermo Fisher. Calf thymus DNA (CT-DNA) was purchased from Sigma Aldrich Chemicals Ltd. Celecoxib was sourced from Sigma. Mitosox Mitochondrial Superoxide indicator and Tetramethylrhodamine E, methyl ester, and perchlorate were sourced from Thermo Scientific. The DAPI used was purchased from CST USA.

3.2 Sample preparation and Instrumentation

3.2.1 RNA synthesis and purification

RNA sequences, including different (CGG)_{exp} RNAs, a library of 11 RNA sequences containing 1 × 1 internal nucleotide motifs, (CAGx6), (CUGx6), (CCGx6), and (AUx6), were synthesized by runoff transcription (In vitro transcription) method using synthetic DNA template for various biophysical studies and gel-based assays. Briefly, synthetic DNA oligos, either amplified by PCR or cloned in a plasmid, were transcribed using T7 RNA polymerase, and then the transcribed products were purified by PD10 Column ^{20,45,46}.

3.2.2 Expression and purification of DGCR8

E. coli cells expressing the DGCR8 RNA-binding domain via a pENTR/D-TOPO vector were cultured in LB with 50 μ g/mL kanamycin at 37 °C. At OD600 = 0.8, protein expression was induced with 0.5 mM IPTG, followed by 4 h incubation at 37 °C. Cells were harvested, resuspended in lysis buffer (50 mM Tris-HCl, 50 mM NaCl, 20 mM imidazole, 1 mM PMSF), and lysed by sonication. After centrifugation (14,000 rpm, 45 min, 4 °C), the supernatant was applied to Ni-NTA resin pre-equilibrated with lysis buffer. The resin was washed with buffer containing 0.1% Triton X-100, and the protein was eluted using 50 mM Tris-HCl (pH 8.0), 50 mM NaCl, and 200 mM imidazole. Eluted protein was aliquoted and stored at -80 °C 47

3.2.3 Fluorescence Titration Assay

Fluorescence binding assays were carried out at room temperature (25 °C) using Corning half-area 96-well black plates. A Synergy H1 multi-mode

microplate reader was used to record the measurements following the assay. Various r(CGG)_{exp} RNAs, RNA controls (5'CNG/3'GNC), AU duplex pairs, G-quadruplex DNAs (C-myc, HRAS-1, HRAS-2, Bcl-2), and CT-DNA were used at a final concentration of 40.0 µM and serially diluted, with the final well serving as a blank (without RNA). The excitation and emission wavelengths for Celecoxib were set at 264 and 368 nm, respectively. Drug molecules were added at a constant concentration of 2.0 nm across all wells to maintain uniformity. SigmaPlot 15.0 software (Systat Software, Chicago, USA) was used for data analysis, according to the following equation ^{17,46,48}.

$$f = Bmax * abs(x) / Kd * abs(x)$$

 K_d is the equilibrium dissociation constant in this analysis, and B_{max} is the maximum number of binding sites.

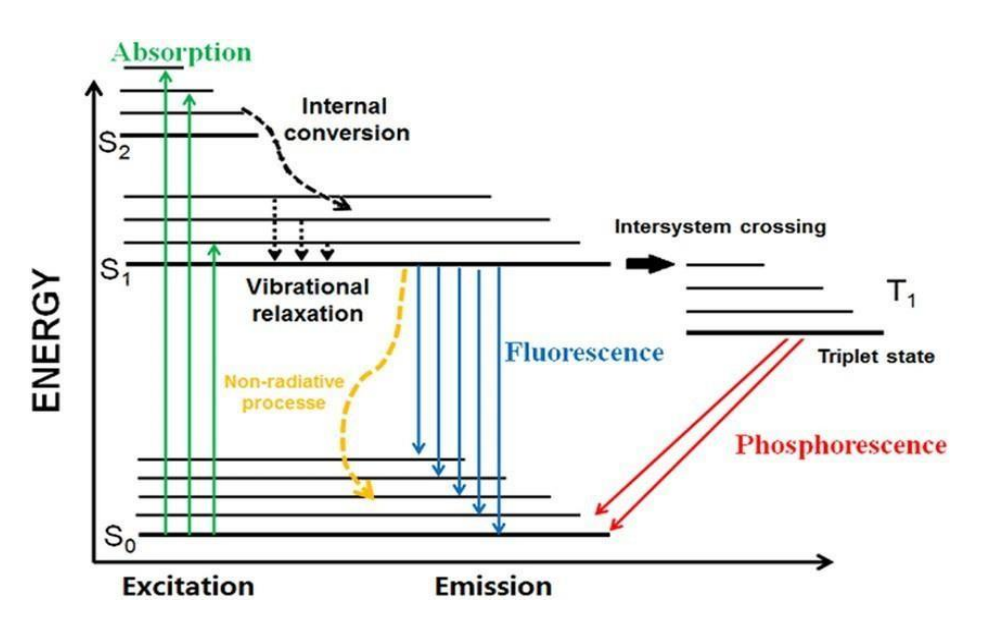


Figure 3.1 Jablonski diagram depicting fluorescence phenomenon where the molecule is excited to a higher energy state followed by the release of energy ⁴⁵.

3.2.4 Isothermal Titration Calorimetry (ITC) Experiment

All ITC experiments were conducted using a MicroCalTM iTC200 isothermal calorimeter (GE Healthcare) at 25 °C. To prepare the RNA solution, RNA was dissolved in 1X KPO4 buffer, then heated at 95 °C for 10 minutes, then gradually cooled down at RT to reanneal properly. For the ITC analysis, 5.0 µM of various r(CGG)_{exp} RNA sequences of varying repeat lengths, along with control RNAs, were loaded into the sample cell. Celecoxib, with concentrations ranging from 0.5 to 1.5 µM, was placed in the syringe. Both the RNA and the drug solution were degassed prior to their respective loading into the sample cell and syringe. Celecoxib was injected in 1.66 µL aliquots, starting with an initial 0.4 µL injection, followed by a 60-second equilibrium delay before each subsequent injection. A total of 22 injections were performed, with 120-second intervals between them. The reference power was maintained at 8 µcal/sec, and the sample was stirred at 1000 rpm throughout the titration. The heat of dilution was assessed by titrating Celecoxib at the same concentration in the buffer alone, without RNA. The resulting RNA-Celecoxib binding thermogram was analyzed using a two-site binding model to calculate the K_d , after accounting for the heat of dilution 46,49 .

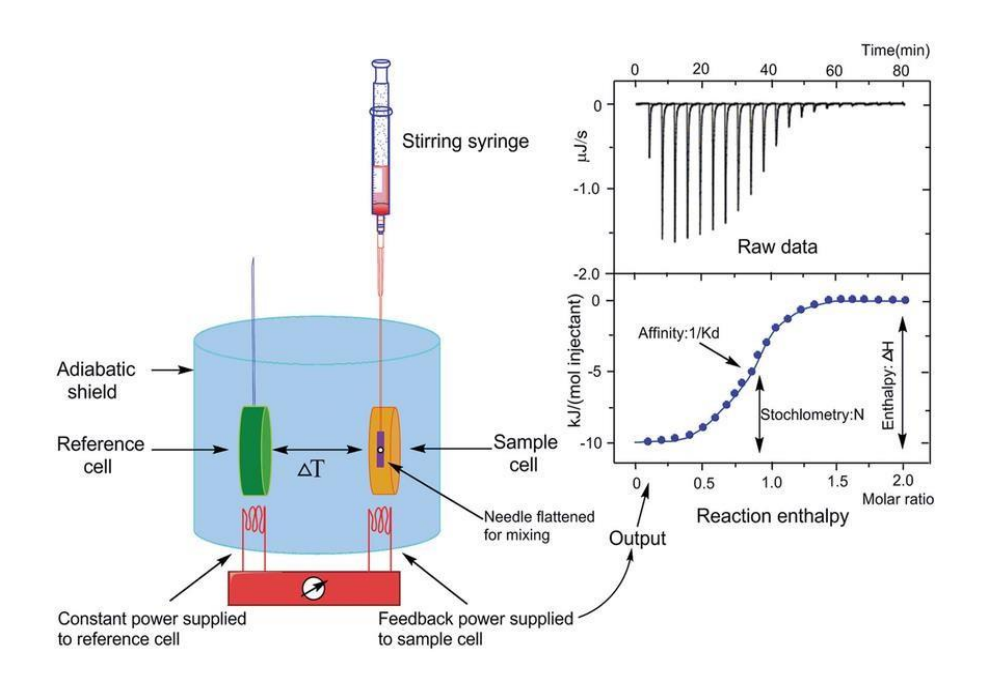


Figure 3.2 Schematic representation of the heat calorimeter in ITC instrument along with example of binding isotherm ⁴⁹.

3.2.5 Circular Dichroism (CD) Spectroscopy

A JASCO J-815 Spectropolarimeter was used for CD spectroscopy, equipped with a Peltier junction temperature controller to maintain the temperature at 298 K. A constant flow of dry nitrogen gas (5 L/min) was aimed into the cuvette chamber to avoid condensation on the outer surface of the cuvette. A cuvette with a 1 mm route length was used to record the measurements at 0.1 nm intervals. Three scans were averaged for each spectrum. RNA samples (CGG and AU) were maintained at a constant concentration of 10.0 μM while titrating increasing concentrations of Celecoxib. Prior to each measurement, a blank spectrum of the buffer (comprising 1X KPO4, KCl, and Milli-Q water) was obtained and subtracted from the sample's CD spectrum to ensure precision. SigmaPlot

15.0 was used to analyze the data, enabling a comprehensive interpretation of the interactions between RNA and Celecoxib ^{46,48,50}.

CD titration experiments were also conducted to analyze the RNA-protein interactions involving pathogenic r(CGGx99) and the purified DGCR8. A constant RNA concentration of 5.0 µM was maintained throughout the experiments, with protein concentrations increased linearly in separate titration assays for both proteins. Upon reaching the saturation in the spectra of the RNA-protein complex, Celecoxib is gradually added to the same solution. All the samples were prepared in 1× KPO₄ buffer. Prior to each measurement, a blank spectrum of the buffer alone was recorded and subtracted from the corresponding sample spectrum to eliminate any background signal contribution. CD spectra were collected over an appropriate wavelength range to monitor conformational changes upon protein binding. Data analysis, including spectral plotting and thermal transition analysis, was carried out using SigmaPlot 15.0 software (Systat Software, Chicago, IL, USA) ⁴⁷.

3.2.6 Electrophoretic Mobility Shift Assay

EMSA was performed using 10.0 μM of each RNA sample, which included different (CGG)_{exp} RNAs and AU duplex control. All the samples were prepared in a 1X KPO4 buffer containing 50.0 mM KCl and heated at 95 °C for 10 minutes, then gradually cooled down to room temperature (RT) to reanneal properly. Celecoxib was then added at the optimum concentration of 1 mM and then serially diluted to the rest of the tubes, keeping the last tube as a control (without Celecoxib) and further incubated for 30 minutes at RT. Following the incubation, 6X DNA loading dye was added to the samples and resolved on a 3% agarose gel in 1X Tris-Borate-EDTA (TBE) buffer. The pre-stained ethidium bromide (EtBr) gels

containing the samples were analyzed using ImageQuant LAS 4000 (GE Healthcare) 46,48.

Celecoxib's effect on the RNA-Protein interactions was also assessed using EMSA with a 3% agarose gel in 1× Tris-Borate-EDTA (TBE) buffer. RNA samples were prepared in Tris-Cl buffer containing 80.0 mM KCl. Varying concentrations of purified proteins and Celecoxib were added to the RNA samples and allowed to equilibrate for 20 minutes at 25 °C. For electrophoresis, 10 μL of each sample was loaded onto the gel, and the separation was carried out at 4 °C using a Bio-Rad Mini-Sub Cell GT Electrophoresis System. The electrophoresis was performed at a constant voltage of 72 V. Following electrophoresis, the bands were visualized by ethidium bromide, and images were captured using the Dual LED Blue/White Light Transilluminator system (Invitrogen, Thermo Fisher Scientific) ⁴⁷.

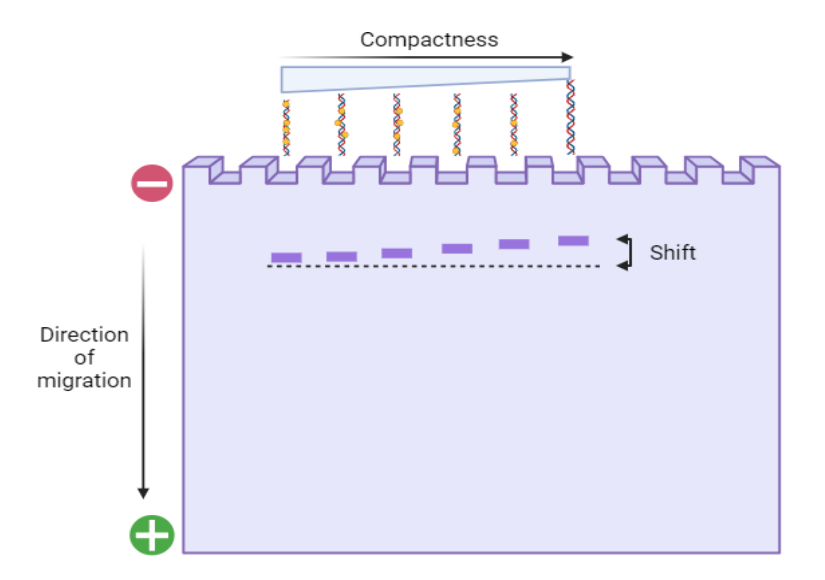


Figure 3.3 Schematic representation of Electrophoretic shift mobility ⁴⁶.

3.2.7 PCR Stop Assay

This experiment was carried out using the GGx1 (5'-GGAGAGGGUUUAAUCGGUACGAAAGUACGGAUUGGAU
CCGCAAGG-3') and GGx6 (5'-GGAGAGGGUUUAAUCGGCGGCGGCGGCGGCGGUACG

AAAGUACGGCGGCGGCGGCGGAUUGGAUCCGCAAGG-3') templates alongside the complementary sequence (GGCCGGATCCTAAGATACGACTCACTATAGGGAGAGGGTTTAA T). The master mix was prepared using 1X PCR reaction buffer (without MgCl₂), 4.0 mM MgCl₂, 10.0 pmol of oligonucleotides, 0.2 mM dNTPs, and 2.5 units of Taq polymerase. The final volume was adjusted to the desired amount (10 µl) using Milli-Q water. Then, Celecoxib was serially diluted, ranging from 0.0 µM to 100.0 µM. The reaction mixtures were then incubated in the thermocycler (HiMedia) in the following conditions: 30 seconds of initial denaturation at 95 °C, 35 cycles of denaturation at 92 °C for 20 seconds, 35 seconds of annealing at 56.5 °C, 1 minute of extension at 72 °C, a final extension at 72 °C, and finally held at 4 °C for infinity. After incubation, the products were mixed with 6X DNA loading dye and resolved on a 3% agarose gel pre-stained with EtBr. The gels were then visualized and analyzed using ImageQuant LAS 4000 (GE

Healthcare) 46.

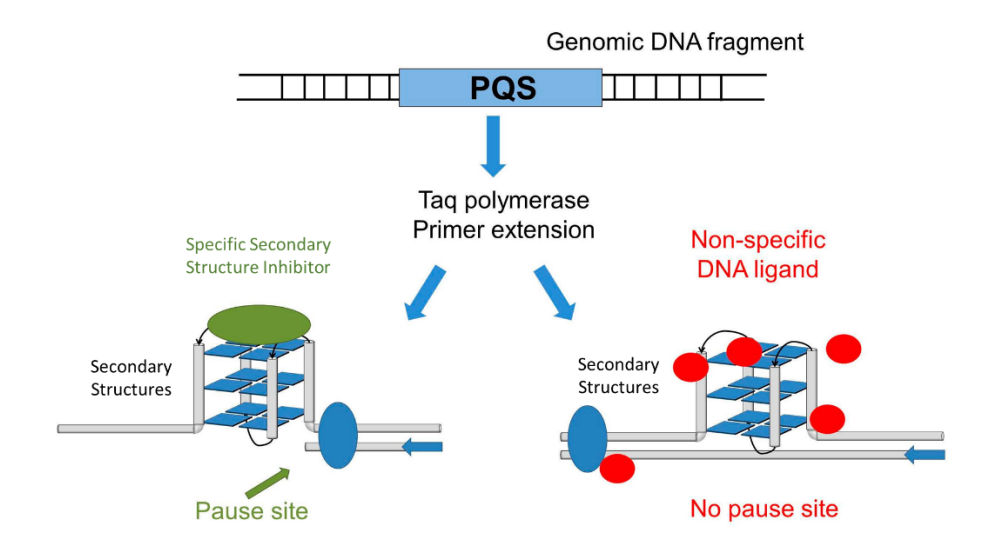


Figure 3.4 Schematic representation of PCR Stop assay ⁴⁶.

3.2.8 Molecular Docking

The three-dimensional (3D) crystal structure of duplex CGG RNA (PDB ID: 3JS2) ⁵¹ was used for the receptor preparation. Then, this macromolecule was prepared for docking using Autodock tools. Subsequently, the 3D structure of Celecoxib was downloaded from the PubChem Database in sdf format (PubChem CID ID: 2662). The ligand preparation was performed using Discovery Studio 3.5 (San Diego, Dassault Systèmes, USA), i.e., both the RNA and celecoxib files were prepared in PDBQT format. A grid box was designed to encompass the entire RNA structure, allowing Celecoxib to explore the entire conformational space. Following the grid box design, docking studies were conducted using Auto Dock Vina (The Scripps Research Institute, La Jolla, CA, USA), with all other parameters set to default values. The docking study results were mainly evaluated by examining the binding affinities of the ligand to the duplex CGG RNA. The best dock result was carried out to prepare the image in Discovery Studio 3.5.

3.2.9 Nuclear Magnetic Resonance (NMR) Spectroscopy

NMR studies for the r(CGG)₆ RNA were carried out using high-resolution Avance III 400 and 500 MHz spectrometers coupled with a broadband inverse probe and z-field gradients (BioSpin International AG, Switzerland). The samples were prepared in a 1X KPO4 buffer (10.0 mM phosphate, pH 7.2, 0.1 M KCl, 50.0 mM EDTA) containing 10% D₂O. For drug titration studies, RNA was incrementally added to the samples. A 7:1 ratio of H₂O to D₂O was used to lock the radio frequency throughout the titration. One-dimensional proton NMR spectra were acquired with 64,000 data points, an 8-second relaxation delay, and 64 to 128 scans at 298 K, achieving a digital resolution of 0.15 to 0.3 Hz/point. The acquired spectra were processed with baseline and phase corrections. Tuning, matching, and shimming were performed to ensure consistency across samples during titration. Data processing, integration, and analysis were conducted using Topspin version 3.5, with DSS (4,4-dimethyl-4-silapentane-1-sulfonic acid) as the NMR reference standard ⁴⁶.

3.2.10 Fluorescence spectroscopy

Proteins were dissolved in 5.0 mM potassium phosphate buffer (K₂HPO₄) at pH 6.8 to obtain working solutions. To investigate RNA-protein interactions, different amounts of FXTAS-related pathogenic and non-pathogenic RNA were incrementally added, maintaining a series of increasing nucleic acid-to-protein (N/P) ratios. Steady-state fluorescence measurements were conducted at 25 °C using a Fluorolog®-3 Spectrofluorometer (Horiba Scientific, Jobin Yvon, Palaiseau, France), with data acquisition controlled via FluorEssence software (Horiba Scientific, Jobin Yvon, Palaiseau, France). Emission spectra were collected

in the range of 330 to 500 nm with 1 nm steps and an integration time of 0.5 seconds, while excitation was set at 295 nm (λ exc). To ensure statistical validity, measurements were performed in triplicate at 120-second intervals. The resulting fluorescence data were analyzed using OriginPro software (© OriginLab Corporation) ⁴⁷.

3.2.11 Western blot analysis

HEK-293T cells cultured in a 12-well plate were transfected with 2.0 µg of CGGx99-EGFP and pcDNA-EGFP plasmids, and further treated with different concentrations of Celecoxib for 24 hours. After treatment, cell lysates were gathered using a RIPA lysis buffer containing Halt Protease Inhibitor Cocktail from Sigma. Following the Bradford assay, the proteins were separated using SDS PAGE at 80 V, then transferred onto a nitrocellulose membrane in a transfer buffer containing 20% methanol for 80 minutes at 4 °C. Blots were blocked for 3 hours in 5% Skimmed Milk (SM) in TBST (50 mM Tris, pH 7.4, 0.15 M NaCl, 0.05% Tween) and probed overnight at 4 °C with primary antibodies at a 1:1000 dilution in TBST. Anti-IgG conjugated with Horseradish Peroxidase (HRP) secondary antibodies were subsequently used at a 1:10,000 dilution prepared in TBST. The Luminata Crescendo Western HRP substrate was utilized for blot detection. The gel images were captured using the Gel Documentation System (Bio-print) and analyzed using ImageJ. The Blots were developed using the Luminata Crescendo Western HRP substrate, and images were captured using the Gel Documentation System (Bio-print). The data were subsequently analyzed using ImageJ software ⁴⁶.

3.2.12 Visualization of FMR1PolyG aggregation

COS-7 cells were seeded and grown in 12-well plates containing complete DMEM media till the cells became 80-90% confluent. To evaluate the impact of Celecoxib on FMR1PolyG-EGFP aggregates, transfection of two plasmid constructs, i.e., CGGx99-EGFP and pcDNA-EGFP, was carried out using Lipofectamine 3000 (Thermo Fisher Scientific) following the manufacturer's instructions. Four hours after transfection, the medium was replaced with fresh media containing different concentrations of Celecoxib. The cells were then incubated at 37 °C for 24 hours with 5% CO₂. Following the incubation, the cells were washed with PBS and fixed with 4% paraformaldehyde for 15 minutes. High-resolution images of protein aggregates were obtained using fluorescence confocal microscopy, and background noise in the images was minimized through processing. In each experiment, a total of 150 EGFP-positive transfected cells per well were manually examined to differentiate between cells with and without FMR1PolyG-EGFP aggregates. The data were subsequently analyzed using ImageJ software ⁴⁶.

3.2.13 Pre-mRNA alternative splicing analysis

To assess the potency of the drug in the context of restoring the pre-mRNA alternative splicing defects in an FXTAS cellular model, HEK-293T cells were cultured in 24-well plates as monolayers at 37 °C with 5% CO₂ in complete DMEM growth medium. On reaching 80–90% confluency, the cells were transfected with plasmid constructs containing CGGx99 repeats along with the Survival Motor Neuron 2 (SMN2) and B-cell lymphoma x (Bcl-x) mini-genes. For the control conditions, the mini-genes SMN2 and Bcl-x were co-transfected with a plasmid that did not contain the CGG repeat in the 5' UTR. Additionally, the CGG repeat plasmid was co-transfected with the mini-genes for cardiac Troponin T (cTnT) exon 5 and Insulin Receptor (IR), as their pre-mRNA splicing is not affected by

Sam68 and DGCR8. After 4 hours of transfection, the transfection medium was replaced with a fresh medium containing different concentrations of Celecoxib. Cells were lysed after 24 hours of treatment, and total RNA was isolated using an RNA extraction kit (Invitrogen) following the manufacturer's instructions. Reverse transcription (RT-PCR) was then performed on the RNA samples using a cDNA synthesis kit from Bio-Rad. From the 500 ng of transcribed mRNA, 100 ng was used for Real-time polymerase chain reaction (RT-PCR), which was carried out with the following conditions: denaturation at 95 °C for 1 minute, annealing at 58 °C for 1 minute, extension at 72 °C for 2 minutes, and a final extension at 72 °C for 10 minutes, with 30–35 cycles. The RT-PCR products were mixed with 6X DNA loading dye and resolved on a 2% pre-stained EtBr agarose gel. The gels were then visualized and analyzed using ImageQuant LAS 4000 (GE Healthcare). The intensities of the splicing isoforms were quantified using ImageJ software ⁴⁶.

3.2.14 *Drosophila* stocks and dietary conditions

The transgenic fly lines expressing the EGFP (*UAS-EGFP*) and the mutant fly lines expressing the 90 PolyG repeats *UAS-(CGG)*₉₀-*EGFP* ⁵² were kind gifts from Prof. Abrar Ahmad Qurashi (University of Kashmir). The pan-neuronal driver line *Elav-GAL4* ⁵³ and the eye-specific driver lines that express in the eye-imaginal discs of the larvae and in the adult eye (*GMR-GAL4*) ⁵⁴ were kindly provided by Dr. Anand K. Tiwari (IAR Gandhinagar). The muscle-specific driver line *Mef2-GAL4* were kindly gifted by Dr. Dhananjay Chaturvedi (CCMB, Hyderabad). Males of all the transgenic lines used in the study were crossed with virgins of *Elav-GAL4*, and *GMR-GAL4* to drive their expression in the fly brain and eye, respectively ⁵⁵. The flies were reared on a standard cornmeal-agar diet at 25±1 °C, with consistent light-dark cycles and humidity ranging from 70%

to 80%. Celecoxib was mixed with the fly food at concentrations of 12.5 μM and 25.0 μM to rear experimental larvae or flies. Control groups were maintained under the same rearing conditions without the drug.

3.2.15 Larval Feeding Assay

A yeast paste containing FD&C Blue Dye No. 1 (Sigma Aldrich) and celecoxib at the specified concentrations was prepared and positioned at the center of a 100 mm × 10 mm petri dish layered with 3% (w/v) agar. For each experimental condition, two sets of ten third-instar larvae were introduced to the yeast paste and allowed to feed for 2 hours. Post-feeding, larvae were rinsed properly with distilled water (containing 0.7% NaCl) to remove any external dye residues and subsequently dried. The larvae were then homogenized in PBS, followed by centrifugation at 15,000 rpm for 15 minutes. The absorbance of the supernatant was measured at 625 nm to determine dye intake ⁵⁶.

3.2.16 Eye Phenotyping

3.2.16.1 Brightfield imaging

The rough eye phenotype of flies expressing CGG₉₀ and EGFP under *GMR-GAL4* regulation was examined. Flies were reared at 25 °C with a standard diet and food containing 12.5 μM and 25.0 μM of Celecoxib. The diseased flies were sorted on the 14th day after eclosion, and the eye's exterior was examined with a Leica S8Apo microscope. 30 flies were analyzed for each condition. The morphological changes in untreated and treated fly eyes were analyzed and quantified using the Flynotyper software (http://flynotyper.sourceforge.net) ⁵⁷. This software calculates a phenotypic score that depicts the extent of disorganization in the ommatidial arrangement within the fly's eye.

3.2.16.2 Confocal imaging

Diseased and EGFP-expressing flies were sorted and fixed in a slide containing mounting media. In *GMR-GAL4>UAS-(CGG)₉₀-EGFP* flies, FMRPolyG-EGFP protein aggregations were observed in the rough eye phenotype. The images were captured at 10X magnification using confocal microscopy, and the intensities of the aggregates were quantified using ImageJ software.

3.2.16.3 FE-SEM imagining

The Critical Point Drying (CPD) method was utilized to prepare *Drosophila* samples for high-magnification FE-SEM, adhering to the protocol described by Kimmel et al ⁵⁸. Whole flies were fixed for 2 hours in a solution containing 1% glutaraldehyde, 1% formaldehyde, and 1M sodium cacodylate buffer (pH 7.2). 0.2% Tween-20 (diluted in water) was added dropwise to the fixative to ensure proper penetration ⁵⁹. Following fixation, the samples were rinsed with water and dehydrated through a stepwise ethanol series. This included 12-hour treatments in 25%, 50%, and 75% ethanol, followed by two 12-hour incubations in 100% ethanol, all performed at room temperature. The dehydrated samples were then processed via CPD and sputter-coated for imaging.

3.2.17 Climbing Assay

The negative geotaxis or climbing assay was performed to assess the flies' locomotor abilities. For each experimental condition, two groups of approximately 15 flies were tested across six trials using a vertical column explicitly designed for the assay. The column measured 18 cm in length

and 2 cm in diameter. The column was gently tapped thrice to begin the test, prompting the flies to climb. The number of flies that successfully climbed beyond the 10.0 cm mark within a 30-second time frame and the number of flies that remained at the bottom were recorded ⁴⁶.

3.2.18 Flight assay

The flight assay was conducted using a cylindrical flight chamber measuring 45.0 cm in height and 7.0 cm in diameter. The interior surface was lined with a polyacrylamide sheet coated with a Tangle-Trap adhesive to serve as the landing substrate for flying insects. Vials containing approximately 15 flies from each experimental set were dropped through a funnel into the cylinder, and their flight capability was evaluated based on landing height. A minimum of 5 vials were examined for each experimental condition. Images of the landing surface were taken with a camera set on a track, and flight positions were evaluated using ImageJ software. Images were converted to grayscale, thresholds were applied, and particles were examined to determine fly positions. The x-coordinates were translated to landing heights, and the results were put into a spreadsheet ⁶⁰. Similar procedure was followed to measure the flight efficiencies of flies expressing (CGG)₉₀ in the muscles.

3.2.19 Larval crawling assay

The larval crawling assay was performed in a $100.0 \text{ mm} \times 10.0 \text{ mm}$ Petri dish with 3 % agar. A track measuring 2.0 mm wide, 30.0 mm long, and 5.0 mm deep was formed in the center of the dish using a previously described process. Each third-instar larva was given 2-3 minutes to settle in before being placed on the track. The larvae were then monitored for 30 seconds, and their total distance traveled was recorded. Each condition was

evaluated with 5 larvae in five independent experiments ^{46,56}. Similar procedure was followed to measure the flight efficiencies of flies expressing (CGG)₉₀ in the muscles.

3.2.20 Western blotting from *Drosophila*

For the western blot analysis, diseased flies were sorted, and the heads of 40 flies from each experimental group were dissected. Proteins were isolated from the brain of the flies treated with different concentrations of Celecoxib, as per the established protocol ⁶¹. The isolated protein concentrations were determined using the Bradford assay, and 50.0 µg of protein was loaded onto SDS-PAGE gels for separation. Subsequently, proteins were then transferred onto PVDF membranes, which were incubated overnight with primary antibodies against FMR1PolyG and EGFP (both obtained from Merck Millipore). Following incubation, an anti-IgG secondary antibody conjugated with horseradish peroxidase was added. Chemiluminescent signals were detected using the Luminata Crescendo Western HRP substrate (Merck Millipore) and visualized with the ImageQuant LAS 4000 system (GE Healthcare). Similar procedure was followed to isolate the protein from the muscles and to measure the FMR1PolyG and EGFP levels in the muscles.

3.2.21 Histology of larval tissue staining

Larval tissue staining was performed as previously described 62 . Larval brains were dissected in 1X PBS and fixed in 4% Paraformaldehyde in PBS at room temperature for 20 minutes. Then, for the PI staining, the fixed brain tissues were incubated with 1.0 μ g/ml PI (P4170; Sigma, St Louis, MO, USA) solution for 15 minutes at room temperature. For the Mitosox (Invitrogen, Thermo Fisher Scientific) staining, the fixed brain

tissues were incubated with $1.0\,\mu\text{M}$ Mitosox solution for $30\,\text{minutes}$ at room temperature. For the TMRM staining, the fixed brain tissues were incubated with $50.0\,\text{nM}$ TMRM (Invitrogen, Thermo Fisher Scientific) for $30\,\text{minutes}$ at room temperature 63 . Finally, the brains were washed three times in PBST for $10\,\text{minutes}$ and mounted in mounting media (FlourSave reagent, Merck Millipore). Images were acquired at $10X\,\text{magnification}$ using FV1200 MPE confocal microscopy. Image brightness and contrast were adjusted using FluoView FV1000 Software.

3.2.22 Eye Pigmentation Analysis

To assess the levels of red eye pigmentation, 40 fourteen-day-old flies were sorted from each experimental group, and their heads were dissected. After dissection, the heads were homogenized in 1.0 ml of methanol containing 0.1% HCl (for acidification). The supernatant was collected, and the pigment levels were determined by measuring its absorbance at 480 nm ⁶⁴.

3.2.23 Lifespan Analysis

Virgin flies were collected within 24 hours of hatching from synchronously laid eggs. Diseased flies were sorted into separate vials, with 30 flies per vial containing either control or experimental food. Celecoxib was incorporated into the experimental food to achieve a final concentration of 12.5 μM and 25.0 μM. Depending on the experimental group, flies were fed Celecoxib starting from different time points—Day 0, Day 1, and Day 7—to evaluate the efficacy of the drug at different stages of development. Dead flies were recorded every 3 days, and the flies were transferred to fresh food vials at the same interval, ensuring no anesthesia was used during transfers. The lifespan experiments were performed two

times independently. Lifespan data were subsequently analyzed using Prism statistical software 65,66 . Similarly, the lifespan of untreated and treated flies expressing (CGG) $_{90}$ in the muscles was measured.

3.2.24 Detection of ROS levels

To assess the steady-state levels of reactive oxygen species (ROS), 2, 7-dichlorofluorescein diacetate (DCF-DA) dye was employed. Following a 14-day treatment period, 20 fourteen-day-old flies were sorted from each experimental group. Further the heads were isolated and homogenized in 20 mM Tris buffer (pH 7.0). The resulting homogenate was subjected to centrifugation at 1600 × g for 10 minutes at 4 °C. The supernatant was collected and incubated with DCF-DA for one hour to allow for the oxidation of DCF-DA to its fluorescent form, 2, 7-dichlorofluorescein (DCF). Fluorescence intensity was subsequently measured using a multimode plate reader, with excitation and emission wavelengths set at 488 nm and 530 nm, respectively. An elevation in DCF fluorescence corresponds to an increase in ROS generation ^{67,68}. Similar procedure was followed to measure the ROS levels in the muscles.

3.2.25 Statistical Analysis

Statistical analyses and graphical representations were performed using GraphPad Prism software (version 9.5). Results were presented as the mean \pm standard error of the mean (SEM) or standard deviation (SD). A one-way ANOVA was conducted to assess the statistical significance across multiple groups, while a two-way ANOVA was applied for subgroup analyses. A P-value of <0.05 was considered indicative of statistical significance.

Chapter 4

Results and discussion

4.1 Primary screening of the molecules using the Fluorescence binding assay

Several studies have demonstrated that planar molecules exhibit high binding efficiency toward RNA motifs, particularly internal loops ^{20-22,46}. Fluorescence-based binding assay of Celecoxib was then performed with RNAs possessing various CGG repeats - r(CGGx2), r(CGGx3), r(CGGx4), r(CGGx20), r(CGGx40), r(CGGx60), and r(CGGx99) (Figure 1a, e and **Table S1**). Celecoxib has shown a progressively enhanced binding affinity, increasing many-fold with the increasing number of CGG repeats. In contrast, no significant binding was detected with r(CAGx6), r(CCGx6), r(CUGx6), and r(AUx6) duplex RNA, which further strengthens the notion of high affinity and selectivity of these compounds for CGG repeat RNA (Figure 4.1b, c, f, g and Table S1). Furthermore, Celecoxib showed no significant binding against different mismatch (5'CNG/3'GNC) RNA internal loops, G-quadruplex forming DNAs (c-Myc, HRAS-1, HRAS-2, Bcl2), and Calf Thymus (CT) duplex DNA (Figure 4.1d, h and Table S1). This primary fluorescence-based screening indicates the higher binding affinity and specificity of celecoxib towards r(CGG)_{exp} RNAs.

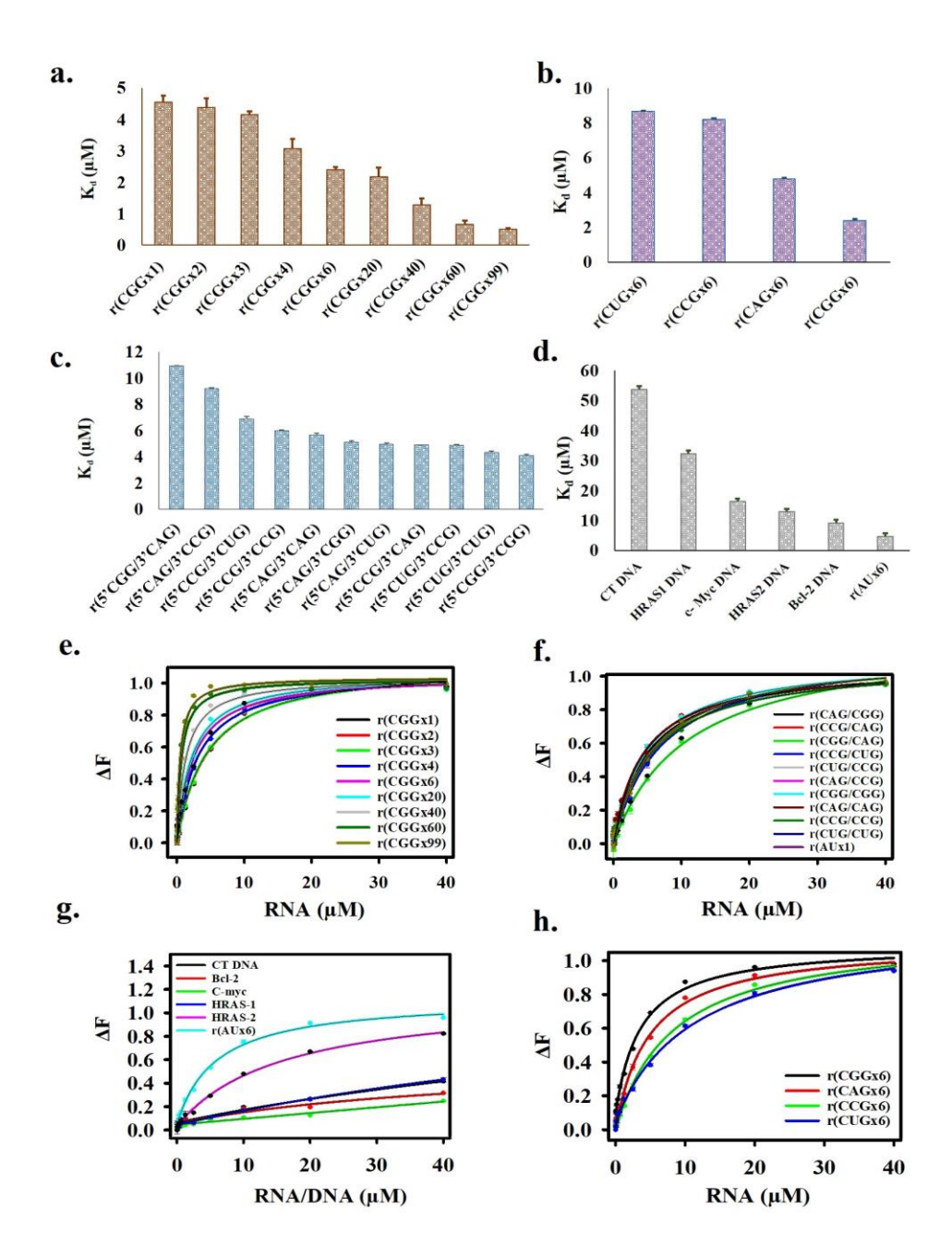


Figure 4.1 Fluorescence-based screening of Celecoxib's binding affinity to FXTAS-associated repeat structures. a. Bar graph represents K_d values of Celecoxib with different $r(CGG)_{exp}$ RNAs. b. Bar graph represents K_d values comparisons of Celecoxib with $r(CGG)_{exp}$ motif and control RNA motifs. c. Bar graph depicts K_d values of Celecoxib with different single mismatch (5'CNG/3'GNC) RNA internal loop. d. Bar graph depicts K_d values of Celecoxib with different DNA and RNA

controls. **e.** The plot represents a curve fitting for fluorescence titration assay of Celecoxib with $r(CGG)_{exp}$ motifs. **f.** The plot represents curves fitting for the fluorescence binding assay of Celecoxib with 1x1 internal loops. **g.** The plot represents the fluorescence titration assay curve fitting of different DNA and RNA controls. **h.** The binding plot illustrates K_d value comparisons of Celecoxib with $r(CGG)_{exp}$ motif and control RNA motifs.

4.2 Thermodynamic Analysis of Celecoxib Binding to CGG Repeat RNAs through Isothermal Titration Calorimetry

Following the fluorescence-based binding assay validation, Isothermal Calorimetry (ITC) was performed to Titration elucidate thermodynamic properties of the interaction between Celecoxib and r(CGG)_{exp} RNAs. This robust technique quantifies the heat exchanged (either released or absorbed) during automated titration, enabling the determination of binding affinity, stoichiometry, and key thermodynamic parameters 49 69 . A negative enthalpy change (ΔH) indicates an exothermic process, often associated with a stable and thermodynamically favorable interaction ^{20,70}. The calorimetric binding isotherm demonstrated that the binding of Celecoxib to r(CGG)_{exp} RNAs was exothermic, as evidenced by negative enthalpy changes, confirming the favorable thermodynamic profile of these interactions. The association constant (K_a) values of Celecoxib with r(CGGx6), r(CGGx20), r(CGGx40), r(CGGx60) and r(CGGx99) were 1.25×10^5 M⁻¹, 6.67×10^6 M⁻¹, 5.27×10^7 M⁻¹, 1.63×10^8 M⁻¹ and 5.89×10⁹ M⁻¹ respectively. Contrastingly, the interaction of Celecoxib with the control r(AUx6) duplex RNA exhibited significantly weaker binding, as indicated by a considerably lower K_a of 8.20×10³ M⁻¹ (Figure **4.2a-f and Table S2**). Notably, Celecoxib exhibited a much greater fold increase in binding affinity for r(CGG) repeat RNAs compared to control r(AUx6) duplex RNA. The binding affinity of Celecoxib for r(CGGx60) RNA was several orders of magnitude higher, underscoring its high specificity for $r(CGG)_{exp}$ RNAs over control RNA sequences. The exothermic nature of these interactions, characterized by negative enthalpy changes, suggests that binding is primarily driven by favorable interactions between the aromatic moieties of Celecoxib and the RNA bases, likely facilitated by π - π interactions ^{21,46,71}. These thermodynamic findings align with fluorescence titration data, further supporting Celecoxib's high affinity and specificity for $r(CGG)_{exp}$ RNAs. These findings highlight the potential of Celecoxib as a highly selective therapeutic candidate for disorders associated with CGG repeat expansions.

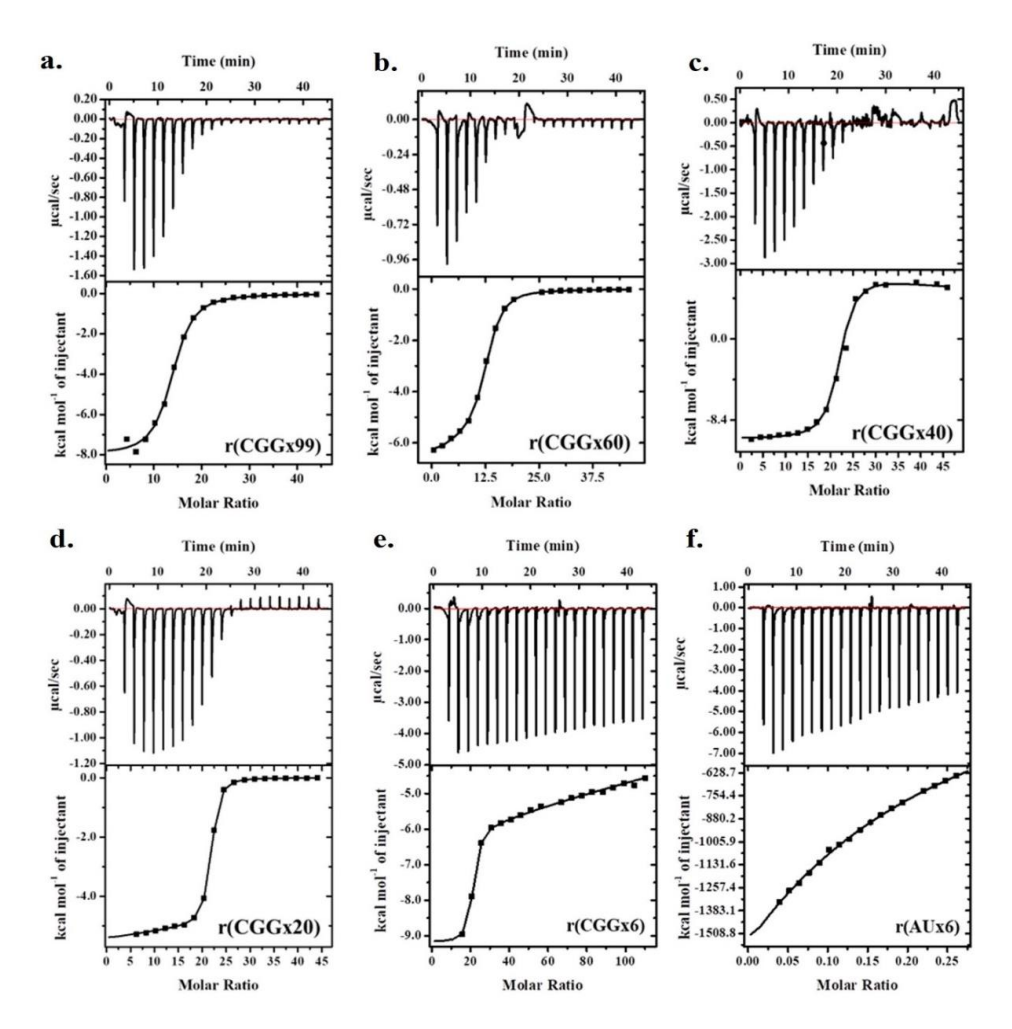


Figure 4.2 Isothermal calorimetry titrations of Celecoxib against different r(CGG)_{exp} and r(AUx6). Celecoxib with **a.** r(CGGx99), **b.** r(CGGx60), **c.** r(CGGx40), **d.** r(CGGx20), **e.** r(CGGx6), **f.** r(AUx6). Normalized Isothermograms, because of titrated peptides, suggest favorable binding interactions with the CGG RNAs. A solid line curve represents the two-mode binding best fitting.

4.3 Validation of Celecoxib-Induced Conformational Changes in CGG Repeat RNA Using Circular Dichroism Assay

CD spectroscopy is a highly potent technique for detecting mere conformational changes in nucleic acid structures induced by ligand

interactions ²², ⁴⁶. To assess structural changes in target CGG RNAs, CD spectra were recorded with increasing Celecoxib concentrations. The CD spectrum of r(CGG)_{exp} has shown a typical characteristic positive peak around 265-270 nm and a negative peak near 215-220 nm, which resembles the double-stranded A-type RNA 72. The gradual addition of Celecoxib to the r(CGG)_{exp} solution, up to a D/N ratio of 7.0, resulted in a significant decrease in ellipticity (hypochromic shift) and a bathochromic (red) shift in the negative peak of all the r(CGG)_{exp} RNAs. Along with that, a hypochromic and bathochromic shift is observed in the positive peak of RNAs comprising higher CGG repeats, thereby indicating the higher binding affinity of the drug towards higher pathogenic CGG repeats (Figure 4.3a-e). A decrease in positive and negative peaks indicates weak van der Waals interactions via π - π stacking between small molecules and target RNAs ²⁰. In contrast, no significant peak shifts were seen in the r(AUx6) duplex RNA (Figure 4.3f) and other RNA controls, even at higher Celecoxib concentrations. All r(CGG)_{exp} samples demonstrated pronounced topological changes upon Celecoxib binding. Significant conformational changes in the r(CGG)_{exp} RNAs, compared to the AU control, highlight Celecoxib's strong selectivity and specificity for G-rich RNA motifs.

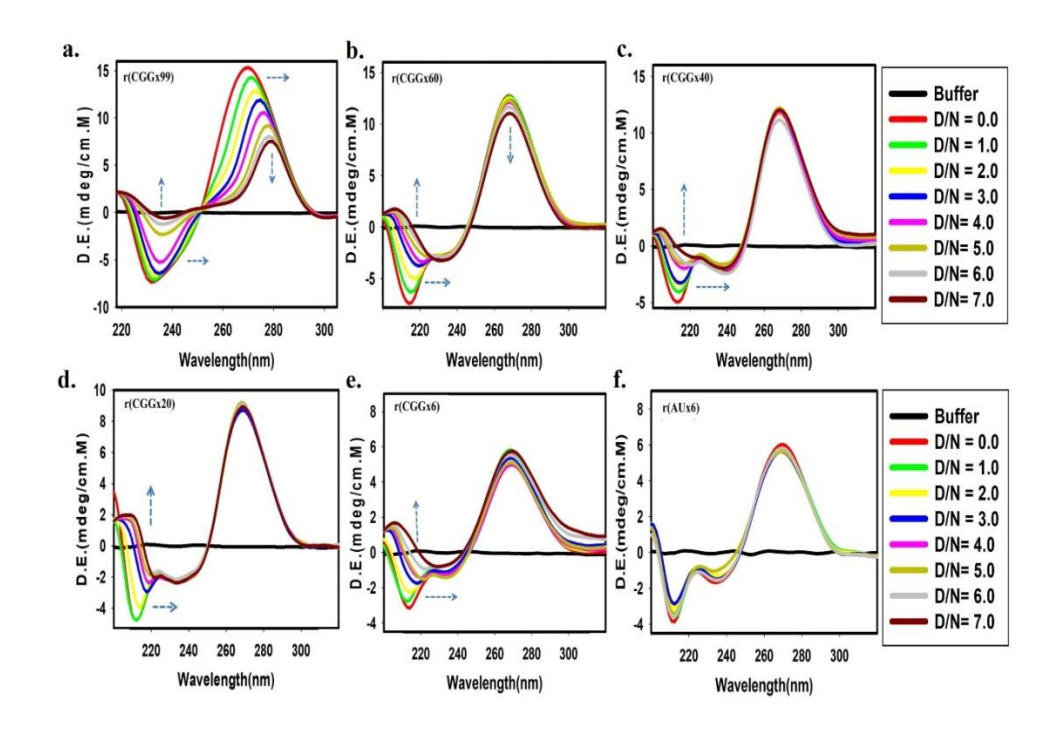


Figure 4.3 CD spectroscopy titration of $r(CCG)_{exp}$ and r(AUx6) duplex RNA in the presence of Celecoxib. CD spectroscopy of with a. r(CGGx99), b. r(CGGx60), c. r(CGGx40), d. r(CGGx20), e. r(CGGx6), f. r(AUx6) duplex control RNA.

4.4 Electrophoretic Mobility Shift Assay and PCR-Based Inhibition of r(CGG) Repeat Expansions by Celecoxib

Gel-based assays were employed to affirm the interaction between Celecoxib and r(CGG)_{exp}, including EMSA and PCR stop assay ⁴⁶. The EMSA showed an observable change in band mobility for all r(CGG)_{exp} samples when Celecoxib concentrations increased to 1.0 mM. However, no mobility change was observed for the control r(AUx6) duplex (**Figure 4.4a**). Additionally, the PCR stop assay was also conducted using (CGGx1) and (CGGx6) templates. This assay relies on the principle that the drug's binding to the CGG template inhibits Taq polymerase activity, resulting in reduced amplification efficiency. Consistent with previous

findings, increasing Celecoxib concentrations significantly reduced the PCR products, as demonstrated by the decreased band intensity. In contrast, no significant decrease in the band intensity was observed for the AU template PCR products, even at Celecoxib concentrations up to $100.0 \, \mu M$ (**Figure 4.4b**). These findings support the conclusion that Celecoxib exhibits a high binding affinity and specificity for GG-mismatch RNA motifs.

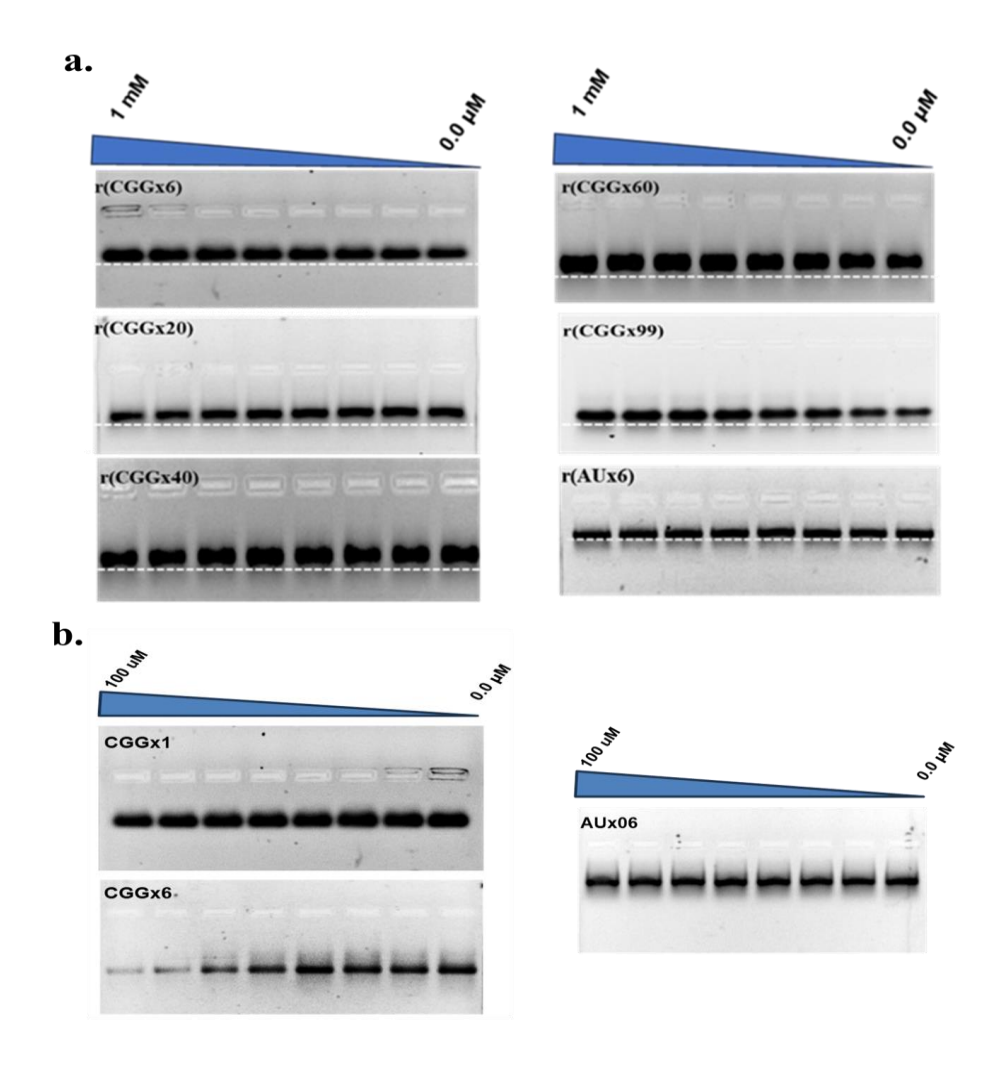


Figure 4.4 Gel retardation assay and PCR stop assay show alteration in $r(CGG)_{exp}$ RNA band patterns on titration with Celecoxib. a. Gel retardation images show that with an increasing concentration of

Celecoxib, the mobility of CGG repeat RNAs significantly increases over AU duplex RNA. **b.** The decreased intensity of the PCR product with increasing concentration of Celecoxib compared with the AU-paired template.

4.5 Molecular Characterization of r(CGG)₆ RNA–Drug Interactions Using Docking Studies and NMR Spectroscopy

Molecular docking analysis was conducted to understand the molecular basis of Celecoxib-r(CGG)_{exp} RNA interactions in silico ^{22,46}. The study showed that Celecoxib possesses a high binding affinity towards the r(CGG)_{exp} RNA motif, with a best docking score of -7.1 kcal/mol. This interaction was primarily facilitated by nucleotide G8 in the RNA duplex, forming a traditional hydrogen bond with Celecoxib. Alongside, nucleotides G11 and G12 formed halogen bonds with the two fluorine atoms in Celecoxib, aligning with the binding site at the GG mismatch loop. These findings align with the initial biophysical studies, as shown in **Figure 4.5a**.

NMR is a widely used technique for studying nucleic acid-drug interactions at the molecular level, where alterations in chemical shifts (upfield and downfield) and peak broadening upon nucleic acid binding offer crucial insights into the involvement of ligand protons in these interactions. After evaluating the binding affinity and specificity of Celecoxib towards r(CGG)_{exp} RNAs, we aimed to gain insights into the atomistic details of this interaction ^{20,22,73}. NMR titration assay was performed using Celecoxib and increasing concentration of r(CGGx6) RNA; subsequently, changes in proton resonance peak height, peak broadening, and ligand chemical shifts were monitored. The incremental addition of r(CGGx6) RNA to the solution containing Celecoxib induced peak broadening along with both downfield and upfield chemical shifts of

resonating protons, observed from a molar ratio of 100:1 to 100:9. Studies have shown that typically, the aromatic ring of planar molecules engages in π - π interactions with nucleic acids. The majority of the exchangeable protons of Celecoxib involved in interacting with the r(CGG)_{exp} RNA lie in the region of 6.8 to 8.0 ppm, suggesting the possibility of π - π interactions. Additionally, peak broadening and downfield chemical shift are observed in H1 and H22 that correspond to the methyl and sulfonamide protons of Celecoxib, suggesting the involvement of both aromatic and aliphatic protons, whether conjugated or unconjugated, participate in the interaction (**Figure 4.5b**). Conclusively, we have elucidated the atomistic details of the interaction between Celecoxib and r(CGG)_{exp} RNAs, confirming Celecoxib's high affinity and specificity towards r(CGG)_{exp} motifs.

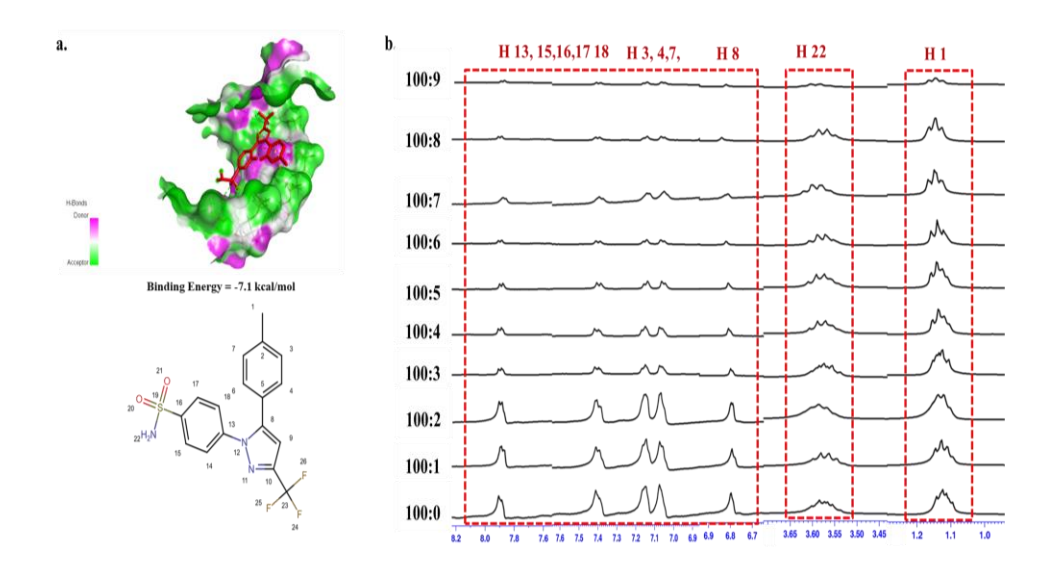


Figure 4.5 Molecular Docking and NMR Broadening of Celecoxib and CGG RNA. a. Docking study showing 3D interaction of Celecoxib with CGG RNA. **b.** Proton spectrum 1D-1H NMR peak broadening of Celecoxib with (CGGx6) RNA.

4.6 Assessment of Celecoxib's effect on alterations in toxic CGG RNA-protein interactions

Toxic CGG repeat RNAs are known to sequester many crucial RBPs, including DiGeorge syndrome critical region gene 8 (DGCR8), DROSHA ⁷⁴, heterogeneous nuclear ribonucleoprotein (hnRNP) A2/B1 ⁷⁵, CUG-binding protein 1 (CUGBP1) ⁷⁵, Src-associated substrate during mitosis of 68 kDa (Sam68) ⁷⁶, and Purine-rich element-binding protein A (Pur-alpha) ⁷⁷. This sequestration of different proteins leads to the formation of toxic RNA foci, a characteristic pathological feature of FXTAS, thereby indicating cellular dysfunction by making the sequestrated RBPs unavailable for their physiological functions. To validate the potential of Celecoxib to bind expanded CGG repeat RNAs and disrupt these pathogenic RNA–protein interactions, we performed three biophysical techniques - EMSA, CD Spectroscopy, and Fluorescence Spectroscopy ⁴⁷. For this study, we utilized pathogenic r(CGGx99) RNA and the most prominent RBPs involved in RNA foci formation, DGCR8.

To validate the effect of celecoxib on the conformational change of the RNA-protein complex, at first, we performed CD spectroscopy. The gradual addition of DGCR8 into the r(CGGx99) RNA solution leads to a hypsochromic (blue) and hypochromic shift in the positive peak and a hypochromic shift in the negative peak (**Figure 4.6a**). This result indicates that DGCR8 shows a favorable interaction with r(CGGx99) RNA. After getting the saturation peak of the RNA-protein complex, Celecoxib was incrementally added to the RNA-protein solution. Increasing concentration of Celecoxib leads to a hypochromic and bathochromic shift in the positive peak and a hypochromic shift and bathochromic shift in the negative peak (**Figure 4.6b**). This spectral change directly correlates with the pattern observed in the RNA-drug complex, indicating a possible displacement of DGCR8 from the r(CGGx99) RNA. Furthermore, EMSA showed a distinct shift in the banding pattern of CGG RNA-protein and CGG RNA-

drug compared to free RNA bands, indicating the complex formation of the drug as well as the protein with r(CGGx99) RNA. Interestingly, with the increase in Celecoxib concentration, the RNA-protein complex band progressively shifted to a position corresponding to the RNA-drug complex (Figure 4.7). This suggests that celecoxib is capable of displacing DGCR8 from the RNA-protein complex. Additionally, fluorescence spectroscopy was performed to investigate the interaction dynamics. At first, r(CGGx99) RNA was gradually added to the solution containing DGCR8. Following the attainment of the saturation peak of the RNAprotein complex, Celecoxib was gradually added to the RNA-protein solution. With increasing concentrations of Celecoxib, there is a decrease in the fluorescence intensity of DGCR8, which also corresponds to the fluorescence intensity observed in spectra of DGCR8 alone (without RNA) (Figure 4.8). Thereby, indicating that the drug is able to interact with the r(CGGx99) RNA in the presence of DGCR8 and able to interfere with the RNA-protein complexes. Together, these biophysical studies indicate that Celecoxib has the potential to displace the proteins from the r(CGGx99)RNA, suggesting its ability to disrupt the RNA foci and release the sequestered proteins, thereby potentially restoring their normal functions.

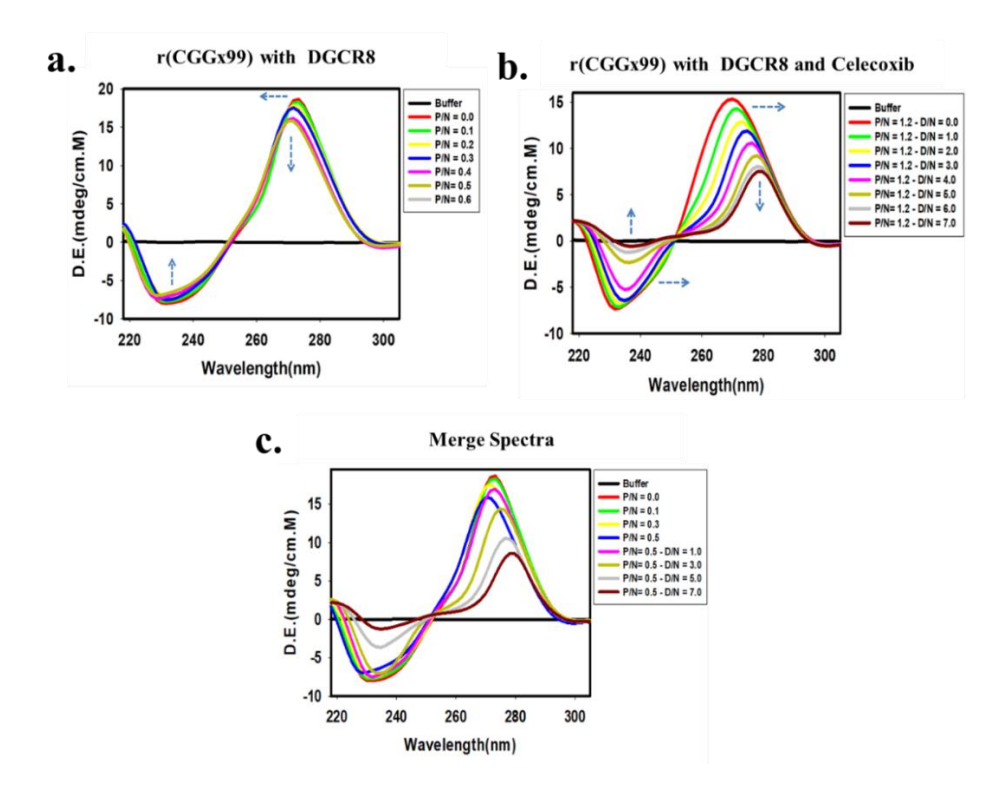


Figure 4.6 CD spectroscopic analysis of r(CGGx99) RNA with increasing concentration of proteins and Celecoxib. a. r(CGGx99) RNA with DGCR8 **b.** r(CGGx99) RNA-DGCR8 complex with Celecoxib **c.** Merged spectra of r(CGGx99) RNA with DGCR8 and Celecoxib.

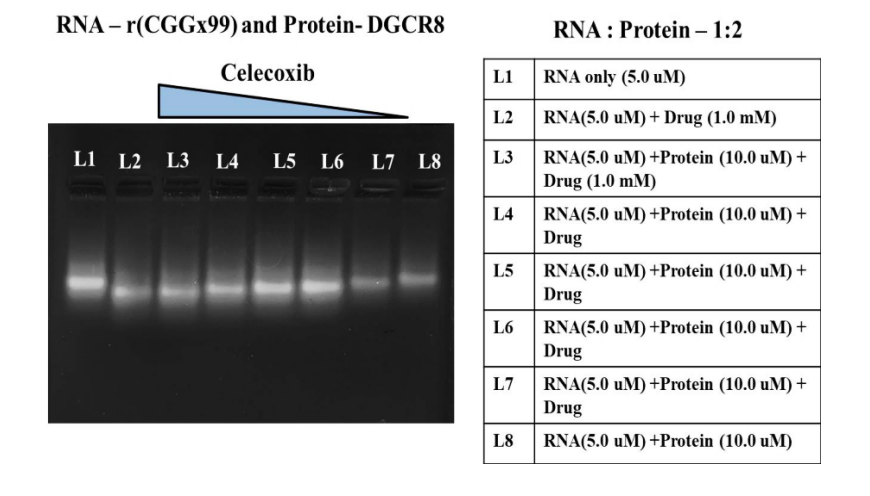


Figure 4.7 Gel images depicting EMSA with r(CGGx99) RNA in the presence of DGCR8 and increasing concentration of Celecoxib.

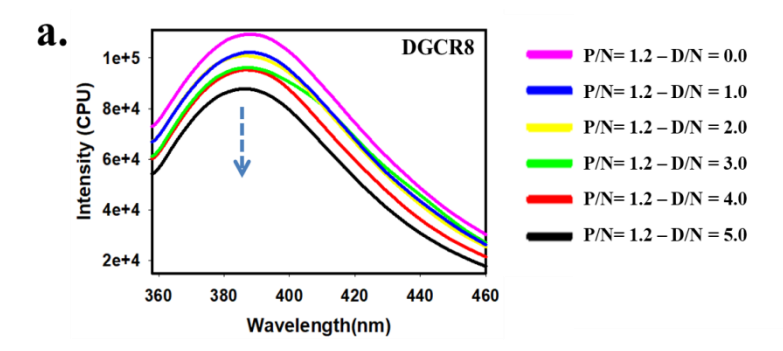


Figure 4.8 Graph depicting the Fluorescence emission spectra of a. DGCR8 in increasing concentrations of r(CGGx99) RNA and Celecoxib.

4.7 Evaluation of Celecoxib-Mediated Inhibition of RAN Translation in FXTAS Cellular Model

The progression of FXTAS relies heavily on non-canonical RAN translation. Past studies have shown that expanded r(CGG), r(CAG), and r(CUG) RNA repeats promote the formation of toxic homopolymeric protein aggregates via RAN translation ^{78,79}. Thereby, we developed a cellular FXTAS model to evaluate Celecoxib's effectiveness in reducing the toxicity caused by these aggregates, particularly FMR1PolyG in FXTAS. For proper visualization of FMR1PolyG aggregates, a comparatively larger-dimension phenotype cell line, COS-7 cells (fibroblast-like cell line), were transfected with a plasmid bearing a CGGx99 repeat in the 5' untranslated region (UTR) of the EGFP gene 46. Celecoxib treatment effectively reduces FMR1PolyG protein aggregates in a dose-dependent manner. The arrowheads in the figure denote intracellular protein aggregates. At a concentration of 5.0 µM, Celecoxib decreased FMR1PolyG aggregates by 55%, with a further reduction to 90% observed at 10.0 µM (Figure 4.9d, e). Whereas the translation of EGFP remained unaffected at these concentrations.

Furthermore, for western blot analysis and cell viability analysis, HEK-293T cells were transfected with the same plasmids abovementioned. Following transfection, cells were treated with varying Celecoxib concentrations. To validate expression patterns, proteins were extracted from cells and examined using immunoblotting with anti-FMR1PolyG, anti-β-actin, and anti-EGFP antibodies. Celecoxib treatment significantly reduced the FMR1PolyG levels by 60% and 92% at 5.0 µM and 10.0 µM concentrations, respectively. Notably, Celecoxib showed minimal effects on EGFP protein expression in control plasmids lacking CGG expansions (Figure 4.9b, c). Importantly, Celecoxib's ability to hinder RAN translation was strongly linked to its affinity for the r(CGG)_{exp} RNA motif and specifically inhibiting non-canonical RAN translation, without interfering with the canonical translation. These findings suggest that the reduction in FMR1PolyG expression is probably driven by Celecoxib interfering with the ribosomal machinery. This interference can occur either by preventing the progression of the ribosome along the RNA or by blocking the initiation of non-canonical translation ^{20,46}. Our results indicate that Celecoxib significantly improved cell viability in HEK293-T cells expressing CGGx99 repeats. This restoration of viability by Celecoxib is likely due to a reduction in cellular inflammation, apoptotic pathways, and oxidative stress 29,41, along with the maintenance of homeostasis between autophagy and oxidative stress 80, which are typically caused by the accumulation of toxic protein aggregates.

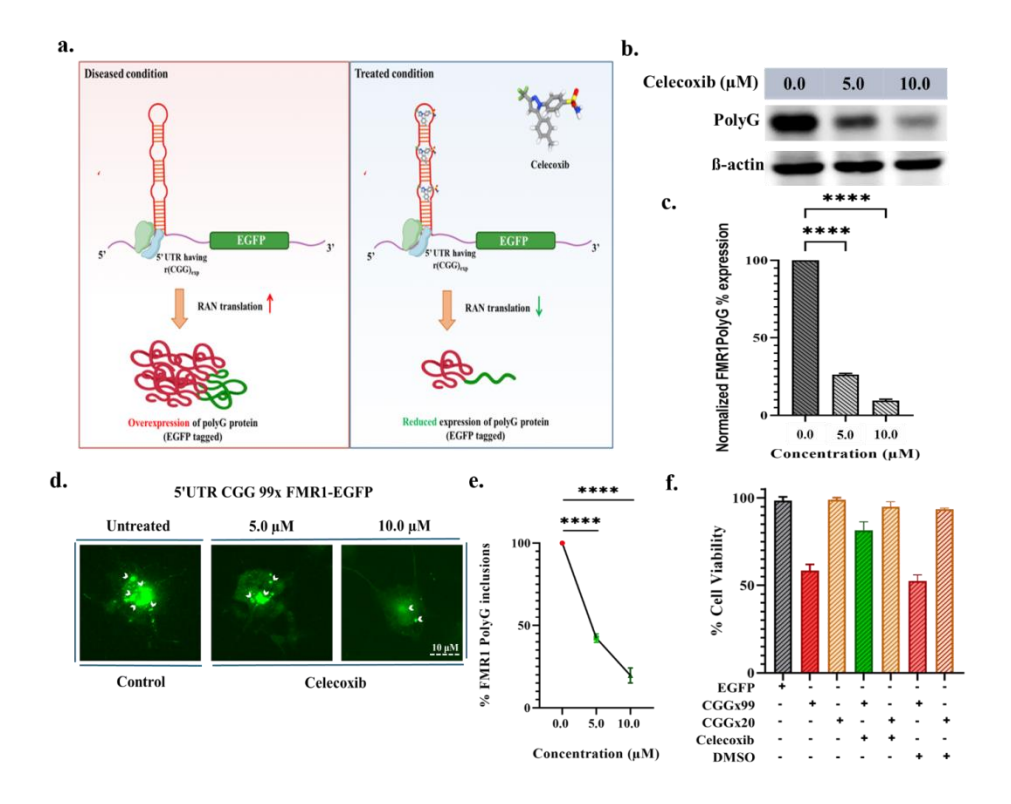


Figure 4.9 In-vitro efficacy of Celecoxib in reducing FMR1PolyG aggregates in FXTAS cellular models a. Schematic representation of reduction in PolyG aggregates upon treatment with Celecoxib. b. Blot showing the reduction in PolyG aggregates formation as a function of Celecoxib concentration with control β-actin and EGFP plasmid (lacking CGG repeat). c. Quantitative analysis of the normalized PolyG protein expression. d. Treatment with Celecoxib reduced the FMR1PolyG-EGFP aggregation in COS7 cells in a concentration-specific manner. e. Graph depicting the percentage reduction in the FMR1PolyG-EGFP inclusions at different concentrations of Celecoxib (12.5 μM and 25.0 μM). f. Bar graph representing improved cell viability in toxic plasmid-transfected HEK-293 cells in the presence of Celecoxib. Statistical significance was determined using one-way ANOVA ****P≤0.00001.

4.8 Improvement of Splicing Defects in FXTAS Cellular Model by Celecoxib Treatment

In healthy cells, RBPs such as DGCR8 and Sam68 regulate SMN2 premRNA alternative splicing; however, expanded CGG repeats hinder this process by sequestering these splicing regulators. An FXTAS cellular model was developed to investigate Celecoxib's potential in rectifying splicing anomalies, mainly focusing on the alternative splicing of Survival Motor Neuron 2 (SMN2) and B-cell lymphoma x (Bcl-x) pre-mRNAs, both of which are dysregulated in FXTAS ^{19,46}. Aberrant splicing patterns in cells possessing CGG repeat, such as increased exon 7 inclusion in SMN2 mRNA (~65% compared to ~42% in healthy cells), demonstrate the effect of r(CGG)_{exp} repeats on mRNA splicing ^{20,22,46}. Co-transfection of CGGx99-EGFP and SMN2 minigene construct in HEK-293T cells was carried out to assess Celecoxib's potency in mitigating splicing abnormalities. Celecoxib improved normal splicing in a dose-dependent manner, with 5.0 µM correcting ~30% of the SMN2 mis-splicing defect and 10.0 µM attaining near-wild-type restoration (~80%) (Figure 4.10b). Similar results were observed for the Bcl-x minigene. Bcl-x minigene contains two isoforms: Bcl-xL and Bcl-xS. In normal conditions, the BclxL isoform accounts for ~47% in healthy cells, whereas in the FXTAS condition, it accounts for ~65%. At 10.0 µM Celecoxib, ~85% of the Bcl-x mis-splicing defect was recovered, whereas 5.0 µM recovered ~20%. While Celecoxib did not influence splicing in cells that lacked CGG repeats, demonstrating its specificity towards CGG repeats (Figure 4.10d). Further investigations suggested that Celecoxib likely displaces splicing regulators (e.g., Sam68, DGCR8) from secondary structures formed due to CGG repeats, restoring their availability for normal RNA processing and reducing splicing defects. Furthermore, Celecoxib binds specifically to r(CGG)_{exp} motifs, primarily targeting CGG-repeat-associated splicing errors, as evidenced by its lack of effect on the cTnT minigene, which

remains unaffected by r(CGG)_{exp}-associated sequestration of proteins. These findings show that Celecoxib efficiently rectifies pre-mRNA splicing abnormalities caused by CGG expansions, suggesting a targeted treatment strategy for FXTAS. Moreover, the splicing results, together with the previous biophysical studies on assessing Celecoxib's impact on modulating the toxic CGG RNA-protein interactions, strongly suggest that Celecoxib may interfere with the interaction of key regulatory proteins involved in RNA foci formation, including CUGBP1, Purα, Sam68, hnRNPA2/B1, DGCR8, and DROSHA, with r(CGG)_{exp} RNA ^{13,20,75-77}. By interfering with their sequestration, Celecoxib may restore the functional availability of these proteins, allowing them to participate in essential cellular processes, including RNA metabolism and splicing regulation. This restoration of protein function could reduce RNA foci-associated toxicity.

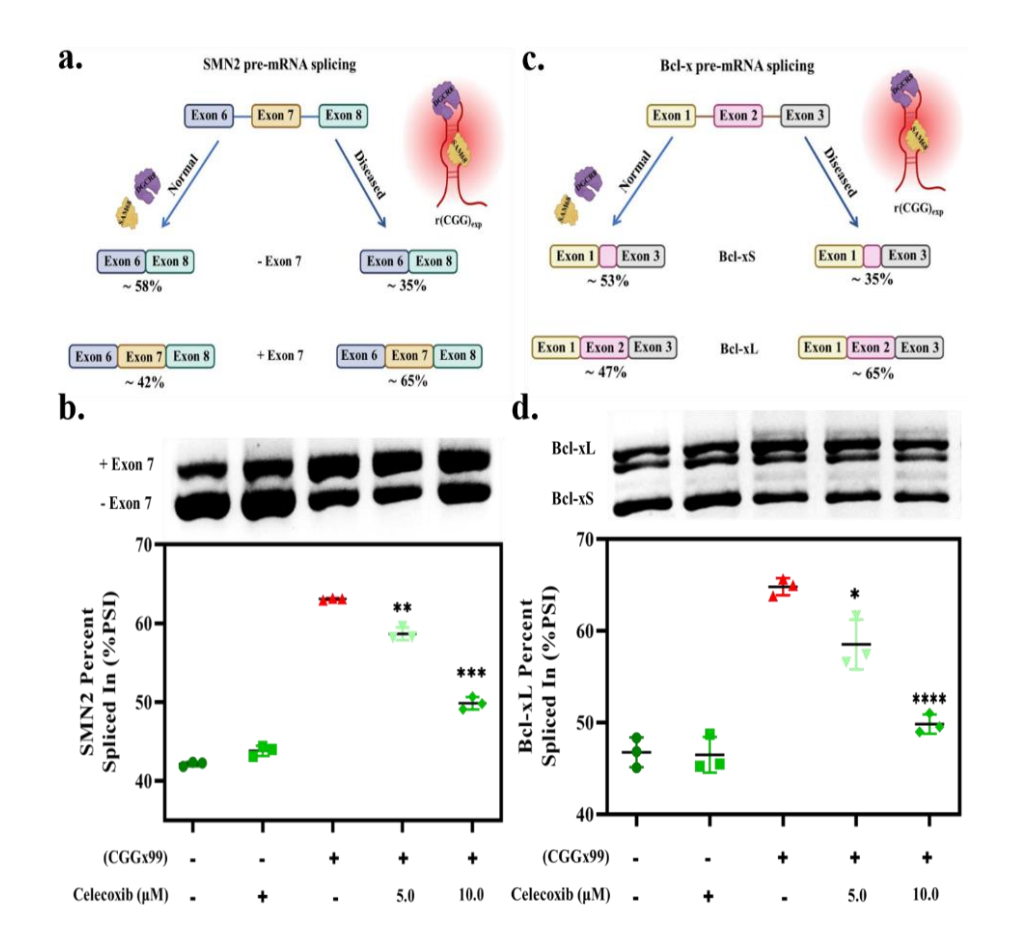


Figure 4.10 In-vitro potency of Celecoxib in ameliorating splicing defects in FXTAS cellular models a. Schematic representing splicing defects associated with SMN2 in the FXTAS model. b. Gel image and graph illustrate that Celecoxib corrects the SMN2 splicing defects in relation to its concentration. c. Schematic representing splicing defects associated with Bcl-x in the FXTAS model. d. Gel image and graph illustrate that the drug corrects the Bcl-x splicing defects in relation to their concentration. e. Blot showing that Celecoxib has no effect on EGFP expression. f. Quantitative analysis of normalized EGFP expression. Statistical significance was determined using one-way ANOVA $****P \le 0.0001; ***P \le 0.001; *P \le 0.01.$

4.9 Assessment of Celecoxib's Effect on the Feeding Behavior of the Flies

Taste plays a key role in helping animals choose safe, nutritious food while avoiding harmful substances. To lay the groundwork for drug-feeding experiments and better interpret future results, we tracked how larvae feed. Larvae were given access to food mixed with different doses of Celecoxib and a blue dye for two hours, and their food intake was later measured using spectrophotometry ⁵⁶. Herein, we found that no difference in the feeding behavior was observed at different Celecoxib concentrations in the case of all four strains used in the study - *GMR-GAL4>UAS-(CGG)*₉₀-EGFP, *GMR-GAL4>UAS-EGFP*, *Elav-GAL4>UAS-(CGG)*₉₀-EGFP, *Elav-GAL4>UAS-EGFP* (**Figure 4.11a-d)**.

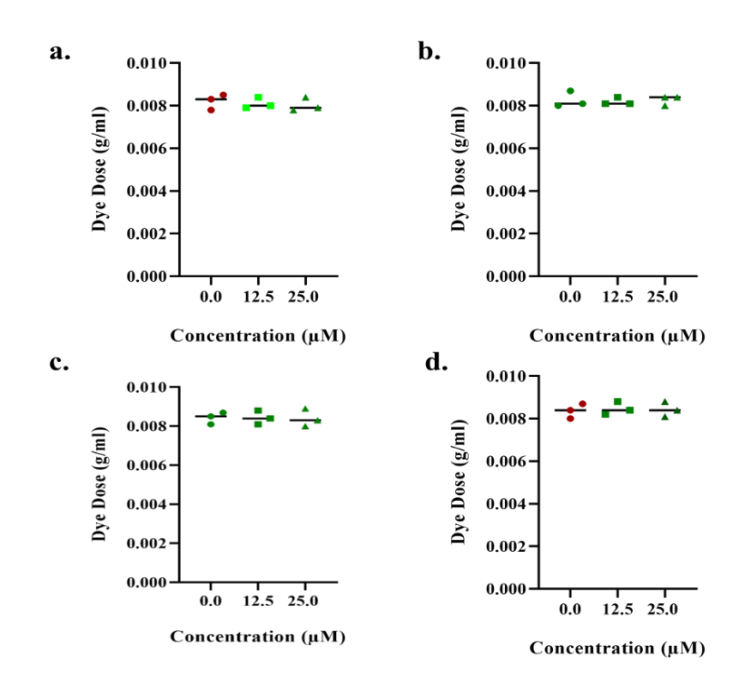


Figure 4.11 Graphs representing feeding intake of a. GMR-GAL4>UAS-(CGG)90-EGFP b. GMR-GAL4>UAS-EGFP c. Elav-GAL4>UAS-(CGG)90-EGFP d. Elav-GAL4>UAS-EGFP

4.10 Celecoxib Counteracts FMR1PolyG-Induced Neurodegeneration, Eye Abnormalities, and Pigment Loss in the *Drosophila* FXTAS Model

4.10.1 Brightfield microscopy

Celecoxib's therapeutic potential was evaluated using an FXTAS *Drosophila* model. The pan-retinal *GMR-GAL4* driver line was used to drive the expression of *UAS-(CGG)90-EGFP* and *UAS-EGFP* transgenes in flies' compound eyes ⁴⁶. Celecoxib was incorporated into food at various concentrations. In diseased flies expressing (CGG)90, increasing dosages of Celecoxib dramatically reduced exterior morphological defects such as pigment loss and rough eye phenotypes (**Figure 4.12a**), but control flies expressing solely EGFP exhibited no significant differences (**Figure S4a**). Notably, treatment with Celecoxib protected pigmented cells, preventing progressive degeneration and improving the degenerated eye phenotype, suggesting sustained therapeutic advantages.

4.10.2 Eye pigmentation Analysis

Moreover, it is observed that in diseased conditions, there is a significant decrease in the red pigmentation in the eyes. To assess the red pigment levels, an eye pigmentation assay was performed by homogenizing the heads of flies expressing (CGG)₉₀ repeats and only EGFP, both grown at varying Celecoxib concentrations. The test findings showed that increasing Celecoxib concentrations resulted in a considerable rise in red pigmentation levels in diseased (CGG)₉₀ repeat flies (**Figure 4.12b**). In contrast, flies that only expressed EGFP showed no change in red pigmentation levels, revealing the specificity of the drug.

4.10.3 FE-SEM

Under pathological conditions, the normally structured *Drosophila* compound eye, which consists of approximately 800 ommatidia arranged in a precise hexagonal pattern with distinct interommatidial bristles,

exhibits a rough eye phenotype ^{81,82}. FE-SEM analysis further validated these findings, demonstrating the potency of Celecoxib in restoring the hexagonal arrangement and spacing of ommatidia with clearly defined interommatidial bristles in a dose-dependent manner. Under disease conditions, flies typically displayed disrupted ommatidia and rough eye morphology, which were significantly improved following treatment (**Figure 4.12a**). Morphological changes were measured using Flynotyper software, which verified reduced ommatidia disorderliness scores in treated flies and correlated with the observed improvements in eye structure.

4.10.4 Confocal microscopy

To further confirm that phenotypic abnormalities, including decreased pigmentation and rough eye morphology, correlate directly with FMR1PolyG expression levels. Confocal imaging of the same flies exhibiting decreased pigmentation revealed prominent FMR1PolyG aggregates through visualization of the EGFP-tagged PolyG in (CGG)₉₀-EGFP-expressing flies (**Figure 4.12a, c**). Notably, these aggregates were not present in control flies expressing solely EGFP, providing further evidence that CGG repeat expansion drives the observed degeneration. The fluorescence intensity of FMR1PolyG aggregates was significantly reduced after Celecoxib treatment, indicating that it effectively reduces FMR1PolyG accumulation. Quantitative analysis confirmed the reduction, emphasizing Celecoxib's therapeutic potential in targeting CGG repeat-induced toxicity.

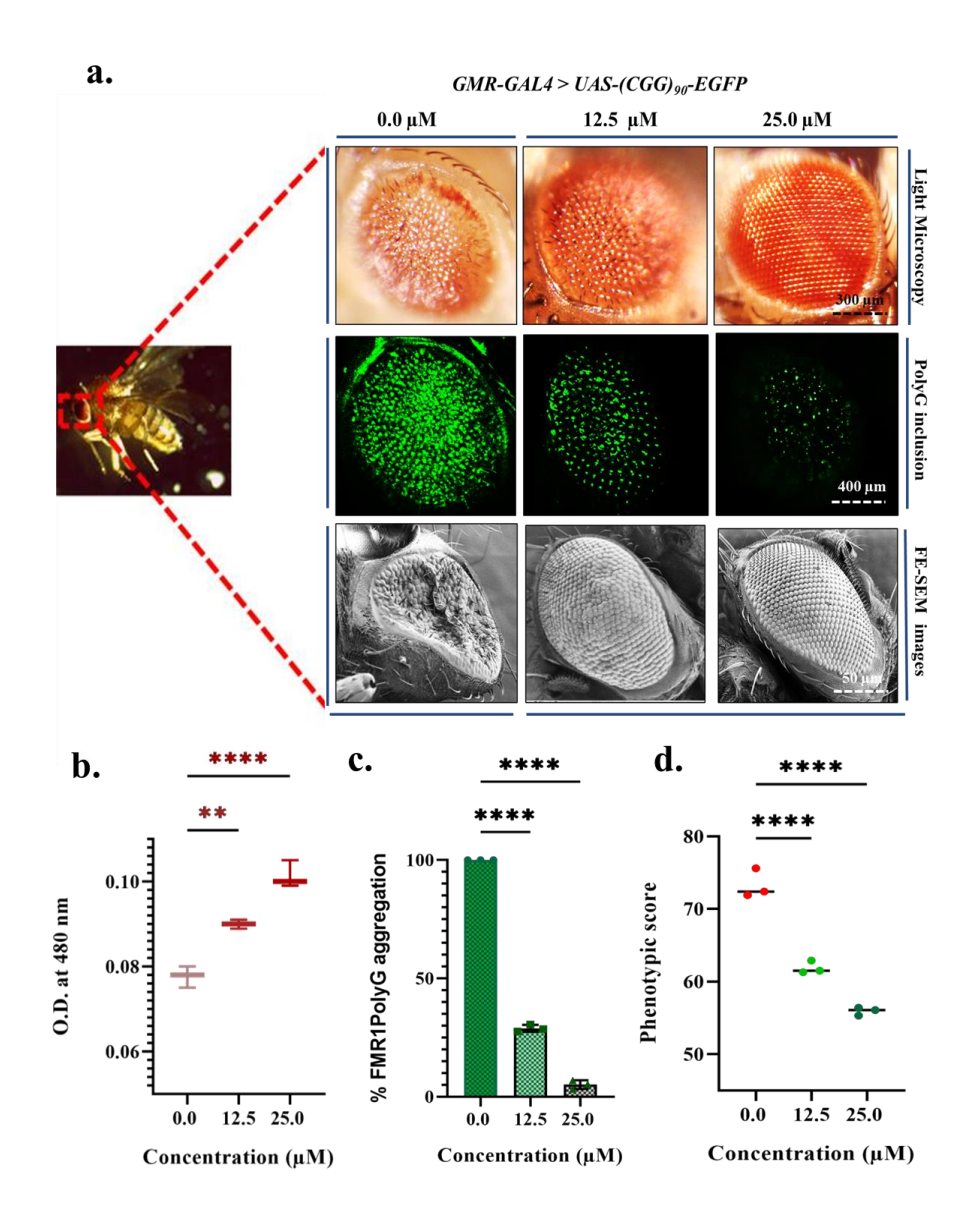


Figure 4.12 Celecoxib mitigates pigment loss and rough eye phenotype caused by PolyG toxicity in the FXTAS Drosophila model. (a-d) Celecoxib mitigates pigment loss and rough eye phenotype caused by PolyG toxicity in the FXTAS *Drosophila* model. **a.** Light, confocal, and FE-SEM microscopy images of the adult fly eyes expressing *GMR-GAL4>UAS-(CGG)90-EGFP* and *GMR-GAL4>UAS-EGFP*. Flies were fed with different concentrations (12.5 μM and 25.0 μM) of Celecoxib. **b.** Eye pigmentation was quantified by measuring red pigment levels in fly heads at O.D. 480 nm. **c.** Bar graph representing the quantitative analysis of

FMR1PolyG inclusions as a percentage. **d.** Quantitative assessment of rough eye morphology based on phenotypic scoring. Data are presented as mean \pm SEM from at least three independent experiments. Statistical significance was determined using one-way ANOVA, ****P \leq 0.00001; **P \leq 0.00.

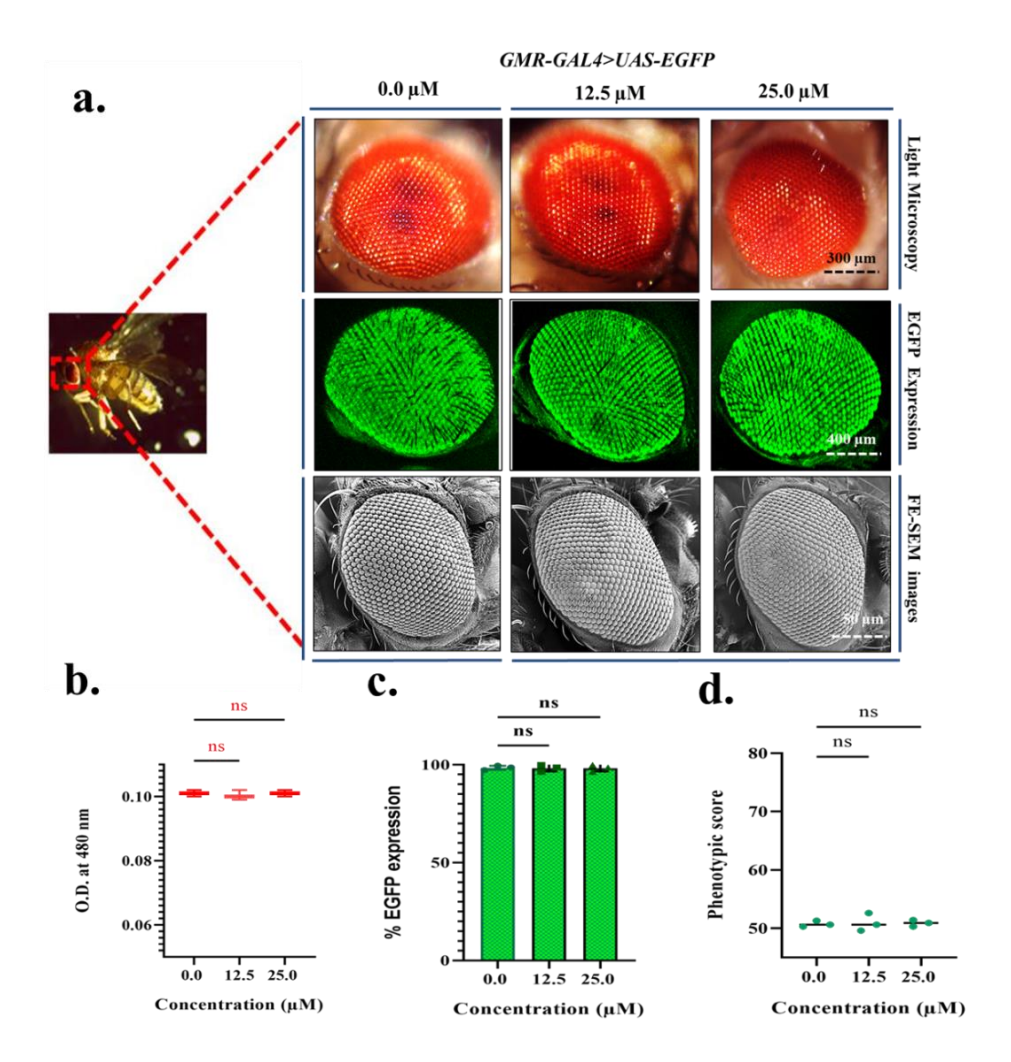


Figure 4.13 Effect of Celecoxib on *Drosophila* FXTAS model. Light, confocal, and FE-SEM microscopy images of the adult fly eyes expressing GMR-GAL4>UAS-EGFP. **a.** Flies were fed with different concentrations (12.5 μ M and 25.0 μ M) of Celecoxib. **b.** Eye pigmentation was quantified by measuring red pigment levels in fly heads at O.D. 480 nm. **c.** Bar graph

representing the quantitative analysis of EGFP expression as a percentage. **d.** Quantitative assessment of rough eye morphology based on phenotypic scoring. Data are presented as mean \pm SEM from at least three independent experiments.

4.11 In vivo potency of celecoxib in reducing the FMR1PolyG inclusion in brain tissues

The toxic FMR1PolyG was expressed in the neuronal cells of flies using a strong pan-neuronal expression driver, *Elav-GALA*. Subsequently, the EGFP-tagged-PolyG aggregation in brain tissues was visualized using confocal microscopy. This aggregation corresponds to the accumulation of the RAN translation product FMR1PolyG, a hallmark of RNA toxicity. Treatment with increasing concentrations of Celecoxib resulted in a significant, dose-dependent reduction in FMR1PolyG aggregation, as evidenced by decreased green fluorescence intensity in brain tissues (Figure 4.14a). Furthermore, Protein extracts from the heads of flies treated with different doses of Celecoxib were subjected to Western blot analysis. Anti-FMR1PolyG antibodies were utilized to assess FMR1PolyG protein levels in treated flies and compared with experimental control (untreated flies). Across all treatment groups, the results showed a substantial decrease in FMR1PolyG protein levels, indicating that Celecoxib effectively prevents FMR1PolyG aggregation (**Figure 4.14b, c**). Celecoxib selectively targets toxic FMR1PolyG aggregates formed due to expanded CGG repeats, as evidenced by the unchanged levels of β -actin. In contrast, flies expressing solely EGFP had no change in the levels of EGFP or β -actin. These findings highlight the in vivo potency of Celecoxib in interfering with pathological RAN translation, effectively reducing the levels of the RAN translation product. The observed decrease in FMR1PolyG aggregation demonstrates Celecoxib's potential to mitigate the downstream toxic effects associated with CGG repeat expansions, a key pathological feature in FXTAS.

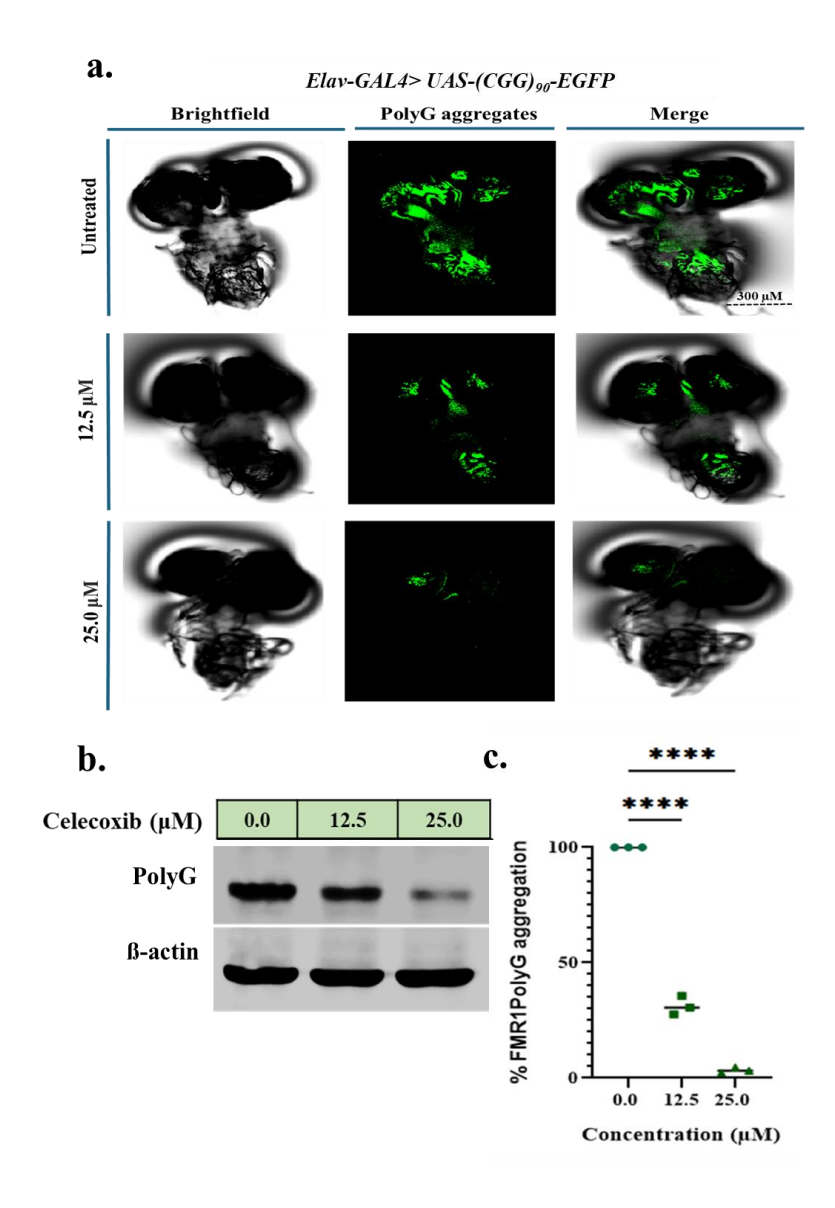


Figure 4.14 Celecoxib helps to mitigate the PolyG aggregates in the FXTAS *Drosophila* model. a. Confocal microscopy of larval brains *GMR-GAL4>UAS-(CGG)*₉₀-*EGFP* fed with different concentrations (12.5 μ M

and 25.0 μ M) of Celecoxib. **b.** Blot showing reduced PolyG expression in proteins isolated from heads of diseased flies (CGG)₉₀ treated with various Celecoxib concentrations. **c.** The graph illustrates the normalized percentage expression of PolyG. Data are presented as mean \pm SEM from at least three independent experiments. Statistical significance was determined using one-way ANOVA, ****P \leq 0.00001.

4.12 Celecoxib Restores Locomotor Activity in FMR1PolyG-Induced FXTAS *Drosophila* Model

We tested Celecoxib's effect on motor function in flies expressing *UAS-EGFP* and *UAS-(CGG)₉₀-EGFP* using the neuron-specific *Elav-GAL4* driver. Larvae from the *Elav-GAL4>UAS-(CGG)₉₀-EGFP* and *Elav-GAL4>EGFP* groups were treated with varying Celecoxib doses. After treatment, third-instar larvae were subjected to a crawling assay to determine their locomotor (crawling) activity ⁸³. The findings revealed that Celecoxib treatment improved the crawling ability of larvae containing (CGG)₉₀ repeats in a dose-dependent manner (**Figure 4.15b**).

Further, the climbing and flight ability of 14-day-old male flies treated with various drug concentrations was tested to assess motor function in adult flies ^{60,84}. Celecoxib did not affect the locomotion of control flies (expressing only EGFP). However, flies expressing FMR1PolyG ((CGG)₉₀) showed considerable enhancements in climbing ability with increasing Celecoxib concentration. At a dose of 25.0 μM, almost 90% of treated flies efficiently crossed the 10 cm mark (**Figure 4.15d**), indicating a significant improvement in motor function. Along with the improvement in climbing abilities, there is a significant increment in the flight percentage of flies with the increase in Celecoxib concentration, as depicted in the screen captures and the bar graph representing their average landing height (**Figure 4.15f-h**).

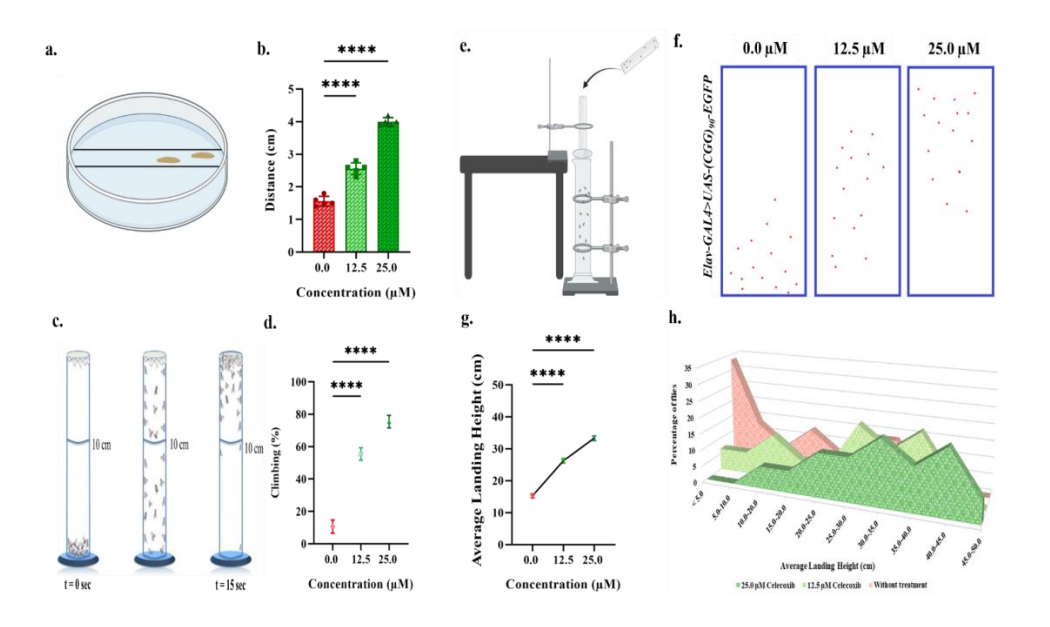


Figure 4.15 Celecoxib improves locomotor dysfunctions in the diseased

fly model. a. Schematic representation of the larval crawling assay. b. Crawling assay results for third-instar larvae (Elav-GAL4>UAS-(CGG)90-EGFP) treated with Celecoxib. c. Schematic for the climbing assay. d. Climbing assay for Elav-GAL4>UAS-(CGG)90-EGFP adult male flies following the treatment with the drug. e. Schematic representation of the apparatus used for the flight assay. f. Screen captures for diseased and control flies displaying the landing heights of individual flies. Each red dot represents the location of an individual fly. These landing heights are used to calculate the average landing height. g. Graph representing the average landing height (cm). h. Graph for the overall distribution of the flies in the sheet. Data are presented as mean \pm SEM from at least three independent experiments. Statistical significance was determined using one-way ANOVA, ****P \leq 0.00001.

4.13 Quantification of arbitrary ROS levels

Previous studies have shown that the accumulation of toxic CGG repeats is associated with the disruption of multiple cellular pathways, including oxidative stress and mitochondrial dysfunction, ultimately leading to increased reactive oxygen species (ROS) production ^{9,85}. To assess the steady-state ROS levels in treated and control flies, a DCF-DA assay was performed. A significant increase in ROS levels was observed in diseased flies, whereas ROS levels decreased significantly with increasing Celecoxib concentrations (**Figure 4.16a**). In contrast, no significant changes in ROS levels were detected in control flies lacking CGG repeats (**Figure 4.16b**). Further investigations are required to elucidate the precise molecular mechanisms underlying Celecoxib's protective role and to determine whether its effects extend to other cellular dysfunctions associated with FMR1PolyG toxicity.

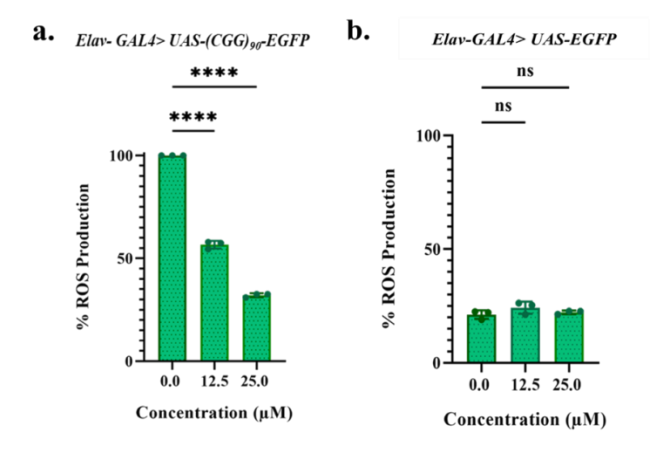


Figure 4.16 Graphs representing % ROS production in a. *Elav-GAL4>UAS-(CGG)*₉₀-*EGFP* fed with different concentrations (12.5 μ M and 25.0 μ M) of Celecoxib. b. *Elav-GAL4>UAS-EGFP* fed with different concentrations (12.5 μ M and 25.0 μ M) of Celecoxib. Statistical significance was determined using one-way ANOVA, ****P \leq 0.00001.

4.14 Effect of Celecoxib on mitochondrial oxidative stress and membrane potential

Mitochondrial dysfunctions result in elevated levels of reactive oxygen species (ROS), a key factor associated with disease pathogenesis and neuronal cell death in neurodegenerative conditions. To evaluate the mitochondrial reactive oxygen species (mtROS) production in the diseased and treated flies, MitoSOX staining was utilized ⁶³. Consistent with the findings from DCFDA staining, increasing concentrations of Celecoxib resulted in a reduction in MitoSOX fluorescence intensity (**Figure 4.17a**, **b**), indicating that Celecoxib treatment may attenuate mtROS production and mitochondrial dysfunction.

To further validate the potential of Celecoxib in mitigating mitochondrial dysfunction, we have measured the change in mitochondrial membrane potential by using Tetramethylrhodamine methyl ester (TMRM) assay ⁶³. TMRM is a cell-permeable fluorescence dye that is predominantly used to assess the mitochondrial membrane potential, which serves as a key indicator of mitochondrial health. TMRM accumulates in the mitochondrial matrix of healthy mitochondria due to a negative charge inside the mitochondria, thereby giving a strong red fluorescence. In contrast, less TMRM is uptaken by dysfunctional mitochondria; thus, decreased fluorescence intensity is obtained 86. The Drosophila FXTAS model shows a notable increase in the TMRM intensity upon increasing the drug concentration (Figure 4.18a, b). The dose-dependent increase in TMRM intensity in the *Drosophila* FXTAS model suggests that the drug enhances mitochondrial membrane potential, suggesting improved mitochondrial health. Whereas, in the case of EGFP-control flies, the fluorescence of TMRM remains stable in untreated and drug-treated flies, indicating the presence of healthy mitochondria in control flies. These results suggest that Celecoxib may improve mitochondrial function by reducing mitochondrial membrane depolarization, enhancing ATP production, and preventing mitochondrial DNA damage, thereby mitigating FMR1PolyG-induced mitochondrial dysfunction.

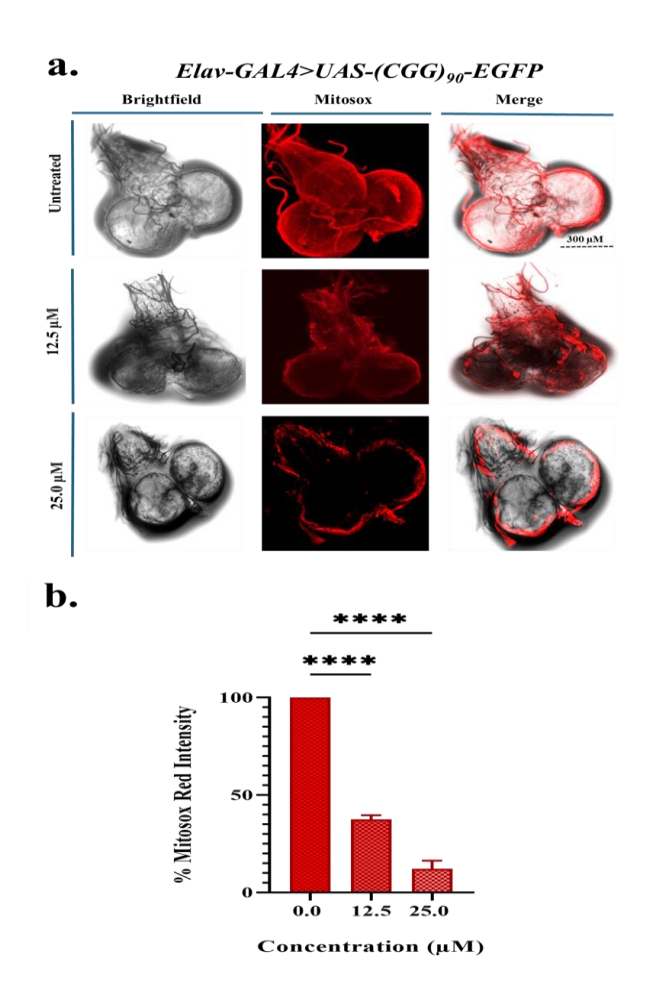


Figure 4.17 Celecoxib treatment restores mitochondrial dysfunction in the FXTAS *Drosophila* model a. Mitosox staining of *Elav-GAL4>UAS-* $(CGG)_{90}$ -EGFP flies fed with different concentrations (12.5 μ M and 25.0 μ M) of Celecoxib. b. Bar graph representing % Mitosox red intensity. Statistical significance was determined using one-way ANOVA, ****P \leq 0.00001.

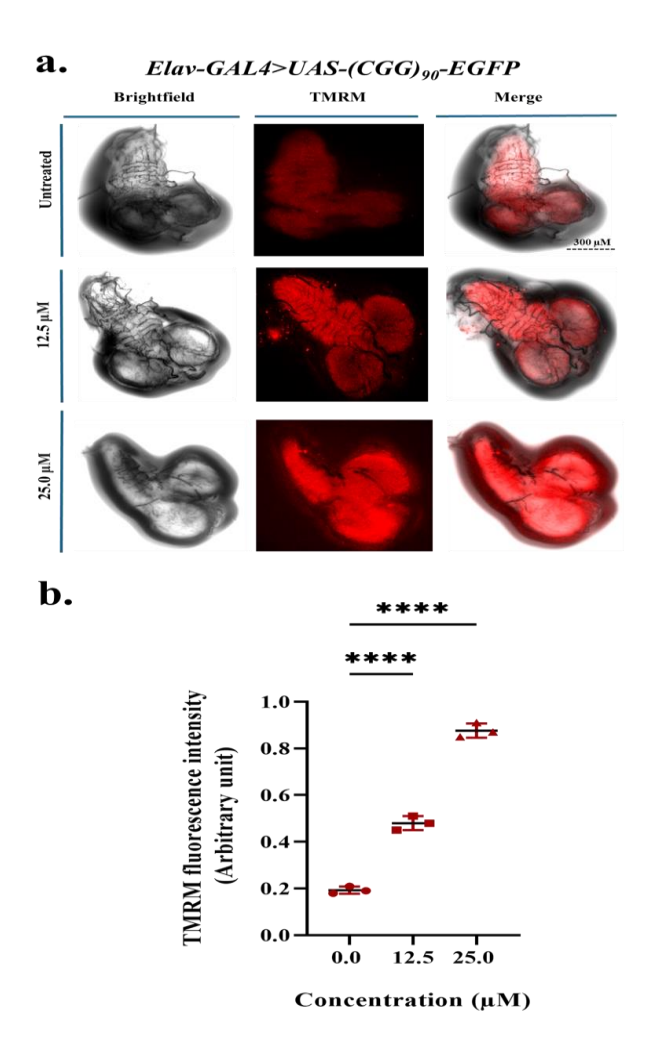


Figure 4.18 Celecoxib treatment restores mitochondrial dysfunction in the FXTAS *Drosophila* model a. TMRM staining of *Elav-GAL4>UAS-* $(CGG)_{90}$ -EGFP flies fed with different concentrations (12.5 μ M and 25.0 μ M) of Celecoxib. b. Bar graph representing TMRM fluorescence intensity. Statistical significance was determined using one-way ANOVA, ****P \leq 0.00001.

4.15 Visualization of neuronal cell death using Propidium Iodide (PI) staining

Emerging studies have shown that multiple interconnected mechanisms, such as inflammation, oxidative stress, mitochondrial dysfunction, and dysregulated autophagy, act as key contributors in driving cellular damage associated with neurodegenerative diseases. These pathological processes ultimately lead to neuronal cell death, a critical event in disease progression, as observed in different repeat-associated neurodegenerative disorders such as FXTAS 87,88. This led us to perform Propidium Iodide (PI) staining to examine the amount of neuronal cell death in control and treated flies ^{88,89}. PI is a nucleic acid-binding dye that cannot penetrate intact cell membranes, making it a useful marker for staining dead cells with compromised membranes. It emits red fluorescence, selectively staining cells with damaged membranes ^{90,91}. Third-instar larval brains expressing *Elav-GAL4>UAS-(CGG)*₉₀-*EGFP* were treated with varying concentrations of Celecoxib and were compared to control UAS-EGFP brains. The brains from untreated flies showed more dead cells than the drug-treated larval brains. The intensity of red fluorescence was significantly reduced with the increase in Celecoxib concentration to 25.0 uM, signifying a notable decrease in cell death on drug treatment. Subsequently, quantifying the PI red intensity showed a significant reduction in red fluorescence, demonstrating the effectiveness of Celecoxib in reducing CGG repeat-induced neuronal cell death (Figure 4.19a, b).

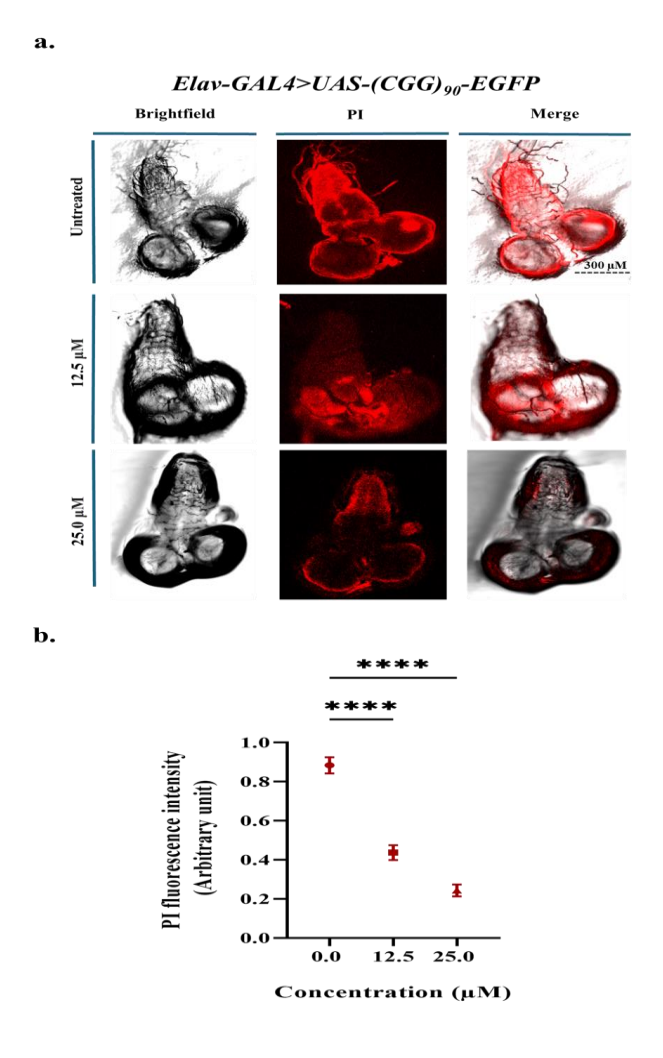


Figure 4.19 Celecoxib treatment reduces neuronal cell death in the FXTAS *Drosophila* model. Confocal microscopy of larval brains a. *Elav-GAL4>UAS-(CGG)*₉₀-*EGFP* fed with different concentrations (12.5 μ M and 25.0 μ M) of Celecoxib and stained with Propidium Iodide (PI). b. Bar graph representing fluorescence intensity (Arbitrary Units) of PI. All data are representative of three independent experiments and are presented as the mean \pm SD, (One-way ANOVA test). ****P \leq 0.00001.

4.16 Analysis of Lifespan in Response to Celecoxib Dosage

Neurodegenerative disorders, such as FXTAS, are frequently associated with a shorter lifespan ⁹². We sought to explore whether a brief period of Celecoxib treatment, applied early or late in life, could extend longevity, as early-life events significantly influence the onset of aging and, in turn, affect overall lifespan. Therefore, a lifespan analysis was conducted by feeding Celecoxib at different time points. The study demonstrated that treatment with 12.5 µM and 25.0 µM Celecoxib, from emergence, significantly improved the survival rates of flies carrying (CGG)₉₀ repeats (Figure 4.20c, d). Interestingly, even when 25.0 µM Celecoxib was administered post-eclosion from day 1 and day 7, an improvement in survivability percentage was observed (Figure 4.20e, f). In contrast, no variations in survival rates were seen in control flies expressing solely EGFP upon Celecoxib administration. These findings demonstrate that Celecoxib specifically extends the lifespan of flies with CGG repeats while not impacting the normal control flies, potentially by preventing damage accumulation and/or enhancing repair mechanisms.

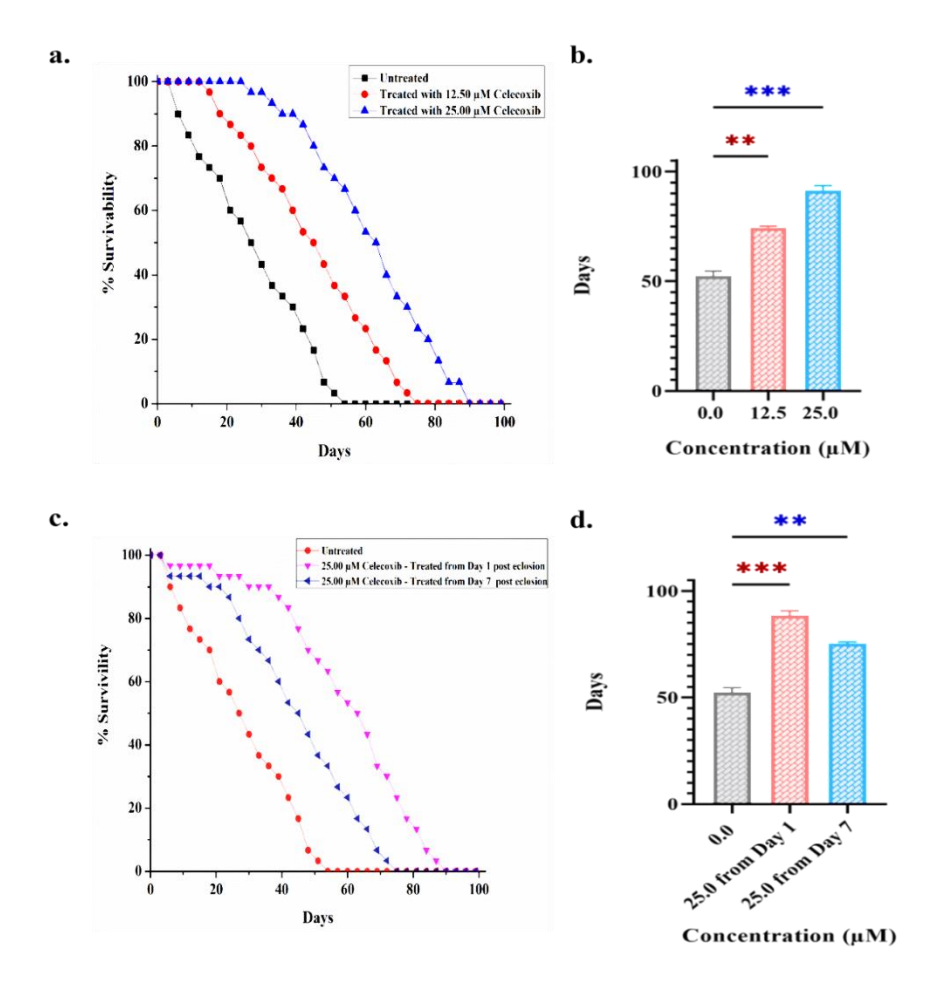


Figure 4.20 Celecoxib treatment extends lifespan in the FXTAS *Drosophila* model. a. Survival curves of *Elav-GAL4>UAS-(CGG)*₉₀-*EGFP* flies fed with different concentrations (12.5 μM and 25.0 μM) of Celecoxib from the larval stage. b. Bar graph representing lifespan (days) of *Elav-GAL4>UAS-(CGG)*₉₀-*EGFP* flies fed with different concentrations (12.5 μM and 25.0 μM) of Celecoxib from the larval stage. c. Survival curves of *Elav-GAL4>UAS-(CGG)*₉₀-*EGFP* flies fed with different concentrations (12.5 μM and 25.0 μM) of Celecoxib from Day 1 and 7 (post eclosion). d. Bar graph representing lifespan (days) of *Elav-GAL4>UAS-(CGG)*₉₀-*EGFP* flies fed with different concentrations (12.5 μM and 25.0 μM) of Celecoxib from Day 1 and 7 (post eclosion). All data are representative of three independent experiments and are presented as the mean ± SD, (One-way ANOVA test), ***P≤0.0001; ***P≤0.001.

4.17 RT-qPCR analysis of various genes involved in autophagic regulation and neuroprotection

Autophagy is a critical cellular process that acts as a quality control of the cells, such as eliminating damaged mitochondria and other cellular components, thereby protecting the cells from inflammation and oxidative stress. Dysregulation of autophagic pathways is a key feature in various neurodegenerative diseases, often contributing to the accelerated progression of neurodegeneration ⁹³. Previously, studies have shown that Celecoxib has the potential to upregulate autophagy. Therefore, we checked the expression levels of some crucial autophagy-related genes in the Drosophila FXTAS model. Specifically, we measured the expression of Atg1, Atg4b, Atg5, Atg7, Atg8a, and Atg101. Atg1 is involved in recruiting downstream Atg proteins and regulating autophagosome formation ⁹⁴; Atg4b a protease is involved in autophagy-related processing 95; Atg5 is involved in the formation and expansion of autophagosome 96; Atg7 is an E1-like enzyme that initiates autophagy by facilitating autophagosomes membrane formation and elongation ⁹⁷; Atg8a is known to support the nervous systems' stability in Drosophila and regulate membrane elongation during autophagosome biogenesis ⁹⁸ and Atg101 acts as a core complex of the Atg1 complex, important for autophagy initiation and autophagosome formation ⁹⁹. In the diseased model, we found a significant downregulation of Atg1, Atg5, Atg7, Atg8a, and Atg101, while the levels of Atg4b remain unchanged. Treatment with 25.0 µM Celecoxib restored the levels of these crucial autophagic genes (Atg1, Atg5, Atg7, Atg8a, and Atg101), whereas no significant change was observed in the levels of Atg4b (Figure 4.21a-f). These findings suggest the potential of Celecoxib to restore impaired autophagic pathways, thereby promoting the clearance of damaged mitochondria and other cellular components. In our previous study, mitochondrial dysfunction was identified in disease states, and we observed that Celecoxib had the ability to attenuate this dysfunction. Thus, the upregulation of autophagy and the subsequent clearance of damaged mitochondria and other cellular components becomes crucial to re-establish cellular homeostasis. This suggests a potential neuroprotective role of Celecoxib through the modulation of autophagic pathways.

Building on previous results demonstrating the neuroprotective effects of Celecoxib, we further investigated the expression levels of selected genes reported to be upregulated by Celecoxib that are directly involved in neuroprotection ^{100,101}. We therefore assessed the expression levels of SOD, Nrf2, and GSTs in the (CGG)₉₀-expressing flies. The diseased flies showed a significant downregulation of SOD and Nrf2 and a slight upregulation of GSTs. Remarkably, treatment with 25.0 μM Celecoxib resulted in notable upregulation of SOD, Nrf2, and GSTs (**Figure 4.21g-i**), Thereby attenuating oxidative stress and subsequent neuroinflammatory cascades. Additionally, the significant upregulation of Nrf2 also suggests a probable upregulation of downstream neuroprotective genes. These findings suggest the therapeutic potential of Celecoxib as a neuroprotective molecule for FXTAS.

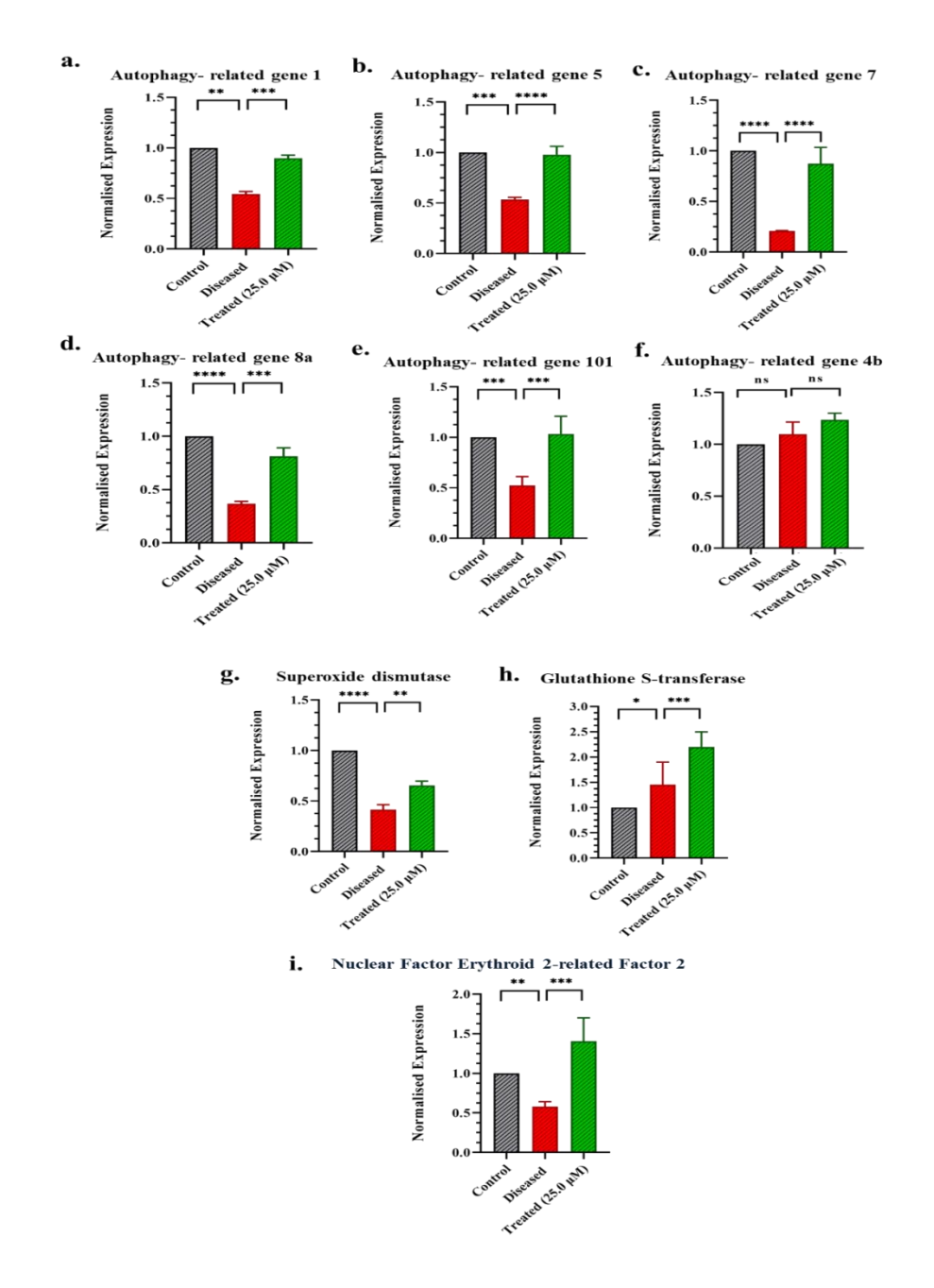


Figure 4.21 Celecoxib treatment upregulates different autophagic and neuroprotective genes in the FXTAS Drosophila model a. Autophagy-related gene 1 b. Autophagy-related gene 5 c. Autophagy-related gene 7 d. Autophagy-related gene 8a e. Autophagy-related gene 101 f. Autophagy-related gene 4b. (g-i) RT-qPCR analysis of various neuroprotective genes. The Bar graphs represent the fold change of genes treated with Celecoxib

(25.0 μ M), diseased control (UT), as well as normal control (without (CGG)₉₀ expression). **g.** Superoxide dismutase **h.** Glutathione S-transferase **i.** Nuclear Factor Erythroid 2-related Factor 2. GAPDH was used as an internal control for data normalization. All data are representative of three independent experiments and are presented as the mean \pm SD, (One-way ANOVA test). ****P\leq 0.00001; ***P\leq 0.0001; **P\leq 0.001.

4.18 Assessment of Celecoxib's Effect on the Feeding Behavior of the Flies

Following the Cross of flies carrying $(CGG)_{90}$ with the muscle specific driver live, Mef2-GAL4, we assessed the feeding behavior of the progenies (expressing $(CGG)_{90}$ in their muscles). Taste plays a key role in helping animals choose safe, nutritious food while avoiding harmful substances. To lay the groundwork for drug-feeding experiments and better interpret future results, we tracked how larvae feed. Larvae were given access to food mixed with different doses of Celecoxib and a blue dye for two hours, and their food intake was later measured using spectrophotometry 56 . Herein, we found that no difference in the feeding behavior was observed at different Celecoxib concentrations in the case of all four strains used in the study - Mef2-GAL4>UAS- $(CGG)_{90}$ -EGFP, Mef2-GAL4>UAS-EGFP (Figure 4.22a, b).

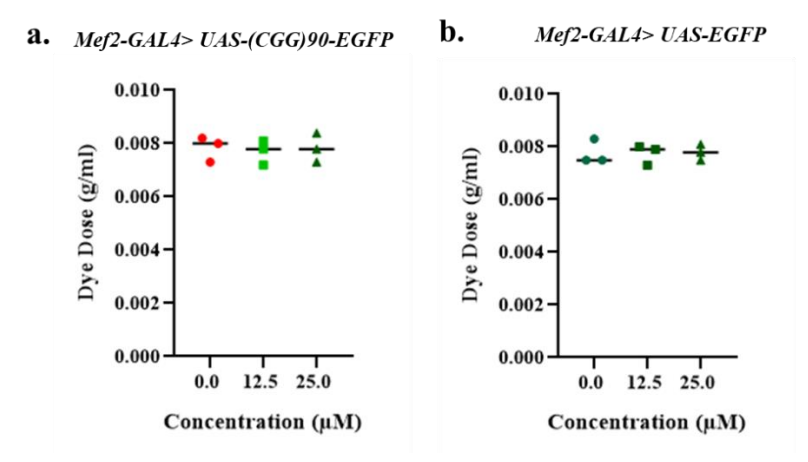


Figure 4.22 Graphs representing feeding intake of muscle specific expression flies of a. Mef2-GAL4>UAS-(CGG)90-EGFP b. Mef2-GAL4>UAS-EGFP

4.19 In vivo potency of celecoxib in reducing the FMR1PolyG inclusion in muscles tissues

Protein were extracted from the muscles of flies treated with different doses of Celecoxib were subjected to Western blot analysis. Anti-FMR1PolyG antibodies were utilized to assess FMR1PolyG protein levels in treated flies and compared with experimental control (untreated flies). Across all treatment groups, the results showed a substantial decrease in FMR1PolyG protein levels, indicating that Celecoxib effectively prevents FMR1PolyG aggregation (**Figure 4.23a, c**). Celecoxib selectively targets toxic FMR1PolyG aggregates formed due to expanded CGG repeats, as evidenced by the unchanged levels of β -actin. In contrast, flies expressing solely EGFP had no change in the levels of EGFP or β -actin (**Figure 4.23b, d**). These findings highlight the in vivo potency of Celecoxib in interfering with pathological RAN translation, effectively reducing the levels of the RAN translation product.

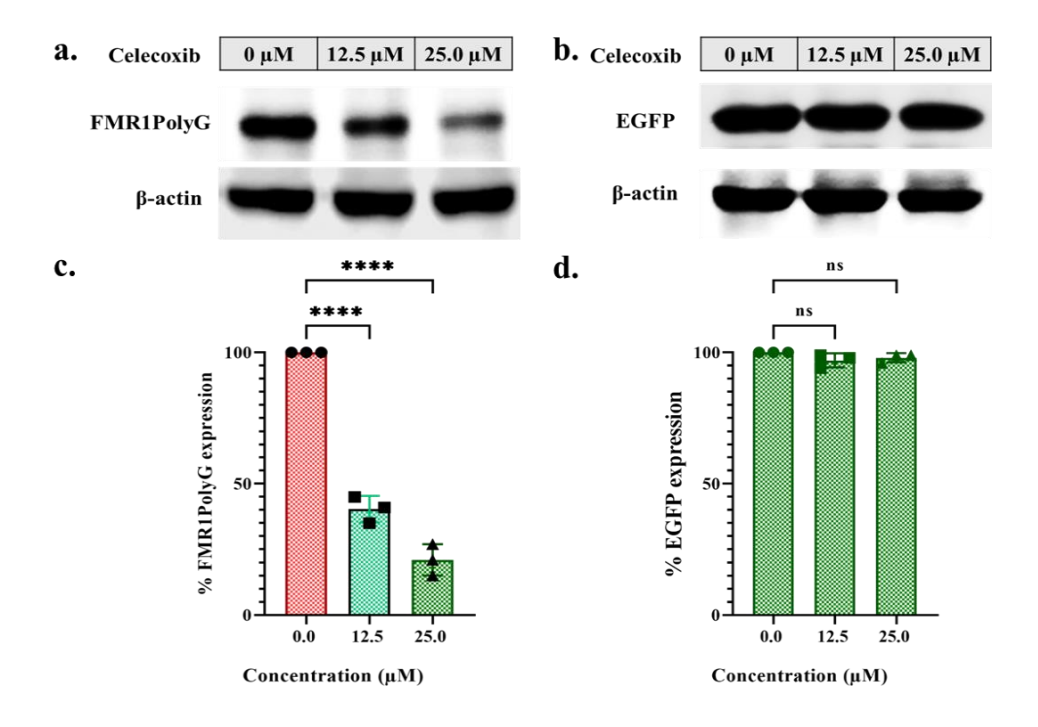


Figure 4.23 Celecoxib helps to mitigate the PolyG aggregates in muscle tissues in the FXTAS *Drosophila* model. a. Blot showing reduced PolyG expression in proteins isolated from heads of diseased flies (CGG)₉₀ treated with various Celecoxib concentrations. c. The graph illustrates the normalized percentage expression of PolyG. Data are presented as mean \pm SEM from at least three independent experiments. c. Blot showing reduced PolyG expression in proteins isolated from heads of diseased flies expressing solely EGFP treated with various Celecoxib concentrations. d. The graph illustrates the normalized percentage expression of EGFP. Data are presented as mean \pm SEM from at least three independent experiments. Statistical significance was determined using one-way ANOVA, ****P \leq 0.00001.

4.20 Celecoxib Restores muscle functioning in FMR1PolyG-Induced FXTAS *Drosophila* Model

We tested Celecoxib's effect on motor function in flies expressing *UAS-EGFP* and *UAS-(CGG)*₉₀-*EGFP* using the muscle-specific *Mef2-GAL4* driver. Larvae from the *Mef2-GAL4>UAS-(CGG)*₉₀-*EGFP* and *Mef2-GAL4>EGFP* groups were treated with varying Celecoxib doses. After treatment, third-instar larvae were subjected to a crawling assay to determine their locomotor (crawling) activity ⁸³. The findings revealed that Celecoxib treatment improved the crawling ability of larvae containing (CGG)₉₀ repeats in a dose-dependent manner. Along with the distance travelled by the larvae, we have also measure the number of contractions in treated and untreated flies. There is significant increase in the number of contraction, which directly signifies that Celecoxib treatment can significantly improve the muscle functioning (**Figure 4.24a**).

Further, the flight ability of 14-day-old male flies treated with various drug concentrations was tested to assess muscle functioning in adult flies ^{60,84}. Celecoxib did not affect the locomotion of control flies (expressing only EGFP) (**Figure 4.25b**). However, flies expressing FMR1PolyG ((CGG)₉₀) showed considerable enhancements in flight ability with increasing Celecoxib concentration. There is a significant increment in the flight percentage of flies with the increase in Celecoxib concentration, as depicted in the screen captures and the bar graph representing their average landing height (**Figure 4.25c-e**).

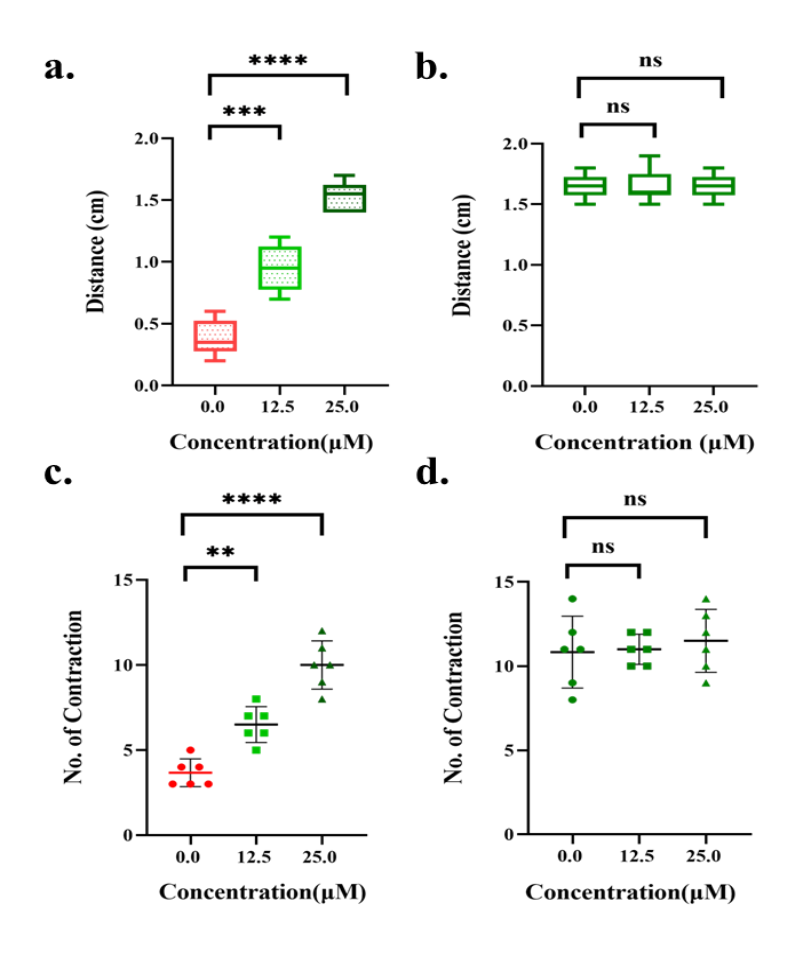


Figure 4.24 Celecoxib Restores muscle functioning in larvae of FMR1PolyG-Induced FXTAS Drosophila Model. a. Graph representing distance travelled of third-instar larvae (Mef2-GAL4>UAS-(CGG)90-EGFP) treated with Celecoxib. b. Graph representing distance travelled of third-instar larvae (Mef2-GAL4>UAS-EGFP) treated with Celecoxib. c. Graph representing number of contraction of third-instar larvae (Mef2- $GAL4 > UAS-(CGG)_{90}-EGFP$ treated with Celecoxib. d. Graph representing number of contraction of third-instar larvae (Mef2-GAL4>UAS-EGFP) treated with Celecoxib. c. Screen captures for diseased and control flies displaying the landing heights of individual flies. Each red dot represents the location of an individual fly. These landing heights are used to calculate the average landing height. d. Graph representing the average landing height (cm). e. Graph for the overall

distribution of the flies in the sheet. Data are presented as mean \pm SEM from at least three independent experiments. Statistical significance was determined using one-way ANOVA, ****P \leq 0.00001; ***P \leq 0.0001.

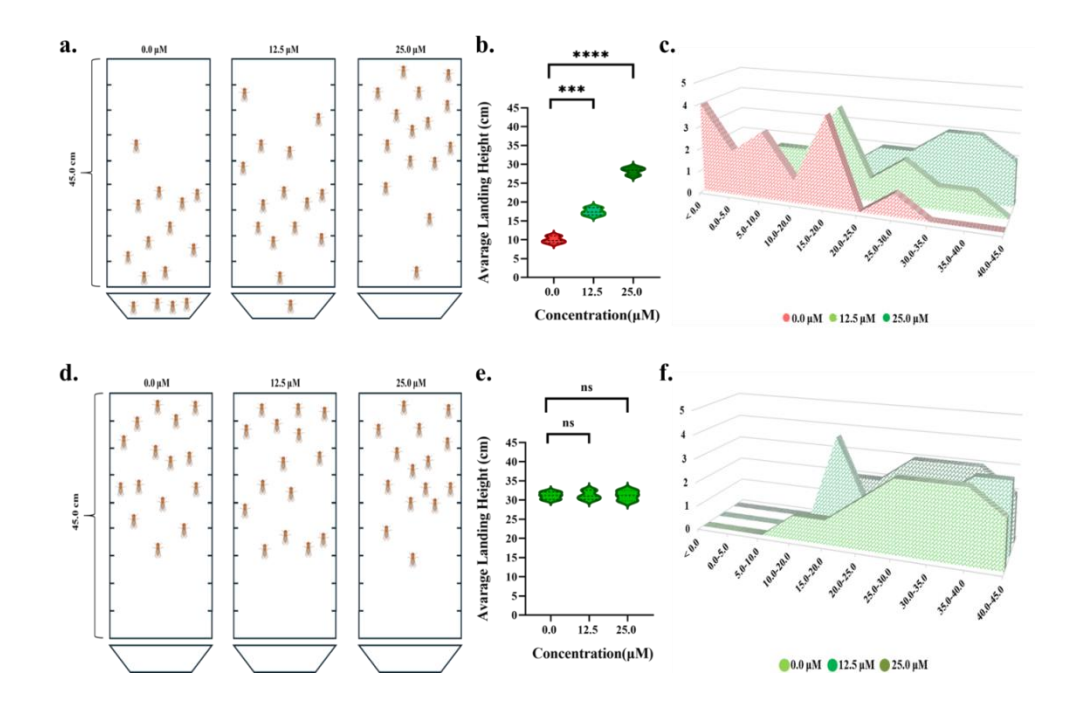


Figure 4.25 Celecoxib Restores muscle functioning in adult flies of FMR1PolyG-Induced FXTAS *Drosophila* Model a. Screen captures for diseased flies displaying the landing heights of individual flies. These landing heights are used to calculate the average landing height. b. Graph representing the average landing height (cm). c. Graph for the overall distribution of the flies in the sheet. d. Screen captures for control flies displaying the landing heights of individual flies. These landing heights are used to calculate the average landing height. e. Graph representing the average landing height (cm). f. Graph for the overall distribution of the flies in the sheet. Data are presented as mean \pm SEM from at least three independent experiments. Statistical significance was determined using one-way ANOVA, ****P \leq 0.00001; ***P \leq 0.0001.

4.13 Quantification of arbitrary ROS levels in muscles

Previous studies have shown that the accumulation of toxic CGG repeats is associated with the disruption of multiple cellular pathways, including oxidative stress and mitochondrial dysfunction, ultimately leading to increased reactive oxygen species (ROS) production ^{9,85}. To assess the steady-state ROS levels in treated and control flies, a DCF-DA assay was performed. A significant increase in ROS levels was observed in diseased flies, whereas ROS levels decreased significantly with increasing Celecoxib concentrations (**Figure 4.26a**). In contrast, no significant changes in ROS levels were detected in control flies lacking CGG repeats (**Figure 4.26b**). Further investigations are required to elucidate the precise molecular mechanisms underlying Celecoxib's protective role and to determine whether its effects extend to other cellular dysfunctions associated with FMR1PolyG toxicity.

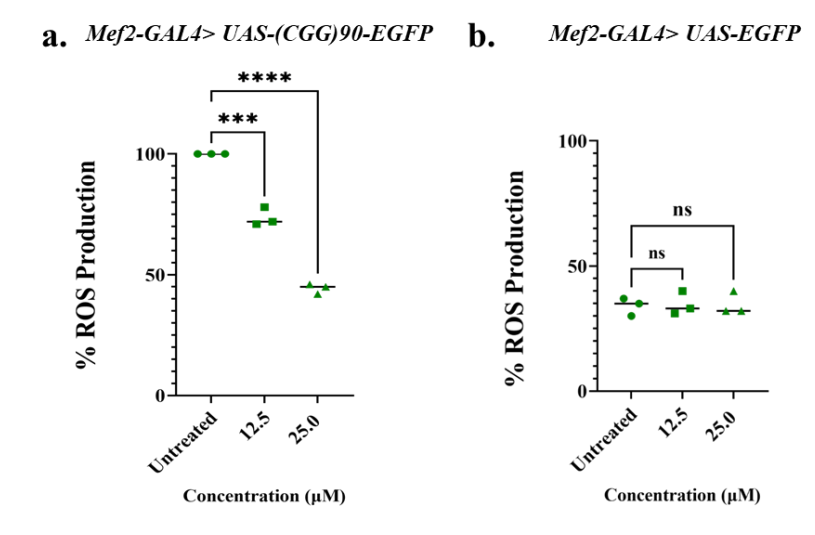


Figure 4.26 Graphs representing % ROS production in Muscle specific expression flies. a. Mef2-GAL4>UAS- $(CGG)_{90}$ -EGFP fed with different concentrations (12.5 μ M and 25.0 μ M) of Celecoxib. b. Mef2-GAL4>UAS-EGFP fed with different concentrations (12.5 μ M and 25.0

 μ M) of Celecoxib. Statistical significance was determined using one-way ANOVA, ****P \leq 0.0000; ***P \leq 0.0001.

4.16 Analysis of Lifespan Response to Celecoxib Dosage in flies expressing $(CGG)_{90}$ in the muscles

Neurodegenerative disorders, such as FXTAS, are frequently associated with a shorter lifespan ⁹². We sought to explore whether a brief period of Celecoxib treatment, applied early or late in life, could extend longevity, as early-life events significantly influence the onset of aging and, in turn, affect overall lifespan. Therefore, a lifespan analysis was conducted by feeding Celecoxib at different time points. The study demonstrated that treatment with 12.5 µM and 25.0 µM Celecoxib, from emergence, significantly improved the survival rates of flies carrying (CGG)₉₀ repeats (Figure 4.27c, d). Interestingly, even when 25.0 µM Celecoxib was administered post-eclosion from day 1 and day 7, an improvement in survivability percentage was observed (Figure 4.27e, f). In contrast, no variations in survival rates were seen in control flies expressing solely EGFP upon Celecoxib administration. These findings demonstrate that Celecoxib specifically extends the lifespan of flies with CGG repeats while not impacting the normal control flies, potentially by preventing damage accumulation and/or enhancing repair mechanisms.

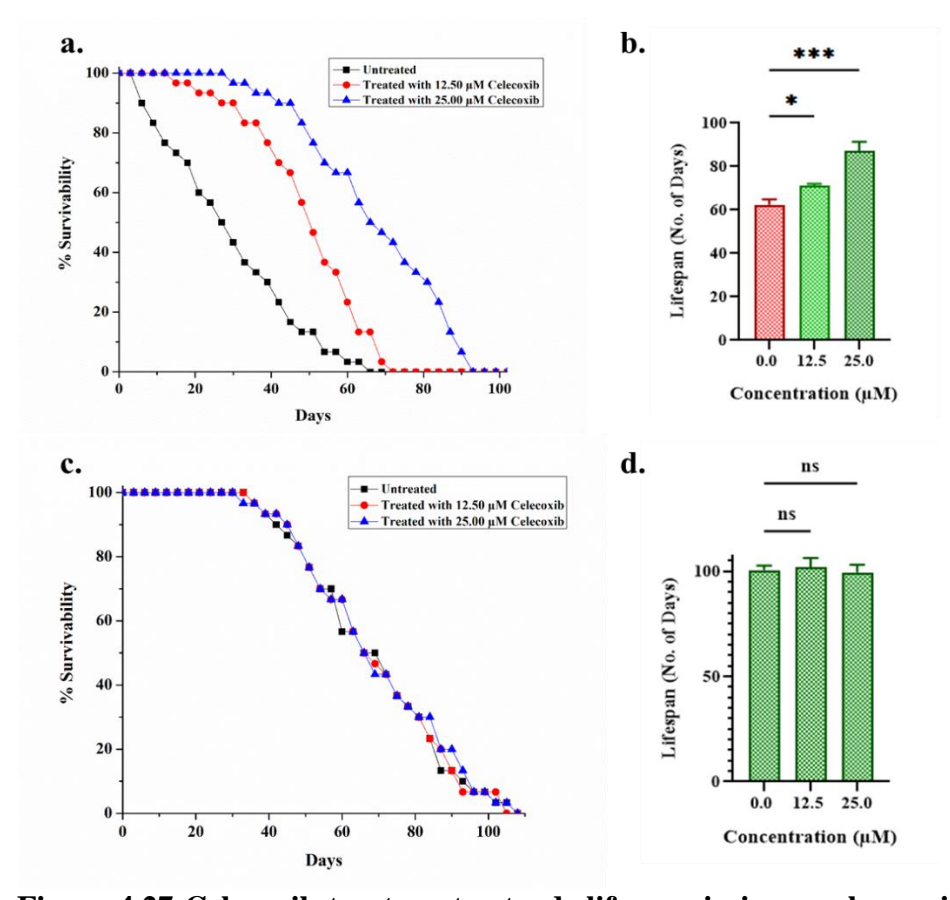


Figure 4.27 Celecoxib treatment extends lifespan in in muscle specific **expression flies a.** Survival curves of Mef2-GAL4>UAS-(CGG)₉₀-EGFP flies fed with different concentrations (12.5 µM and 25.0 µM) of Celecoxib from the larval stage. **b.** Bar graph representing lifespan (days) of *Mef2-GAL4>UAS-(CGG)*₉₀-EGFP flies fed with different concentrations (12.5 µM and 25.0 µM) of Celecoxib from the larval stage. c. Survival curves of Mef2-GAL4>UAS -EGFP flies fed with different concentrations (12.5 µM and 25.0 µM) of Celecoxib from the larval stage. **d.** Bar graph representing lifespan (days) of *Mef2-GAL4>UAS-EGFP* flies fed with different concentrations (12.5 µM and 25.0 µM) of Celecoxib from the larval stage. All data are representative of three independent experiments and are presented as the mean \pm SD, (One-way ANOVA test), *** $P \le 0.0001$; ** $P \le 0.001$.

Chapter 5

Discussion and future perspectives

The expansion of CGG repeats in the 5' UTR of mutant FMR1 transcripts is a well-established cause of FXTAS ^{4,5}. These CGG repeat sequences are known to form 1×1 GG internal hairpin and tetraplex structures, which play fundamental roles in the pathophysiology of FXTAS ^{21,46}. The CGG hairpin structures exert toxic gain-of-function effects by sequestering RNA-binding proteins into RNA foci, thereby causing widespread splicing defects ⁵. Additionally, CGG repeats undergo RAN translation, producing the toxic FMR1PolyG aggregation and further leading to several detrimental outcomes, including neuroinflammation. The selective targeting of toxic repeats bearing motifs using small molecules has emerged as a promising therapeutic strategy for neurodegenerative diseases by effectively reducing harmful consequences caused by RNA foci and FMR1PolyG aggregate formation^{20,22,23,46}. NSAIDs, which have shown efficacy in modulating neuroinflammation, a key driver of neuronal damage, hold potential as therapeutic agents in neurological diseases. Furthermore, planar small molecules exhibit an enhanced binding affinity for RNA motifs, making planar NSAIDs a compelling strategy to mitigate r(CGG)_{exp}-induced toxicity ³¹⁻³³. This approach integrates the dual benefits of targeting CGG RNA structures and reducing neuroinflammation and its downstream effects, offering a promising avenue for therapeutic development in FXTAS.

We first conducted several biophysical experiments to assess the interaction between Celecoxib and r(CGG)_{exp} RNA. Fluorescence binding assays revealed that Celecoxib exhibited a progressively enhanced binding as the number of CGG repeats increased. Circular Dichroism (CD)

spectroscopy further confirmed the binding, showing significant conformational changes in the RNA structure, including hypochromic and bathochromic shifts in the CD spectra upon binding. Gel-based assays, including Electrophoretic Mobility Shift Assay (EMSA) and PCR stop assays provided additional evidence for Celecoxib's selective binding, showing changes in band mobility and reduced PCR product amplification in the presence of the drug. Molecular docking studies further supported these findings, revealing that Celecoxib binds effectively to the GG mismatch RNA motif, primarily through hydrogen and halogen bonds with specific nucleotides (G8, G11, and G12) in the RNA structure. Together, these results mark the strong and selective interaction between Celecoxib and GG-rich RNA motifs.

Further, Celecoxib demonstrated significant therapeutic potential in a cellular FXTAS model by reducing the toxicity associated with FMR1PolyG protein aggregates and correcting pre-mRNA alternative splicing defects. In HEK-293T cells transfected with a plasmid containing (CGGx99) repeats, Celecoxib treatment reduced FMR1PolyG expression by up to 90% at concentrations of 10.0 µM, likely by interfering with the ribosomal machinery involved in non-canonical RAN translation. Confocal imaging further supported these findings by showing a decrease in FMR1PolyG protein inclusions inside the cells. Additionally, Celecoxib effectively restored normal splicing patterns in SMN2 and Bcl-x premRNAs, both of which are dysregulated in FXTAS due to the sequestration of splicing regulators by CGG repeats. A dose-dependent improvement in splicing was observed, with near-wild-type restoration achieved at 10.0 µM Celecoxib. Celecoxib's specificity for CGG repeats was confirmed, as it did not affect splicing in control cells lacking CGG repeats and showed no influence on canonical translation. These results highlight Celecoxib's potential as a targeted treatment for mitigating both the toxic effects of protein aggregation and the splicing abnormalities in FXTAS.

Thereafter, Celecoxib demonstrated potent therapeutic effects in the FXTAS Drosophila model as well, significantly mitigating pathological features associated with FXTAS. The treatment led to a marked reduction in external morphological defects, such as pigment loss and rough eye phenotypes, while protecting pigmented cells from degeneration and improving the eye phenotype at both 7 and 14 days posteclosion. Celecoxib also reduced FMR1PolyG protein aggregation, as confirmed by western blot analysis and confocal microscopy, emphasizing its ability to target CGG repeat-induced toxicity. The drug's therapeutic potential extended to improved motor function, with enhanced crawling, climbing, and flight abilities in CGG repeat-expressing flies. Furthermore, Celecoxib has shown the potential to mitigate key pathological features of FXTAS, including neuroinflammation, mitochondrial dysfunction, and cell death. Notably, by mitigating these disease-associated consequences, the treatment significantly enhances the lifespan of the treated flies compared to the diseased flies. These findings suggest that it is a promising candidate for treating FXTAS, offering both symptomatic relief and potential disease-modifying benefits.

In conclusion, Celecoxib demonstrates the potential to modulate CGG repeat-containing sequences, making it a promising candidate for the prevention and treatment of FXTAS, a neurodegenerative disorder linked to CGG expansions. Experimental data from FXTAS cellular and *Drosophila* models show Celecoxib's in vitro and in vivo potency in efficiently inhibiting the RNA toxicity and aggregation of the RAN translation product (FMR1PolyG) and associated downstream consequences, supporting its further exploration in higher FXTAS animal models. This approach offers a transformative strategy for a wide range of

diseases having comparable mechanisms, with the potential to lead to innovative therapeutic interventions for RNA-mediated diseases.

Appendix

Table S1. The dissociation constant (K_d) values of Celecoxib with $r(CGG)_{exp}$ and different RNA and DNA controls were determined through fluorescence titration assays.

Sl No.	RNA	$\underline{K}_{\underline{d}}(\mu M)$
1.	r(CGGx1)	4.548
2.	r(CGGx2)	4.3697
3.	r(CGGx3)	4.1549
4.	r(CGGx4)	3.0737
5.	r(CGGx6)	2.3893
6.	r(CGGx20)	2.1666
7.	r(CGGx40)	1.2784
8.	r(CGGx60)	0.6467
9.	r(CGGx99)	0.4909
10.	r(5'CAG/3'CGG)	5.1187
11.	r(5'CCG/3'CAG)	4.8905
12.	r(5'CGG/3'CAG)	10.9387
13.	r(5'CCG/3'CUG)	6.8818
14.	r(5'CAG/3'CCG)	9.2113
15.	r(5'CUG/3'CCG)	4.8562
16.	r(5'CGG/3'CGG)	4.3239
17.	r(5'CAG/3'CAG)	5.6682
18.	r(5°CCG/3°CCG)	5.9893

19.	r(5'CUG/3'CUG)	4.0881
20.	r(AUx1)	4.9591
21.	r(AUx6)	4.6863
22.	CT DNA	53.8281
23.	c- Myc DNA	16.3310
24.	Bcl-2 DNA	9.1998
25.	HRAS1 DNA	32.3357
26.	HRAS2 DNA	12.8853
27.	r(CUGx6)	8.8488
28.	r(CAGx6)	5.0437
29.	r(CCGx6)	8.7908

Table S2. Thermodynamic parameters of $r(CGG)_{exp}$ and $r(AU)_6$ duplex RNAs with Celecoxib derived from isothermal titration calorimetry utilizing dual-mode curve fitting.

Sl.no	Parameters	Celecoxib					
		r(CGGx6)	r(CGGx20)	r(CGGx40)	r(CGGx60)	r(CGGx99)	r(AUx6)
1.	N1 (sites)	1.33	0.260	2.13	1.67	13.3	0.900
2.	K1 (M ⁻¹)	1.9E5	6.78E7	2.6E7	8.39E7	5.76E8	2.9E3

3.	ΔH1 cal/mol	0.541E4	6.552E6	1.631E7	5.252E4	-7998	5.232E4
		***************************************	3.00	-100-1-1		.,,,	
4.	ΔS1	4.17E4	2.20E4	5.47E4	290	-0.446	2.20E4
	cal/mol/deg						
	G						
5.	N2 (sites)	7.68	20.7	8.48	3.18	4.22E-8	18.7
	Ì						
6.	K2 (M ⁻¹)	0.95E5	6.80E6	1.85E6	9.00E5	6.29E4	5.10E3
7.	∆H2 cal/mol	-1.130E4	-8.772E4	-1.030E4	-6.546E4	2799	-8.772E3
8.	ΔS1	495	-263	85.5	-105	31.3	263
] "		.,,,	203	00.0	100	00	200
	cal/mol/deg						

Table S3. Sequences of PCR primers used for the assay of alternative splicing defects.

Sl.	Gene	Forwards primer	Reverse primer
No.			
1.	SMN2	5'GGTGTCCACTCCCAGTTC	5'GCCTCACCACCGTGCTGG
	mini-	AA	
	gene		
2.	cTNT	5'GTTCACAACCATCTAAAG	5'GTTGCATGGCTGGTGCAGG
	mini-	CAAGATG	
	gene		
3.	β-Actin	5'	5' GGGCCGGACTCGTCATAC
		CCTGGCACCCAGCACAAT	

4.	(CGG)99	5'GCACGACTTCTTCAAGTC	5'GCGGATCTTGAAGTTCACC
	-EGFP	CGCCATGCC	TTGATGCC

Table S4. Sequences of PCR primers used for the assay of alternative splicing defects.

Sl.	Gene	Forwards primer	Reverse primer
No.			
1.	Atg1	5'GGATTTTGGGTTTGCGCG	5'CAGAGATCCGCCTTGGAG
		AT	TC
2.	Atg4b	5'GACCATTGTAGAGGGTAG	5'CGATGAATCGTCTGTATG
		CCG	GGG
3.	Atg5	5'ATATGCTTCCAGGCGGAT	5'
		CG	AACCACACAGCTCCATCCT
			G
4.	Atg7	5'GATGTTACGGCCCCTGGA	5'
		AA	GCCAGCTCCTTACGAGGAT
			G

_	Atg8a	5'TCTAGCCACAGCAGTTAG	5'
5.	Aigoa		
		CG	TTGTGTAGAGTGACCGTGC
			G
6.	Atg101	5'	5' GATGTGTCGAAGATCAG
		GAGGTGTGGACGGTGCACC	
7.	Nrf2	5'	5'
		AGCTTCTGTCGCATGGTTG	AGCCGTTGCTAACATGTCC
		A	A
8.	GSTs	5'	5'
		CAGACCGTCAAGGACAAC	TCGCGCTTGACCATGTAGT
		GA	Т 3'
9.	SOD	5'	5'
		ACCGACTCCAAGATTACGC	GTTGCCCGTTGACTTGCTC
		TCT	
10.	GAPDH	5'TAAATTCGACTCGACTCA	5'CTCCACCACATACTCGGC
		CGGT	TC

References

- (1) Ibañez, K.; Jadhav, B.; Zanovello, M.; Gagliardi, D.; Clarkson, C.; Facchini, S.; Garg, P.; Martin-Trujillo, A.; Gies, S. J.; Galassi Deforie, V.; Dalmia, A.; Hensman Moss, D. J.; Vandrovcova, J.; Rocca, C.; Moutsianas, L.; Marini-Bettolo, C.; Walker, H.; Turner, C.; Shoai, M.; Long, J. D.; Fratta, P.; Langbehn, D. R.; Tabrizi, S. J.; Caulfield, M. J.; Cortese, A.; Escott-Price, V.; Hardy, J.; Houlden, H.; Sharp, A. J.; Tucci, A. Increased Frequency of Repeat Expansion Mutations across Different 30 Populations. Nat. Med.2024. (11),3357-3368. https://doi.org/10.1038/s41591-024-03190-5.
- (2) Depienne, C.; Mandel, J.-L. 30 Years of Repeat Expansion Disorders: What Have We Learned and What Are the Remaining Challenges? *Am. J. Hum. Genet.* **2021**, *108* (5), 764–785. https://doi.org/10.1016/j.ajhg.2021.03.011.
- (3) Paulson, H. Chapter 9 Repeat Expansion Diseases. In *Handbook of Clinical Neurology*; Geschwind, D. H., Paulson, H. L., Klein, C., Eds.; Neurogenetics, Part I; Elsevier, 2018; Vol. 147, pp 105–123. https://doi.org/10.1016/B978-0-444-63233-3.00009-9.
- (4) Sellier, C.; Buijsen, R. A. M.; He, F.; Natla, S.; Jung, L.; Tropel, P.; Gaucherot, A.; Jacobs, H.; Meziane, H.; Vincent, A.; Champy, M.-F.; Sorg, T.; Pavlovic, G.; Wattenhofer-Donze, M.; Birling, M.-C.; Oulad-Abdelghani, M.; Eberling, P.; Ruffenach, F.; Joint, M.; Anheim, M.; Martinez-Cerdeno, V.; Tassone, F.; Willemsen, R.; Hukema, R. K.; Viville, S.; Martinat, C.; Todd, P. K.; Charlet-Berguerand, N. Translation of Expanded CGG Repeats into FMRpolyG Is Pathogenic and May Contribute to Fragile X Tremor Ataxia Syndrome. *Neuron* **2017**, *93* (2), 331–347. https://doi.org/10.1016/j.neuron.2016.12.016.

- (5) Glineburg, M. R.; Todd, P. K.; Charlet-Berguerand, N.; Sellier, C. Repeat-Associated Non-AUG (RAN) Translation and Other Molecular Mechanisms in Fragile X Tremor Ataxia Syndrome. *Brain Res.* **2018**, *1693*, 43–54. https://doi.org/10.1016/j.brainres.2018.02.006.
- (6) Leehey, M. A. Fragile X-Associated Tremor/Ataxia Syndrome: Clinical Phenotype, Diagnosis, and Treatment. *J. Investig. Med. Off. Publ. Am. Fed. Clin. Res.* **2009**, *57* (8), 830–836. https://doi.org/10.2310/JIM.0b013e3181af59c4.
- (7) Kong, H. E.; Zhao, J.; Xu, S.; Jin, P.; Jin, Y. Fragile X-Associated Tremor/Ataxia Syndrome: From Molecular Pathogenesis to Development of Therapeutics. *Front. Cell. Neurosci.* **2017**, *11*. https://doi.org/10.3389/fncel.2017.00128.
- (8) Role of neuroinflammation in neurodegeneration development / Signal Transduction and Targeted Therapy. https://www.nature.com/articles/s41392-023-01486-5#citeas.
- (9) Gohel, D.; Berguerand, N. C.; Tassone, F.; Singh, R. The Emerging Molecular Mechanisms for Mitochondrial Dysfunctions in FXTAS. *Biochim. Biophys. Acta BBA Mol. Basis Dis.* **2020**, *1866* (12), 165918. https://doi.org/10.1016/j.bbadis.2020.165918.
- (10) Alvarez-Mora, M. I.; Garrabou, G.; Molina-Porcel, L.; Grillo-Risco, R.; Garcia-Garcia, F.; Barcos, T.; Cantó-Santos, J.; Rodriguez-Revenga, L. Exploration of SUMO2/3 Expression Levels and Autophagy Process in Fragile X-Associated Tremor/Ataxia Syndrome: Addressing Study Limitations and Insights for Future Research. *Cells* **2023**, *12* (19), 2364. https://doi.org/10.3390/cells12192364.
- (11) Grandi, M.; Galber, C.; Gatto, C.; Nobile, V.; Pucci, C.; Schaldemose Nielsen, I.; Boldrin, F.; Neri, G.; Chiurazzi, P.; Solaini, G.; Baracca, A.; Giorgio, V.; Tabolacci, E. Mitochondrial Dysfunction Causes

- Cell Death in Patients Affected by Fragile-X-Associated Disorders. *Int. J. Mol. Sci.* **2024**, *25* (6), 3421. https://doi.org/10.3390/ijms25063421.
- (12) Muzar, Z.; Lozano, R. Current Research, Diagnosis, and Treatment of Fragile X-Associated Tremor/Ataxia Syndrome. *Intractable Rare Dis. Res.* **2014**, *3* (4), 101–109. https://doi.org/10.5582/irdr.2014.01029.
- (13) Boivin, M.; Willemsen, R.; Hukema, R. K.; Sellier, C. Potential Pathogenic Mechanisms Underlying Fragile X Tremor Ataxia Syndrome: RAN Translation and/or RNA Gain-of-Function? *Eur. J. Med. Genet.* **2018**, *61* (11), 674–679. https://doi.org/10.1016/j.ejmg.2017.11.001.
- (14) Evers, M. M.; Toonen, L. J. A.; van Roon-Mom, W. M. C. Antisense Oligonucleotides in Therapy for Neurodegenerative Disorders. *Adv. Drug Deliv. Rev.* **2015**, *87*, 90–103. https://doi.org/10.1016/j.addr.2015.03.008.
- (15) Angelbello, A. J.; Chen, J. L.; Disney, M. D. Small Molecule Targeting of RNA Structures in Neurological Disorders. *Ann. N. Y. Acad. Sci.* **2020**, *1471* (1), 57–71. https://doi.org/10.1111/nyas.14051.
- (16) Kumar, A.; Parkesh, R.; Sznajder, L. J.; Childs-Disney, J. L.; Sobczak, K.; Disney, M. D. Chemical Correction of Pre-mRNA Splicing Defects Associated with Sequestration of Muscleblind-like 1 Protein by Expanded r(CAG)-Containing Transcripts. *ACS Chem. Biol.* **2012**, *7* (3), 496–505. https://doi.org/10.1021/cb200413a.
- (17) Discovery of a potent small molecule inhibiting Huntington's disease (HD) pathogenesis via targeting CAG repeats RNA and Poly Q protein / Scientific Reports. https://www.nature.com/articles/s41598-019-53410-z.
- (18) Myricetin Reduces Toxic Level of CAG Repeats RNA in Huntington's Disease (HD) and Spino Cerebellar Ataxia (SCAs) | ACS

- Chemical Biology. https://pubs.acs.org/doi/10.1021/acschembio.7b00699 (accessed 2024-12-01).
- (19) Yang, W.-Y.; Wilson, H. D.; Velagapudi, S. P.; Disney, M. D. Inhibition of Non-ATG Translational Events in Cells via Covalent Small Molecules Targeting RNA. *J. Am. Chem. Soc.* **2015**, *137* (16), 5336–5345. https://doi.org/10.1021/ja507448y.
- (20) Verma, A. K.; Khan, E.; Mishra, S. K.; Kumar, A. Small Molecule Screening Discovers Compounds That Reduce FMRpolyG Protein Aggregates and Splicing Defect Toxicity in Fragile X-Associated Tremor/Ataxia Syndrome. *Mol. Neurobiol.* **2022**, *59* (3), 1992–2007. https://doi.org/10.1007/s12035-021-02697-z.
- (21) Verma, A. K.; Khan, E.; Mishra, S. K.; Mishra, A.; Charlet-Berguerand, N.; Kumar, A. Curcumin Regulates the r(CGG)Exp RNA Hairpin Structure and Ameliorate Defects in Fragile X-Associated Tremor Ataxia Syndrome. *Front. Neurosci.* **2020**, *14*. https://doi.org/10.3389/fnins.2020.00295.
- (22) Verma, A. K.; Khan, E.; Mishra, S. K.; Jain, N.; Kumar, A. Piperine Modulates Protein Mediated Toxicity in Fragile X-Associated Tremor/Ataxia Syndrome through Interacting Expanded CGG Repeat (r(CGG)Exp) RNA. *ACS Chem. Neurosci.* **2019**, *10* (8), 3778–3788. https://doi.org/10.1021/acschemneuro.9b00282.
- (23) Disney, M. D.; Liu, B.; Yang, W.-Y.; Sellier, C.; Tran, T.; Charlet-Berguerand, N.; Childs-Disney, J. L. A Small Molecule That Targets r(CGG)Exp and Improves Defects in Fragile X-Associated Tremor Ataxia Syndrome. *ACS Chem. Biol.* **2012**, *7* (10), 1711–1718. https://doi.org/10.1021/cb300135h.
- (24) Hoskins, J. W.; Ofori, L. O.; Chen, C. Z.; Kumar, A.; Sobczak, K.; Nakamori, M.; Southall, N.; Patnaik, S.; Marugan, J. J.; Zheng, W.; Austin,

- C. P.; Disney, M. D.; Miller, B. L.; Thornton, C. A. Lomofungin and Dilomofungin: Inhibitors of MBNL1-CUG RNA Binding with Distinct Cellular Effects. *Nucleic Acids Res.* **2014**, *42* (10), 6591–6602. https://doi.org/10.1093/nar/gku275.
- (25) Design of a Bioactive Small Molecule That Targets the Myotonic Dystrophy Type 1 RNA via an RNA Motif—Ligand Database and Chemical Similarity Searching / Journal of the American Chemical Society. https://pubs.acs.org/doi/10.1021/ja210088v (accessed 2024-12-01).
- (26) Rationally Designed Small Molecules Targeting the RNA That Causes Myotonic Dystrophy Type 1 Are Potently Bioactive / ACS Chemical Biology. https://pubs.acs.org/doi/10.1021/cb200408a.
- (27) Saranraj, K.; Kiran, P. U. Drug Repurposing: Clinical Practices and Regulatory Pathways. *Perspect. Clin. Res.* 10.4103/picr.picr_70_24. https://doi.org/10.4103/picr.picr_70_24.
- (28) Drug Repurposing (DR): An Emerging Approach in Drug Discovery | IntechOpen. https://www.intechopen.com/chapters/72744.
- (29) Dutra, M.; Covas da Silva, S.; da Silva Beggiora Marques, P.; Oliveira Amaral, I.; Funo de Souza, S. N.; Dutra, L. A.; Volpon Santos, M.; Machado, H. R.; da Silva Lopes, L. Celecoxib Attenuates Neuroinflammation, Reactive Astrogliosis and Promotes Neuroprotection in Young Rats with Experimental Hydrocephalus. *J. Chem. Neuroanat.* **2023**, *133*, 102344. https://doi.org/10.1016/j.jchemneu.2023.102344.
- (30) Frontiers | Ibuprofen Treatment Reduces the Neuroinflammatory Response and Associated Neuronal and White Matter Impairment in the Growth Restricted Newborn. https://www.frontiersin.org/journals/physiology/articles/10.3389/fphys.201 9.00541/full (accessed 2025-03-20).

- (31) Rivers-Auty, J.; Mather, A. E.; Peters, R.; Lawrence, C. B.; Brough, D.; Alzheimer's Disease Neuroimaging Initiative. Anti-Inflammatories in Alzheimer's Disease—Potential Therapy or Spurious Correlate? *Brain Commun.* **2020**, 2 (2), fcaa109. https://doi.org/10.1093/braincomms/fcaa109.
- (32) Moussa, N.; Dayoub, N. Exploring the Role of COX-2 in Alzheimer's Disease: Potential Therapeutic Implications of COX-2 Inhibitors. *Saudi Pharm. J.* **2023**, *31* (9), 101729. https://doi.org/10.1016/j.jsps.2023.101729.
- (33) Zhu, Y.; Yao, R.; Li, Y.; Wu, C.; Heng, L.; Zhou, M.; Yan, L.; Deng, Y.; Zhang, Z.; Ping, L.; Wu, Y.; Wang, S.; Wang, L. Protective Effect of Celecoxib on Early Postoperative Cognitive Dysfunction in Geriatric Patients. *Front. Neurol.* **2018**, 9. https://doi.org/10.3389/fneur.2018.00633.
- (34) Microglial cell activation and senescence are characteristic of the pathology FXTAS Martínez Cerdeño 2018 Movement Disorders Wiley Online Library. https://movementdisorders.onlinelibrary.wiley.com/doi/10.1002/mds.2755 3.
- (35) Composition of the Intranuclear Inclusions of Fragile X-associated Tremor/Ataxia Syndrome | Acta Neuropathologica Communications | Full Text. https://actaneurocomms.biomedcentral.com/articles/10.1186/s40478-019-0796-1.
- (36) Klegeris, A.; McGeer, P. L. Non-Steroidal Anti-Inflammatory Drugs (NSAIDs) and Other Anti-Inflammatory Agents in the Treatment of Neurodegenerative Disease. http://www.eurekaselect.com.
- (37) Vieira, C. P.; Lelis, C. A.; Ochioni, A. C.; Rosário, D. K. A.; Rosario, I. L. S.; Vieira, I. R. S.; Carvalho, A. P. A.; Janeiro, J. M.; da

- Costa, M. P.; Lima, F. R. S.; Mariante, R. M.; Alves, L. A.; Foguel, D.; Junior, C. A. C. Estimating the Therapeutic Potential of NSAIDs and Linoleic Acid-Isomers Supplementation against Neuroinflammation. *Biomed. Pharmacother.* **2024**, *177*, 116884. https://doi.org/10.1016/j.biopha.2024.116884.
- (38) Guzman-Martinez, L.; Maccioni, R. B.; Andrade, V.; Navarrete, L. P.; Pastor, M. G.; Ramos-Escobar, N. Neuroinflammation as a Common Feature of Neurodegenerative Disorders. *Front. Pharmacol.* **2019**, *10*. https://doi.org/10.3389/fphar.2019.01008.
- (39) Clemett, D.; Goa, K. L. Celecoxib. *Drugs* **2000**, *59* (4), 957–980. https://doi.org/10.2165/00003495-200059040-00017.
- (40) Gong, L.; Thorn, C. F.; Bertagnolli, M. M.; Grosser, T.; Altman, R. B.; Klein, T. E. Celecoxib Pathways: Pharmacokinetics and Pharmacodynamics. *Pharmacogenet. Genomics* **2012**, *22* (4), 310. https://doi.org/10.1097/FPC.0b013e32834f94cb.
- (41) Dassati, S.; Schweigreiter, R.; Buechner, S.; Waldner, A. Celecoxib Promotes Survival and Upregulates the Expression of Neuroprotective Marker Genes in Two Different in Vitro Models of Parkinson's Disease. *Neuropharmacology* **2021**, *194*, 108378. https://doi.org/10.1016/j.neuropharm.2020.108378.
- (42) Kury, L. T. A.; Zeb, A.; Abidin, Z. U.; Irshad, N.; Malik, I.; Alvi, A. M.; Khalil, A. A. K.; Ahmad, S.; Faheem, M.; Khan, A.-U.; Shah, F. A.; Li, S. Neuroprotective Effects of Melatonin and Celecoxib against Ethanol-Induced Neurodegeneration: A Computational and Pharmacological Approach
 P>. Drug Des. Devel. Ther. 2019, 13, 2715–2727. https://doi.org/10.2147/DDDT.S207310.
- (43) Gou, J.; Liang, S.; Cheng, W.; Wu, S.; Ye, Z.; Ma, Y.; Yin, Y.; Wang, H. Neuroprotective Effect of Combined Use of Nicotine and

Celecoxib by Inhibiting Neuroinflammation in Ischemic Rats. *Brain Res. Bull.* **2021**, *175*, 234–243. https://doi.org/10.1016/j.brainresbull.2021.07.022.

- (44) Zheng, X.; Zhang, C.; Li, L.; Ye, J.; Ren, S.; Zhang, Z.; He, X.; Chu, S.; Chen, N. Improvement of Astrocytic Gap Junction Involves the Anti-Depressive Effect of Celecoxib through Inhibition of NF-κB. *Brain Res. Bull.* **2024**, 207, 110871. https://doi.org/10.1016/j.brainresbull.2024.110871.
- (45) Targeting RNA with Small Molecules To Capture Opportunities at the Intersection of Chemistry, Biology, and Medicine | Journal of the American Chemical Society. https://pubs.acs.org/doi/10.1021/jacs.8b13419.
- (46) Singh, K.; Shukla, S.; Ghosh, T.; Das, A. K.; Kumar, A. Tyrosine Peptides Alleviates Multifaceted Toxicity Linked to Expanded CGG Repeats in Fragile X-Associated Tremor/Ataxia Syndrome. *ACS Pharmacol. Transl. Sci.* **2025**. https://doi.org/10.1021/acsptsci.4c00647.
- (47) Elucidating the pathobiology of Cerebellar Ataxia with Neuropathy and Vestibular Areflexia Syndrome (CANVAS) with its expanded RNA structure formation and proteinopathy / Scientific Reports. https://www.nature.com/articles/s41598-024-78947-6.
- (48) Repurposing Oseltamivir Against CAG Repeat Mediated Toxicity in Huntington's Disease and Spinocerebellar Ataxia Using Cellular and Drosophila Model / ACS Omega. https://pubs.acs.org/doi/10.1021/acsomega.4c10338.
- (49) Salim, N. N.; Feig, A. L. Isothermal Titration Calorimetry of RNA. *Methods* **2009**, *47* (3), 198–205. https://doi.org/10.1016/j.ymeth.2008.09.003.

- (50) Characterization of highly conserved G-quadruplex motifs as potential drug targets in Streptococcus pneumoniae | Scientific Reports. https://www.nature.com/articles/s41598-018-38400-x.
- (51) A Crystal Structure of a Model of the Repeating r(CGG) Transcript Found in Fragile X Syndrome Kumar 2011 ChemBioChem Wiley Online Library. https://chemistry-europe.onlinelibrary.wiley.com/doi/10.1002/cbic.201100337.
- (52) Genetic Suppression of Polyglutamine Toxicity in Drosophila / Science. https://www.science.org/doi/10.1126/science.287.5459.1837.
- (53) Koushika, S. P.; Lisbin, M. J.; White, K. ELAV, a *Drosophila* Neuron-Specific Protein, Mediates the Generation of an Alternatively Spliced Neural Protein Isoform. *Curr. Biol.* **1996**, *6* (12), 1634–1641. https://doi.org/10.1016/S0960-9822(02)70787-2.
- (54) The commonly used eye-specific sev-GAL4 and GMR-GAL4 drivers in Drosophila melanogaster are expressed in tissues other than eyes also / Journal of Genetics. https://link.springer.com/article/10.1007/s12041-015-0535-8.
- (55) Increase in brain glycogen levels ameliorates Huntington's disease phenotype and rescues neurodegeneration in Drosophila | Disease Models & Mechanisms | The Company of Biologists. https://journals.biologists.com/dmm/article/16/10/dmm050238/333679/Inc rease-in-brain-glycogen-levels-ameliorates.
- (56) Chongtham, A.; Agrawal, N. Curcumin Modulates Cell Death and Is Protective in Huntington's Disease Model. *Sci. Rep.* **2016**, *6*, 18736. https://doi.org/10.1038/srep18736.
- (57) Quantitative Assessment of Eye Phenotypes for Functional Genetic Studies Using Drosophila melanogaster | G3 Genes|Genomes|Genetics |

Oxford Academic. https://academic.oup.com/g3journal/article/6/5/1427/6027498.

(58) Stages of embryonic development of the zebrafish - Kimmel - 1995 - Developmental Dynamics - Wiley Online Library. https://anatomypubs.onlinelibrary.wiley.com/doi/10.1002/aja.1002030302.

- (59) Wolff, T. Preparation of Drosophila Eye Specimens for Scanning Electron Microscopy. *Cold Spring Harb. Protoc.* **2011**, *2011* (11), pdb.prot066506. https://doi.org/10.1101/pdb.prot066506.
- (60) Babcock, D. T.; Ganetzky, B. An Improved Method for Accurate and Rapid Measurement of Flight Performance in Drosophila. *J. Vis. Exp. JoVE* **2014**, No. 84, e51223. https://doi.org/10.3791/51223.
- (61) Protein Extraction From Drosophila Heads / SpringerLink. https://link.springer.com/protocol/10.1007/978-1-59745-257-1_27.
- (62) Hafer, N.; Schedl, P. Dissection of Larval CNS in Drosophila Melanogaster. *J. Vis. Exp. JoVE* **2006**, No. 1, e85. https://doi.org/10.3791/85.
- (63) Verma, P.; Singh, A.; Nthenge-Ngumbau, D. N.; Rajamma, U.; Sinha, S.; Mukhopadhyay, K.; Mohanakumar, K. P. Attention Deficit-Hyperactivity Disorder Suffers from Mitochondrial Dysfunction. *BBA Clin.* **2016**, *6*, 153–158. https://doi.org/10.1016/j.bbacli.2016.10.003.
- (64) Identification of methotrexate as a heterochromatin-promoting drug / Scientific Reports. https://www.nature.com/articles/s41598-019-48137-w.
- (65) Analysis of Drosophila melanogaster Lifespan / SpringerLink. https://link.springer.com/protocol/10.1007/978-1-0716-0592-9_4.

- (66) Diet-MEF2 interactions shape lipid droplet diversification in muscle to influence Drosophila lifespan Zhao 2020 Aging Cell Wiley Online Library. https://onlinelibrary.wiley.com/doi/10.1111/acel.13172.
- (67) Measurement of DCF fluorescence as a measure of reactive oxygen species in murine islets of Langerhans Analytical Methods (RSC Publishing).

https://pubs.rsc.org/en/content/articlelanding/2014/ay/c4ay00288a.

- (68) Exposure of Drosophila melanogaster to Mancozeb Induces Oxidative Damage and Modulates Nrf2 and HSP70/83 Saraiva 2018 Oxidative Medicine and Cellular Longevity Wiley Online Library. https://onlinelibrary.wiley.com/doi/10.1155/2018/5456928.
- (69) Survey of the year 2009: applications of isothermal titration calorimetry Falconer 2011 Journal of Molecular Recognition Wiley Online Library. https://onlinelibrary.wiley.com/doi/10.1002/jmr.1073.
- (70) Applications of isothermal titration calorimetry in RNA biochemistry and biophysics Feig 2007 Biopolymers Wiley Online Library. https://onlinelibrary.wiley.com/doi/10.1002/bip.20816 (accessed 2025-05-01).
- (71) Energetics of DNA Intercalation Reactions / Biochemistry. https://pubs.acs.org/doi/10.1021/bi000474a.
- (72) Circular dichroism and conformational polymorphism of DNA / Nucleic Acids Research / Oxford Academic. https://academic.oup.com/nar/article/37/6/1713/1030465.
- (73) Structural Insight into the interaction of Flavonoids with Human Telomeric Sequence / Scientific Reports. https://www.nature.com/articles/srep17574.

- (74) Sellier, C.; Freyermuth, F.; Tabet, R.; Tran, T.; He, F.; Ruffenach, F.; Alunni, V.; Moine, H.; Thibault, C.; Page, A.; Tassone, F.; Willemsen, R.; Disney, M. D.; Hagerman, P. J.; Todd, P. K.; Charlet-Berguerand, N. Sequestration of DROSHA and DGCR8 by Expanded CGG RNA Repeats Alters MicroRNA Processing in Fragile X-Associated Tremor/Ataxia Syndrome. *Cell Rep.* **2013**, *3* (3), 869–880. https://doi.org/10.1016/j.celrep.2013.02.004.
- (75) Sofola, O. A.; Jin, P.; Qin, Y.; Duan, R.; Liu, H.; de Haro, M.; Nelson, D. L.; Botas, J. RNA-Binding Proteins hnRNP A2/B1 and CUGBP1 Suppress Fragile X CGG Premutation Repeat-Induced Neurodegeneration in a *Drosophila* Model of FXTAS. *Neuron* **2007**, *55* (4), 565–571. https://doi.org/10.1016/j.neuron.2007.07.021.
- (76) Sellier, C.; Rau, F.; Liu, Y.; Tassone, F.; Hukema, R. K.; Gattoni, R.; Schneider, A.; Richard, S.; Willemsen, R.; Elliott, D. J.; Hagerman, P. J.; Charlet-Berguerand, N. Sam68 Sequestration and Partial Loss of Function Are Associated with Splicing Alterations in FXTAS Patients. *EMBO J.* **2010**, *29* (7), 1248–1261. https://doi.org/10.1038/emboj.2010.21.
- (77) Jin, P.; Duan, R.; Qurashi, A.; Qin, Y.; Tian, D.; Rosser, T. C.; Liu, H.; Feng, Y.; Warren, S. T. Pur α Binds to rCGG Repeats and Modulates Repeat-Mediated Neurodegeneration in a *Drosophila* Model of Fragile X Tremor/Ataxia Syndrome. *Neuron* **2007**, *55* (4), 556–564. https://doi.org/10.1016/j.neuron.2007.07.020.
- (78) Cleary, J. D.; Pattamatta, A.; Ranum, L. P. W. Repeat-Associated Non-ATG (RAN) Translation. *J. Biol. Chem.* **2018**, 293 (42), 16127–16141. https://doi.org/10.1074/jbc.R118.003237.
- (79) Wojciechowska, M.; Olejniczak, M.; Galka-Marciniak, P.; Jazurek, M.; Krzyzosiak, W. J. RAN Translation and Frameshifting as Translational Challenges at Simple Repeats of Human Neurodegenerative Disorders.

- *Nucleic Acids Res.* **2014**, *42* (19), 11849–11864. https://doi.org/10.1093/nar/gku794.
- (80) Talebi, M.; Mohammadi Vadoud, S. A.; Haratian, A.; Talebi, M.; Farkhondeh, T.; Pourbagher-Shahri, A. M.; Samarghandian, S. The Interplay between Oxidative Stress and Autophagy: Focus on the Development of Neurological Diseases. *Behav. Brain Funct.* **2022**, *18* (1), 3. https://doi.org/10.1186/s12993-022-00187-3.
- (81) Bao, S. Two Themes on the Assembly of the *Drosophila* Eye. In *Current Topics in Developmental Biology*; Cagan, R. L., Reh, T. A., Eds.; Invertebrate and Vertebrate Eye Development; Academic Press, 2010; Vol. 93, pp 85–127. https://doi.org/10.1016/B978-0-12-385044-7.00004-7.
- (82) Diez-Hermano, S.; Ganfornina, M. D.; Vegas-Lozano, E.; Sanchez, D. Machine Learning Representation of Loss of Eye Regularity in a Drosophila Neurodegenerative Model. *Front. Neurosci.* **2020**, *14*. https://doi.org/10.3389/fnins.2020.00516.
- (83) Sun, X.; Heckscher, E. S. Using Linear Agarose Channels to Study Drosophila Larval Crawling Behavior. *J. Vis. Exp. JoVE* **2016**, No. 117, e54892. https://doi.org/10.3791/54892.
- (84) Madabattula, S. T.; Strautman, J. C.; Bysice, A. M.; O'Sullivan, J. A.; Androschuk, A.; Rosenfelt, C.; Doucet, K.; Rouleau, G.; Bolduc, F. Quantitative Analysis of Climbing Defects in a Drosophila Model of Neurodegenerative Disorders. *J. Vis. Exp. JoVE* **2015**, No. 100, e52741. https://doi.org/10.3791/52741.
- (85) Pagano, G.; Lyakhovich, A.; Pallardó, F. V.; Tiano, L.; Zatterale, A.; Trifuoggi, M. Mitochondrial Dysfunction in Fragile X Syndrome and Fragile X-Associated Tremor/Ataxia Syndrome: Prospect Use of Antioxidants and Mitochondrial Nutrients. *Mol. Biol. Rep.* **2024**, *51* (1), 480. https://doi.org/10.1007/s11033-024-09415-7.

- (86) Joshi, D. C.; Bakowska, J. C. Determination of Mitochondrial Membrane Potential and Reactive Oxygen Species in Live Rat Cortical Neurons. *J. Vis. Exp. JoVE* **2011**, No. 51, e2704. https://doi.org/10.3791/2704.
- (87) Gohel, D.; Sripada, L.; Prajapati, P.; Currim, F.; Roy, M.; Singh, K.; Shinde, A.; Mane, M.; Kotadia, D.; Tassone, F.; Charlet-Berguerand, N.; Singh, R. Expression of Expanded *FMR1*-CGG Repeats Alters Mitochondrial miRNAs and Modulates Mitochondrial Functions and Cell Death in Cellular Model of FXTAS. *Free Radic. Biol. Med.* **2021**, *165*, 100–110. https://doi.org/10.1016/j.freeradbiomed.2021.01.038.
- (88) Neuronal necrosis and spreading death in a Drosophila genetic model / Cell Death & Disease. https://www.nature.com/articles/cddis2013232.
- (89) Klemm, J.; Stinchfield, M. J.; Harris, R. E. Necrosis-Induced Apoptosis Promotes Regeneration in Drosophila Wing Imaginal Discs. *Genetics* **2021**, *219* (3), iyab144. https://doi.org/10.1093/genetics/iyab144.
- (90) Gupta, R.; Rajpoot, K.; Tekade, M.; Sharma, M. C.; Tekade, R. K. Chapter 7 Methods and Models for in Vitro Toxicity. In *Pharmacokinetics and Toxicokinetic Considerations*; Tekade, R. K., Ed.; Advances in Pharmaceutical Product Development and Research; Academic Press, 2022; Vol. 2, pp 145–174. https://doi.org/10.1016/B978-0-323-98367-9.00006-8.
- (91) *Measuring Cell Death by Propidium Iodide Uptake and Flow Cytometry*. https://cshprotocols.cshlp.org/content/2016/7/pdb.prot087163.
- (92) Dumurgier, J.; Sabia, S. Life Expectancy in Dementia Subtypes: Exploring a Leading Cause of Mortality. *Lancet Healthy Longev.* **2021**, 2 (8), e449–e450. https://doi.org/10.1016/S2666-7568(21)00166-5.

- (93) Autophagy in neurodegenerative diseases: pathogenesis and therapy Guo 2018 Brain Pathology Wiley Online Library. https://onlinelibrary.wiley.com/doi/10.1111/bpa.12545.
- (94) Papinski, D.; Kraft, C. Regulation of Autophagy By Signaling Through the Atg1/ULK1 Complex. *J. Mol. Biol.* **2016**, *428* (9, Part A), 1725–1741. https://doi.org/10.1016/j.jmb.2016.03.030.
- (95) ATG4B and pS383/392-ATG4B serve as potential biomarkers and therapeutic targets of colorectal cancer | Cancer Cell International | Full Text. https://cancerci.biomedcentral.com/articles/10.1186/s12935-023-02909-7.
- (96) ATG5: A central autophagy regulator implicated in various human diseases Changotra 2022 Cell Biochemistry and Function Wiley Online

 Library.

 https://analyticalsciencejournals.onlinelibrary.wiley.com/doi/10.1002/cbf.3
 740.
- (97) Insights on E1-like enzyme ATG7: functional regulation and relationships with aging-related diseases / Communications Biology. https://www.nature.com/articles/s42003-024-06080-1.
- (98) Xu, Y.; Liu, W.; Sun, Z.; Yu, Y.; Yang, T.; Lu, X.; Zhang, G.; Jiao, J.; Duan, X. The Two Autophagy-Related Proteins 8a and 8b Play Distinct Physiological Roles in *Drosophila*. *Genomics* **2024**, *116* (3), 110853. https://doi.org/10.1016/j.ygeno.2024.110853.
- (99) Guo, T.; Nan, Z.; Miao, C.; Jin, X.; Yang, W.; Wang, Z.; Tu, Y.; Bao, H.; Lyu, J.; Zheng, H.; Deng, Q.; Guo, P.; Xi, Y.; Yang, X.; Ge, W. The Autophagy-Related Gene *Atg101* in *Drosophila* Regulates Both Neuron and Midgut Homeostasis. *J. Biol. Chem.* **2019**, *294* (14), 5666–5676. https://doi.org/10.1074/jbc.RA118.006069.

- (100) Celecoxib exerts protective effects in the vascular endothelium via COX-2-independent activation of AMPK-CREB-Nrf2 signalling | Scientific Reports. https://www.nature.com/articles/s41598-018-24548-z.
- (101) Demircan, B.; Çelik ,Gülnaz; Süleyman ,Halis; and Akçay, F. Effects of Indomethacin, Celecoxib and Meloxicam on Glutathione, Malondialdehyde and Myeloperoxidase in Rat Gastric Tissue. *Pain Clin*. **2005**, *17* (4), 383–388. https://doi.org/10.1163/156856905774482797.